NASA Technical Paper 3103

September 1991

Static Internal Performance of Ventral and Rear Nozzle Concepts for Short-Takeoff and Vertical-Landing Aircraft

Richard J. Re and George T. Carson, Jr.

NASA

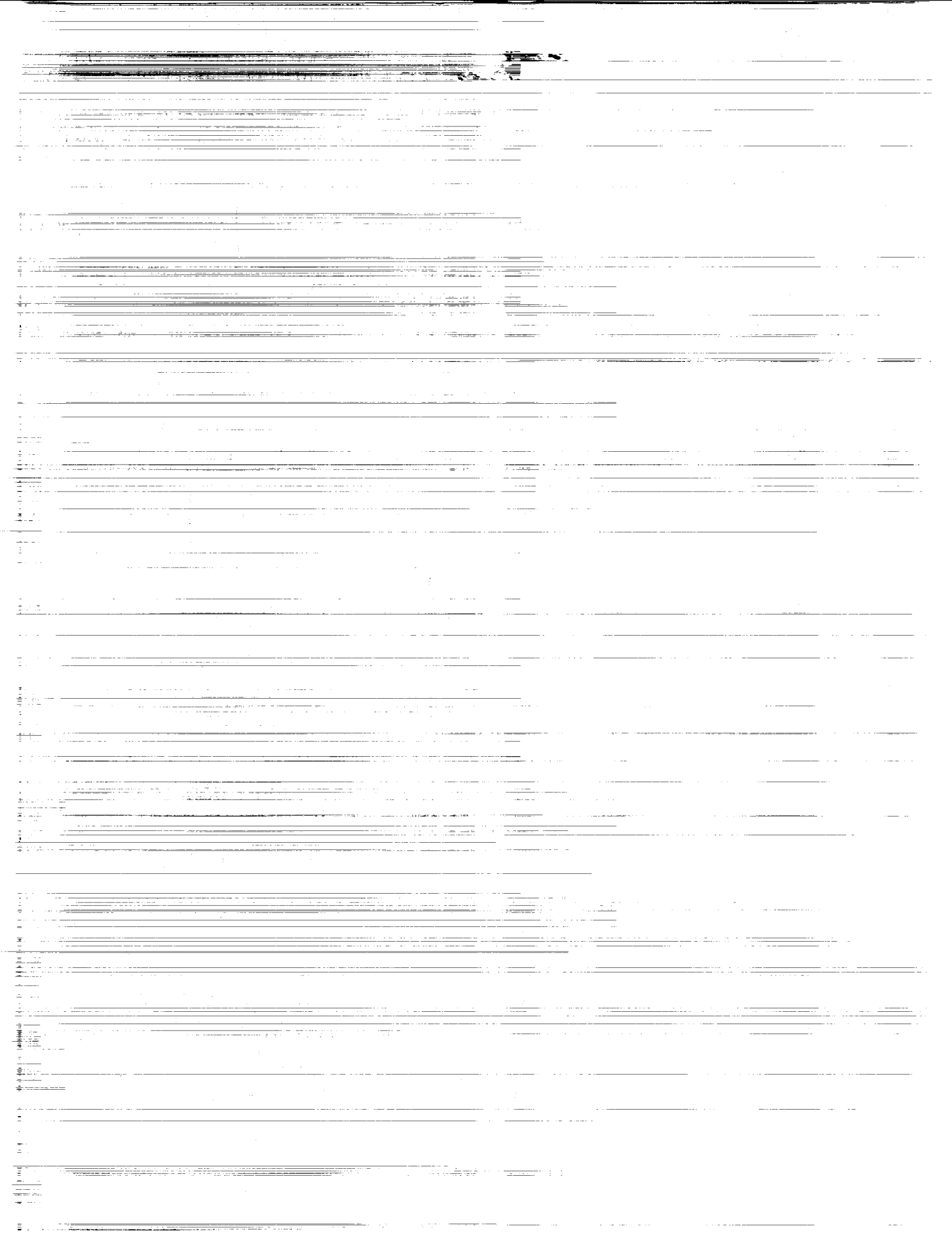

NASA Technical Paper 3103

1991

Static Internal Performance of Ventral and Rear Nozzle Concepts for Short-Takeoff and Vertical-Landing Aircraft

Richard J. Re and George T. Carson, Jr.
Langley Research Center
Hampton, Virginia

National Aeronautics and Space Administration

Office of Management

Scientific and Technical Information Program

Summary

An investigation has been conducted to determine the internal performance of two exhaust system concepts applicable to single-engine short-takeoff and vertical-landing tactical fighter configurations. These concepts involved blocking (or partially blocking) tail-pipe flow to the rear (cruise) nozzle and diverting it through an opening to a ventral nozzle for vertical thrust. A set of variable-angle vanes at the ventral nozzle exit was used to vary ventral nozzle thrust angle between 45° and 110° relative to the positive-axial-force direction. In the vertical flight mode the rear nozzle (or tail-pipe flow to it) was completely blocked. In the transition flight mode flow in the tail pipe was split between the rear and ventral nozzles, and the flow was vectored at both exits for aircraft control purposes throughout this flight regime. In the cruise flight mode the ventral nozzle was sealed and all flow exited through the rear nozzle.

The tests were conducted in the static test facility of the Langley 16-Foot Transonic Tunnel at nozzle pressure ratios from 1.5 to 6.0 (measured in the tail pipe ahead of the passage opening to the ventral nozzle). The results are presented as basic nozzle internal performance data and consist of discharge coefficient, internal thrust ratio, normal-force ratio, pitching-moment ratio, resultant-thrust ratio, and thrust vector angle. Ventral nozzle plume-total-pressure surveys indicate that plume-total-pressure decay with distance from the exit increased significantly when the nozzle exit area was segmented. However, the ventral nozzles with segmented exit area had lower thrust performance than unsegmented nozzles because of a suckdown effect on the base areas between the flowing segments.

Introduction

Operational flexibility of multimission turbofan-powered tactical aircraft would be greatly expanded if they were designed with short-takeoff and vertical-landing (STOVL) capability. The necessity for long, vulnerable runways required for conventional takeoff and landing (CTOL) tactical aircraft would be lessened and aircraft could be deployed for dispersal purposes or based closer to a changing line of battle for rapid response. Recovery of airborne aircraft with vertical-landing capability would always be feasible at alternate sites when operations at the home base have been disrupted; in effect the aircraft would loiter on the ground. With the present state of propulsion technology, STOVL is considered to be a more practical capability for a tactical aircraft than vertical takeoff and landing (VTOL) capability, since a VTOL aircraft would require a larger power plant or additional propulsion capability for vertical takeoff when fully loaded with fuel and ordnance expendables. This increased power plant capability, and hence greater fuel consumption, for vertical takeoff would have detrimental effects on operating range or configuration sizing. Some advantages for attack aircraft with STOVL and VTOL capabilities are discussed in references 1 and 2.

Many vertical (hover) and transition flight systems that could fulfill the needs of STOVL tactical aircraft have been considered. The effectiveness and practicality of proposed systems vary considerably and a discussion of some of these approaches is contained in reference 3. In general, incorporation of STOVL capabilities into an aircraft complicates the design and restricts the designer, depending on the exhaust system features selected. At a minimum, additional ducting, valving, reaction control systems, ventral nozzles, or thrust vectoring systems result in some additional weight, so the increased operational flexibility provided must be traded off against CTOL designs. For configuration balancing purposes it is also desirable to place as much of the reaction lift portion of the propulsion system as near as possible to the vehicle center of gravity so that the configuration can be more easily trimmed in transition or vertical flight. However, such propulsion system placement conflicts with the need to place consumables such as munitions and fuel near the center of gravity. This tends to cause STOVL tactical aircraft configurations to have a large maximum cross-sectional area in the vicinity of the center of gravity and to have a part of the internal volume committed to vertical lift apparatus such as ducting. In spite of the compromises and potential penalties involved, STOVL-related aircraft and propulsion technologies are developing rapidly. The evolution of practical military configurations is likely since mission effectiveness can be enhanced by operating a shorter range STOVL aircraft closer to the combat area to provide an improvement in response time and an increase in mission frequency.

The present investigation was conducted to determine the internal performance of a single-engine STOVL exhaust system in which tail-pipe (or rear nozzle) flow is blocked (or partially blocked) and diverted to a ventral nozzle through an opening in the bottom of the tail pipe. Knowledge of the exhaust system internal performance is a key to assuring that the appropriate back pressure is maintained to avoid engine stalling or overspeeding. Two blocking concepts were examined. One concept incorporated self-closing rear nozzles and longitudinally hinged butterfly doors in the wall of the tail

pipe. The doors opened to permit flow to enter a ventral nozzle passage. The other concept incorporated a tail-pipe blocking system of clamshell diverters that rotated out of the tail-pipe wall to open up the entrance to the ventral nozzle passage while blocking the tail-pipe flow. Both concepts utilized a set of variable-angle vanes at the ventral nozzle exit to vary ventral nozzle thrust angle. Two types of self-closing rear nozzles were investigated. One was a model of a thrust-vectoring two-dimensional convergent-divergent (2D-CD) nozzle with the ability to alter convergent section geometry enough to partially or completely close the throat. The other was a model of a thrust-vectoring axisymmetric nozzle with fixed divergent flap geometry and clamshell blockers in its convergent section that rotated to partially or completely close the throat.

In the vertical flight mode, the rear nozzle was completely closed (i.e., tail-pipe flow to the rear nozzle was blocked aft of the ventral nozzle) to divert the flow to the ventral nozzle. During transition flight the rear nozzle was partially closed (tail-pipe flow to the rear nozzle was partially blocked) to divert some of the flow to the ventral nozzle. In cruise flight the rear nozzle was completely open and all diverter components were stowed flush in the walls of the tail pipe so that the entrance to the ventral nozzle flow passage was blocked. In the vertical flight mode, a vertical thrust port is required on the forward portion of an aircraft configuration to trim the ventral nozzle thrust when aerodynamic surfaces become ineffective. Such a port is likely to be required for flight at the lower transition speeds as well. However, the apparatus developed for the present investigation did not include a forward port.

This investigation was conducted in the static test facility of the Langley 16-Foot Transonic Tunnel at nozzle pressure ratios from 1.5 to 6.0 in the duct tail pipe ahead of the ventral nozzle flow passage opening (simulated variable-area turbine section). The results are presented as basic nozzle internal performance data and consist of discharge coefficient, internal thrust ratio, normal-force ratio, pitching-moment ratio, resultant-thrust ratio, and thrust vector angle. A summary of some of the results obtained in this investigation is contained in reference 4.

Symbols and Abbreviations

All forces (with the exception of resultant gross thrust) and angles are referred to the model centerline (body axis). A detailed discussion of the data reduction and system calibration procedures as well as definitions of forces, angles, and propulsion relationships used herein can be found in reference 5.

A_n	minimum internal area (throat) of rear nozzle or partially blocked duct ahead of it, in^2
A_t	sum of minimum internal areas of ventral and rear nozzles (or duct), $A_n + A_v$, in^2
A_v	minimum internal area (throat) at ventral nozzle exit, butterfly doors, or exit vanes, in^2
c_d	nozzle discharge coefficient based on A_t, w_p/w_i
d	local diameter, in.
F	measured thrust along body axis, positive in forward direction, lbf
F_i	ideal gross thrust, $w_p\sqrt{\frac{R_j T_{t,j}}{g}\frac{2\gamma}{\gamma-1}\left[1-\left(\frac{p_a}{p_{t,j}}\right)^{(\gamma-1)/\gamma}\right]}$, lbf
F_N	normal force, lbf
F_r	resultant gross thrust, $\sqrt{F^2+F_N^2}$, lbf
g	acceleration due to gravity, 32.174 ft/sec^2
MS	model station, in.
M_Y	pitching moment about the force balance moment center, in-lbf
NPR	nozzle pressure ratio, $p_{t,j}/p_a$
p	local static pressure, psi
p_a	ambient (atmospheric) pressure, psi
p_t	local total pressure, psi
$p_{t,j}$	jet total pressure measured in the duct, psi
R_j	jet gas constant, 53.36 ft/°R
r	local radius, in.
STOVL	short takeoff and vertical landing
$T_{t,j}$	jet total temperature measured in the duct, °R
2D-CD	two-dimensional convergent-divergent
w	width of throat of two-dimensional nozzle or diameter of tail-pipe duct, 4.0 in.

w_i	ideal weight-flow rate, lbf/sec
w_p	measured weight-flow rate, lbf/sec
x	local abscissa, in.
y	distance of plume total-pressure survey probes from tip of ventral nozzle exit vanes, in.
α	lower clamshell diverter angle, deg
β	ventral nozzle butterfly door angle, deg
γ	ratio of specific heats, 1.3997 for air
δ	resultant-thrust-vector angle, $\tan^{-1}(F_N/F)$, deg
δ_n	geometric pitch-vector angle of rear nozzle with respect to centerline of simulated turbine discharge section, deg
θ	angle measured clockwise (looking aft) about the model centerline, deg
ϕ	ventral nozzle exit vane angle, deg

Model Component Designations:

B_0	fully open ventral nozzle exit (all five vane passages open)
B_1	rear two ventral nozzle exit vane passages blocked
B_2	forward two ventral nozzle exit vane passages blocked
B_3	second and fourth ventral nozzle exit vane passages blocked
B_4	center ventral nozzle exit vane passage blocked
C	0.6-in.-long downstream extension of centerbody of simulated variable-area turbine section
D_2	cylindrical duct insert section aft of ventral nozzle housing to create long-duct configurations for rear nozzle
E_1	fully open 2D-CD rear nozzle, A_n = 4.00 in^2
E_2	fully open 2D-CD rear nozzle vectored 20°, A_n = 4.00 in^2
E_3	partially open 2D-CD rear nozzle vectored 20°, A_n = 2.67 in^2
E_4	partially open 2D-CD rear nozzle vectored 20°, A_n = 1.32 in^2
E_5	blocking plate to replace 2D-CD rear nozzle
E_6	fully open axisymmetric convergent-divergent rear nozzle vectored 15°, A_n = 4.00 in^2
E_7	partially open axisymmetric convergent-divergent rear nozzle vectored 15°, A_n = 3.28 in^2
E_8	partially open axisymmetric convergent-divergent rear nozzle vectored 15°, A_n = 1.71 in^2
E_9	blocking plate to replace axisymmetric rear nozzle
N_b	nozzle housing and ventral nozzle with internal butterfly doors
N_c	nozzle housing and ventral nozzle used in conjunction with duct clamshell diverters
S_1	both 0.65-in.-long ventral nozzle spacers downstream of ventral nozzle housing
S_2	one 0.65-in.-long ventral nozzle spacer downstream and one spacer upstream of ventral nozzle housing
S_3	both 0.65-in.-long ventral nozzle spacers upstream of ventral nozzle housing
V_c	simulated variable-area turbine section representing engine core flow only
V_{fc}	simulated variable-area turbine section representing engine core and fan flow
W_7	wedge-shaped duct insert to produce 7° bend in duct
W_{17}	wedge-shaped duct insert to produce 17° bend in duct

Apparatus and Methods

Static Test Facility

This investigation was conducted in the static test facility of the Langley 16-Foot Transonic Tunnel. This facility uses a central high-pressure air system that provides a continuous flow of clean, dry air at a controlled temperature of approximately 530°R at the test nozzle for propulsion simulation. Test nozzles exhaust to atmospheric conditions within the facility and the building pressure is equalized through

louvered vents in the roof. Calibration of mass-flow instrumentation and bellows force restraints are conducted as needed for each investigation.

Propulsion Simulation System

A schematic of the propulsion simulation system to which the calibration and test hardware were attached is shown in figure 1. The high-pressure air is brought through the dolly-mounted support strut to a high-pressure plenum and then discharged radially into a low-pressure plenum through eight multiholed nozzles equally spaced around the high-pressure plenum. The force-balance-mounted low-pressure plenum is isolated from the nonmetric high-pressure plenum by two flexible metal bellows that serve to contain the flow and compensate for axial forces caused by pressurization. Attachment of flow transition adapters or instrumentation sections to the downstream end of the low-pressure plenum (at MS 36.485) tailors the system to specific test installation hardware requirements.

Calibration of Assembled System

For this investigation the assembled propulsion simulation system was calibrated using a series of Stratford choke nozzles having their own jet-total-pressure measuring instrumentation section. These nozzles had known internal performance and their throat areas spanned the range of rear and ventral nozzle throat areas to be tested. Force and moment tares due to physical restraint and internal flow were determined with the calibration hardware installed over the anticipated range of jet induced loads to be encountered during the test. This was done by applying known forces and moments to the model and computing correction factors as a function of measured balance loads and bellows pressure with the jet operating. The calibration nozzle (including the total-pressure measuring section) was then removed and the test hardware (including a total-pressure measuring section with a centerbody) was installed (fig. 2). In this way the performance of the entire test model flow system, including the upstream duct and moveable flow-blocking devices in the duct, was measured.

Instrumentation and Measurements

The mass flow through the system was measured with two critical flow venturis in the high-pressure portion of the propulsion air supply. Uncorrected forces and moments produced by the rear and/or ventral nozzle exhausts were measured with a six-component strain-gage force balance. Total and static internal pressures were measured on individual strain-gage transducers sized to the maximum pressure expected at each location. Jet total temperature was measured with iron-constantan thermocouples located in the portion of the duct containing the centerbody. The raw data recorded for each data channel at each data point (a given nozzle pressure ratio setting) was the average of 50 samples taken at a rate of 10 samples per second. Only steady-state data measurements were made.

Model Description

The model simulated the internal flow path of a STOVL exhaust system and consisted of the components necessary to assemble cruise, transition, or vertical lift propulsion systems for static testing. (See fig. 2, e.g.) The portion of the model with the centerbody in the duct represented a variable-area portion of the system simulating the engine turbine discharge section and flow valve for the forward lift system (not simulated for this investigation). Two of these sections (fig. 3) were built, one with an open area to simulate fan-plus-core flow (cruise operation) and a second with an open area to simulate core flow only (transition and vertical lift operation). A cylindrical spacer could be inserted in the aft portion of the centerbody (see fig. 3) so that the centerbody was extended 0.6 in. downstream over the entrance to the ventral nozzle passage to introduce greater blockage in the flow path to the ventral nozzle. The two simulated variable-area turbine sections were instrumented with four total-pressure probes on each of the four centerbody support struts and had a ring of eight static-pressure orifices spaced 45° apart in the surface of the duct wall. Two thermocouples were installed in the plane of the total-pressure probes.

The entrance to the ventral nozzle flow passage was just aft of the simulated variable-area turbine section. (See fig. 4.) The longitudinal location in the tail pipe of the opening to the ventral nozzle flow passage could be changed by movement of one or two narrow spacers upstream or downstream of the ventral nozzle housing. In this way ventral nozzle proximity to the turbine section could be varied while the tail-pipe length remained constant. Two ventral nozzle housings were fabricated, one with provisions for attaching clamshell-type flow diverter components in the main duct (fig. 5) and a second to house a butterfly-type door system at the entrance to the ventral nozzle flow passage (fig. 6). Three ventral nozzle inserts with butterfly doors fixed at angles of 45°, 65°, and 90° relative to a horizontal plane were constructed. The flow at the ventral nozzle exit was vectored in the vertical plane with fixed cascade vane sets (fig. 7) with vane angles of 45°, 70°, 90°, and 110° relative to the

positive-axial-force direction. The ventral nozzle system was designed to operate at a constant throat area that would not change as the exit vanes were vectored. Conceptually this would be done by having two of the five cascade vanes move relative to the other three to compensate for throat area changes that would occur if all five vanes moved in the same manner. To simulate the constant-throat-area concept using the model hardware, blocker plates (fig. 8) were inserted between the ventral nozzle exit and the cascade vanes to block flow through two of the vane passages for the vertical lift configuration (exit vanes at 90°). The blocker plates were removed for a vane angle setting of 45° so that the open area of that set of vanes would match the open area of the partially blocked 90° vanes. Blocker plates with alternate openings were used to obtain segmented nozzle exits. A total-pressure rake with 13 probes could be mounted at various distances from the ventral nozzle exit to survey the exhaust plume total-pressure decay in the centerline plane of the model for configurations with the exit vanes at 90°.

The tail-pipe duct downstream of the ventral nozzle housing could be assembled with various combinations of components (fig. 2). These included cylindrical and wedge (7° or 17°) sections that, when added, simulated long and offset tail-pipe configurations. When a 7° upward wedge was inserted ahead of the cylindrical duct section followed by a 7° downward wedge after the cylindrical section, an S-shaped duct (tail pipe) was formed with the rear nozzle (unvectored) centerline displaced from the model centerline but remaining parallel to it. When the 7° downward wedge was replaced with the 17° downward wedge the duct remained offset but the rear nozzle vector angle was changed by 10°.

Rear nozzle geometry was one of the model variables; internal flow transition and instrumentation sections for either axisymmetric or 2D-CD nozzles (fig. 2) could be installed at the downstream end of the tail pipe ahead of the convergent portion of the nozzle. There were seven rear nozzles of various vector angles and flow areas. Some of these nozzles had reduced throat areas to represent intermediate flight (transition) conditions (i.e., flow split between rear and ventral nozzles). The axisymmetric nozzle throat geometry (fig. 9) was altered with spherical clamshell blocker sections that would come out of the convergent section (conceptually) of the nozzle to partially close the throat. The resulting throat was essentially rectangular (figs. 9(b) and 9(c)) with a rearward-facing base area in the plane of the throat. Reduction of throat area for the 2D-CD nozzles (fig. 10) would be accomplished (conceptually) by using the variable-geometry mechanical features incorporated in the nozzle for thrust vectoring. For the 2D-CD nozzles with reduced throat areas no rearward-facing internal base area resulted. All the rear nozzles, except the partially closed axisymmetric nozzles, had an expansion ratio of 1.09 (ratio of exit area to throat area), which corresponds to a design nozzle pressure ratio (for full flow expansion) of 3.0.

For hover configurations with the clamshell diverter in the tail pipe, the flow to the rear nozzle was blocked in the duct just aft of the ventral nozzle housing (fig. 5(c)). For hover configurations with the butterfly door ventral nozzle, the rear nozzle was removed and replaced with a blocking plate or cap at the end of the tail pipe to block the flow.

Presentation of Results

The basic data obtained during this investigation are presented in graphical form as a function of nozzle pressure ratio (NPR) as measured in the simulated variable-area turbine section. The hardware was designed to generate forces and moments only in the longitudinal plane. These forces and moments are presented as nondimensionalized parameters. Thrust vector angle is presented in degrees and was the angle of the resultant-force vector generated by the flowing nozzles relative to the centerline of the model. Discharge coefficient was based on the sum of the throat areas when more than one nozzle was open. In some cases the minimum area for the rear nozzle flow system was in the tail pipe, where the clamshell diverter closed enough to create a smaller geometric area than the minimum area in the rear nozzle. In the case of the ventral nozzle, the butterfly doors (at 45°) sometimes created a smaller geometric area at the door location than existed at the ventral nozzle exit or in the exit vanes. When either of the aforementioned situations occurred, the smallest area was used as the throat area for the nozzle and is listed in the data figure keys as the throat area for that nozzle. In nondimensionalizing pitching moment, the diameter of the tail-pipe duct (4.0 in.) was arbitrarily used as the reference length. The longitudinal location of the force balance pitching-moment center (MS 29.390) was arbitrarily selected as the pitch reference center for the basic data. Forces and moments measured in the lateral plane were negligible.

In general, each basic data figure presents data for configurations simulating only one flight regime (e.g., hover, cruise, or transition). In addition, the data presented in a given figure are for several configurations having one or two model components systematically varied. Most summary data figures are

presented for NPR = 3.0, which is the design pressure ratio for full flow expansion in the cruise nozzles.

Results and Discussion

In general, the data are discussed in separate sections, one for each flight regime. That is, there is a section on vertical flight (or hover, ventral nozzle open), a section on cruise flight (rear nozzle open), and a section on transition flight (ventral and rear nozzles open). The data for a few configurations with one nozzle partially open are included in the transition flight basic data figures when that nozzle open area is pertinent only to transition flight conditions. For example, a partially open rear nozzle is not a realistic cruise nozzle configuration when tested with the ventral nozzle closed since the reduced area would cause a back pressure increase on the engine.

Vertical Flight (or Hover)

Effect of ventral nozzle axial location and turbine section centerbody length. The axial location of the opening to the ventral nozzle flow passage relative to the turbine discharge section was varied by moving one or two cylindrical spacer rings (fig. 4) either forward or aft of the ventral nozzle housing to determine whether significant flow problems would be caused by having the ventral nozzle passage opening close to the turbine exit station. Location of the ventral nozzle close to the turbine exit is desirable since the vertical thrust vector would be closer to the configuration center of gravity and therefore decrease the pitching-moment contribution. In conjunction with the changes in ventral nozzle location, a cylindrical spacer was inserted in the turbine section centerbody just ahead of the boattail (fig. 3) to determine the effect of a longer centerbody on ventral nozzle performance. These variations of ventral nozzle location and turbine centerbody length were made for the butterfly door (figs. 11 and 12) and clamshell diverter (figs. 13 and 14) ventral nozzles with 90° nozzle exit vanes (rear two vane passages blocked). Summary data (at NPR = 3.0) showing the effects of ventral nozzle axial location and turbine section centerbody length are presented in figure 15 for the butterfly door ($\beta = 90°$) and clamshell diverter ventral nozzles. As shown in the data of figure 15 the effects were small, with the largest effect being the predictable changes in pitching-moment ratio that result from movement of the ventral nozzle forward or aft relative to the force-balance moment center.

The circumferential variation of turbine discharge section wall static-pressure ratio at the total-pressure measuring station (fig. 3) is shown in figure 16 for the butterfly door and clamshell diverter ventral nozzles as a function of nozzle pressure ratio for the three nozzle axial locations and two turbine centerbody lengths. The effect of ventral nozzle axial location on the circumferential distribution of static-pressure ratio is shown in figure 17 for NPR = 3.0 for both ventral nozzle configurations with and without the lengthened turbine centerbody. In all cases, the turning of the flow into the opening of the ventral nozzle passage caused a small decrease in static pressure at the bottom of the turbine section between 135° and 225°. Movement of the butterfly door ventral nozzle to its most rearward location (S_3) decreased the maximum static-pressure distortion from about 2.6 to 1.8 percent. Movement of the clamshell diverter ventral nozzle rearward had almost no effect on maximum static-pressure distortion (which was 1.8 percent). The larger effect of the butterfly door ventral nozzle in its most forward location (S_1) was probably due to protrusion of the butterfly doors ($\beta = 90°$) into the main duct (fig. 6) and their proximity to the centerbody.

Effect of butterfly door angle on ventral nozzle performance. The effect of butterfly door angle on ventral nozzle internal performance over the range of nozzle pressure ratios is presented in figure 18 for door angles of 45°, 65°, and 90° with the nozzle exit vanes at 90° and the ventral nozzle in the forward location. With two nozzle exit vane passages blocked, angular rotation of the butterfly doors caused the minimum area (throat) to move from the butterfly doors (at $\beta = 45°$) to the ventral nozzle exit at some door angle between 45° and 65°. The reduced throat area in the ventral nozzle system is more representative of transition flight conditions, but the data are presented here since the rear nozzle was closed and the ventral nozzle exit vanes were at 90°. The variation of ventral nozzle internal performance parameters with butterfly door angle at NPR = 3.0 is presented in figure 19. The data for the three door angle settings are connected with straight lines because the variation between 45° and 65° was not necessarily smooth since the minimum area moved abruptly from the butterfly door location to the nozzle exit. As shown in the data of figures 18 and 19, discharge coefficient was much larger and resultant-thrust ratio was much smaller when the minimum area was at the butterfly doors ($\beta = 45°$). Examination of the normal-force and thrust-ratio data of figure 18 indicates that the smaller resultant-thrust ratio with the butterfly doors at 45° was due to a large loss in normal-force ratio. This was probably due to a suckdown effect on the projected area in

the horizontal plane of the butterfly doors when the throat occurred at the butterfly door location.

Effect of ventral nozzle exit open area on internal performance. Open area at the ventral nozzle exit was changed by inserting blocker plates between the nozzle exit and the exit vanes to create different open areas or open-area patterns (fig. 8). Both ventral nozzles were investigated with the nozzles in the most forward location. The nozzle exit vanes were at 90° and the butterfly doors were at 90° when that nozzle was tested. The basic internal performance data showing the effect of nozzle pressure ratio for a series of open areas are presented in figure 20 for the butterfly door ventral nozzle and in figure 21 for the clamshell diverter ventral nozzle. The open-area variations were not systematic enough for graphical presentation of summary performance data as a function of open area. However, a few internal performance parameters are presented in bar chart form for NPR = 3.0 in figure 22.

In general, the ventral nozzles with $A_v = 2.43$ in^2 had the highest discharge coefficients above NPR = 2.5 (figs. 20(a) and 21(a)). The butterfly door ventral nozzle had a higher discharge coefficient than the clamshell diverter ventral nozzle for a configuration with a given exit area. As nozzle exit open area increased above 2.43 in^2, discharge coefficient decreased for both ventral nozzles.

Resultant-thrust ratio was the largest for the five nonsegmented nozzle exits with $A_v = 2.43$ in^2 (blockers B_1 and B_2), varying from 0.84 to 0.95 over the range of nozzle pressure ratios (figs. 20(a) and 21(a)). For those five ventral nozzles, resultant-thrust ratio peaked at between 0.93 and 0.95 at nozzle pressure ratios between 4.0 and 6.0. With no area blockage at the nozzle exit (blocker B_0), resultant-thrust ratio was between 7 and 9 percent lower than those for the nonsegmented 2.43 in^2 nozzle exits at the lowest nozzle pressure ratio. However, resultant-thrust ratio steadily increased with nozzle pressure ratio until it reached the same level as those of the nonsegmented configurations (with vanes) at the highest nozzle pressure ratios of this investigation. The worst performance for the configuration with the clamshell diverter occurred when there was no area blockage at the exit (less flow convergence in the nozzle) and the exit vanes were removed (fig. 21). Without the exit vanes the flow overturned (i.e., $\delta > 90°$) by between 2.5° and 6.5° over the nozzle pressure ratio range.

Effect of ventral nozzle exit segmentation on plume-total-pressure decay. Rapid decay of the exhaust plume from the ventral nozzle in the vertical landing mode is desirable to minimize recirculation of flow (or debris) from the ground and to reduce jet velocity and temperature effects on paved surfaces or decks. To determine the decay of plume total pressure with distance from the ventral nozzle exit, some configurations were surveyed with a 13-probe total-pressure rake attached to the model in the centerline longitudinal plane of the model and positioned at three distances from the trailing edge of the exit vanes. The rake position farthest from the exit vanes approximates the distance from the ground that the ventral nozzle exit would be for a typical fighter aircraft at touchdown (vertical landing). These measurements, which were made for the butterfly door ventral nozzle ($\beta = 90°$ and $\phi = 90°$) with blocker B_1 and with segmented blockers B_3 and B_4, are presented in figure 23 for NPR = 3.0. At this pressure ratio, the nozzle exit with blocker B_3 (largest number of open-area segments) had the most rapid decay in plume maximum total pressure with distance (52 percent). The other segmented nozzle exit, with blocker B_4, had a total-pressure decay of 32 percent, while the unsegmented nozzle exit, with blocker B_1, had a total-pressure decay of only 26 percent.

However, the internal performance data (F_r/F_i and F_N/F_i) shown in figure 20 indicate there was a significant thrust loss over the entire nozzle pressure range because of segmenting the nozzle exit. This can be partially explained by the segmented nozzle total-pressure measurements shown in figure 23 for the rake position closest to the ventral nozzle exit. The rake total pressures measured in the blocked areas between the flowing vane passages were below ambient and indicate the presence of a suckdown effect on the projected areas. Since the rake in this position was downstream of the exit vane trailing edges, it is probable that the pressure on the surfaces of the blocked areas was even lower than that measured by the rake since the adjacent flowing jets acted as ejector flows.

Effect of exit vane angle on ventral nozzle performance. The ventral nozzle exit vane angle was varied from 45° to 110° for both ventral nozzle configurations to determine its effect on internal performance. As exit vane angle was varied from 90°, the minimum flow passage area (throat) decreased and moved from the nozzle exit into the vane passages (fig. 7); that is, throat area and location were a function of vane angle for a given exit blocker. The basic internal performance data as a function of nozzle pressure ratio for the four exit vane angle settings

are presented in figure 24 for the butterfly door ventral nozzle (with blocker B_0) and in figure 25 for the clamshell diverter ventral nozzle (with blocker B_1).

The exit vanes were effective in turning the flow to the geometric vector (vane) angle at NPR = 3.0, with a maximum variation in resultant-thrust-vector angle of 20° (for the clamshell diverter nozzle with the exit vanes at 45°) over the range of nozzle pressure ratios tested. In general, the resultant-thrust-vector angle was within 1° or 2° of the geometric vector angle at NPR = 3.0 for all the vane angle settings investigated (figs. 24 and 25). A summary of the effect of vane angle on internal nozzle performance at NPR = 3.0 is presented in figures 26(a) and 26(b) for the butterfly door and clamshell diverter ventral nozzles, respectively. The major difference in performance between the two ventral nozzle configurations was in discharge coefficient, which was about 2 percent higher over the range of nozzle pressure ratios for the clamshell diverter ventral nozzle. This, however, was not necessarily due to nozzle exit vane angle, since the two configurations were investigated with different nozzle exit blockers. As shown in figures 20 to 22, a given ventral nozzle had a measurably higher discharge coefficient with blocker B_1 than with blocker B_0 because of greater flow convergence in the nozzle with blocker B_1. The large variation in pitching-moment ratio with vane angle for both ventral nozzles was primarily due to the change in the length of the moment arm as vane angle is changed rather than any significant change in thrust ratio (figs. 26(a) and 26(b)).

Cruise (or Vectored Cruise) Flight

2D-CD rear nozzles. The 2D-CD rear nozzle was investigated at the cruise power setting (A_n = 4.0 in^2) unvectored and vectored 20°. The nozzles had a throat aspect ratio of 4.0 (ratio of throat width to height), an expansion ratio of 1.09 (ratio of exit area to throat area), a sharp corner on the upper and lower flaps at the throat, and a flat-walled convergent section from the rectangular duct to the rectangular nozzle throat. These nozzles were similar in design to those investigated in references 6 and 7. The basic internal performance data, presented in figure 27, are for a long S-shaped duct unvectored and vectored configuration, a short straight duct vectored configuration, and a long S-shaped duct unvectored configuration having an internal cavity in the duct at the ventral nozzle location. In other words, the clamshell diverter ventral nozzle was blocked at the exit and the duct entrance to the ventral nozzle passage was open.

The thrust ratios and discharge coefficients for unvectored and vectored nozzles shown in figure 27 are comparable to but somewhat lower than those presented in references 6 and 7. These performance differences can be attributed to larger internal losses in the current configurations because of the centerbody, the nonoptimum area convergence to the nozzle throat, and the sharp corners on the upper and lower flaps at the nozzle throat. The effects of the S-shaped duct and of lengthening the duct on resultant-thrust ratio and discharge coefficient were small, as shown in figure 27. Vectoring the long-duct nozzle configuration produced a 3-percent decrease in discharge coefficient over the nozzle pressure ratio range (above NPR = 2.0). This decrease was due to a reorientation of the nozzle throat that occurred when only the divergent portion of the nozzle flaps rotated downward to achieve the vector angle. (See fig. 10(a).) In the vectored configuration, the corner at the throat of the lower flap became sharper than before and the plane of the minimum geometric area (throat) rotated about the corner of the lower flap such that its upper end was moved downstream onto the divergent portion of the upper flap. This approach to vectoring increased the amount of turning required around the sharp corner of the lower flap and the repositioned throat altered the flow convergence, especially in the vicinity of the upper flap.

The resultant-thrust-vector angle varied with nozzle pressure ratio, decreasing from 22.3° at the lowest nozzle pressure ratio to 16.7° at the highest nozzle pressure ratio. At the design nozzle pressure ratio of 3.0 the measured and geometric thrust vector angles were equal (20°). The decrease in thrust vector angle above the design pressure ratio for a vectoring nozzle of this type is customary and is due to the flow leaving the trailing edge of the upper divergent flap (flow becomes unbounded) before it leaves the trailing edge of the lower divergent flap. (See fig. 10(a).) This caused exhaust flow to turn away from the plane of the lower flap and resulted in a smaller component of normal force. (See fig. 27(b).)

The pitching-moment-ratio data of figure 27(b) show the effects of vectoring the nozzle and the combined effects of lengthening the duct and making it S-shaped. Since model hardware was not available to assemble a straight long-duct configuration, the effect of making the duct S-shaped could not be isolated experimentally. However, if the normal force and thrust are assumed to have acted at the nozzle exit for the unvectored S-shaped duct configurations and their pitching-moment-ratio contributions are computed and subtracted from the measured pitching-moment-ratio data, the pitching-moment-ratio curves collapse

to within 0.02 of 0. Therefore, the unvectored configuration pitching-moment ratios presented in figure 27(b) were the effect of the duct being S-shaped. Similar computations for the vectored configurations therefore will isolate the effect on pitching-moment ratio of vectoring the long- and short-duct configurations. The decrease in pitching-moment ratio with increasing nozzle pressure ratio was caused by the decrease in resultant-thrust-vector angle (normal-force ratio) with increasing nozzle pressure ratio.

Axisymmetric convergent-divergent rear nozzle. Only two configurations with the axisymmetric nozzle (expansion ratio of 1.09) were tested at a cruise throat area ($A_n = 4.00$ in^2) and they were both vectored configurations. These configurations were vectored 15° (fig. 9(a)), which represented the maximum vector angle capability of the conceptual axisymmetric mechanical design. The two configurations essentially duplicated the long and short 2D-CD vectored configurations except for nozzle shape and vector angle.

The internal performance data for the axisymmetric cruise nozzle configurations are presented in figure 28. As would be expected, the trends in internal performance for the axisymmetric nozzles were similar to those of the 2D-CD configurations. One noteworthy difference was the constant value of resultant-thrust-vector angle over the range of nozzle pressure ratios (fig. 28(a)). The reason for this is apparent from the nozzle geometry shown in figure 9(a). The vectoring concept for the axisymmetric nozzle included angular rotation of the entire nozzle as a unit so that the plane of the nozzle exit also rotated 15°. Therefore, flow leaving the exit left symmetrically and did not cause a change in normal-force ratio with pressure ratio, as was the case for the 2D-CD vectored nozzle configurations.

Transition Flight

Turbojet and turbofan engines are designed to operate with a constant back pressure on the turbine section. Therefore, the exhaust system downstream of the turbine must provide the proper amount of restriction to maintain that back pressure to avoid engine stall or overspeeding. This is an especially important consideration in a STOVL application where there are at least three different exhaust system configurations to consider. The most difficult flight regime of the three is transition flight where a ventral nozzle is opening up as the rear (cruise) nozzle starts closing and blockers and diverters are being deployed within the exhaust system, thus altering the flow restrictions (losses) within the different legs of the system. In some cases the transition flight exhaust systems can also have a shifting of the location of the minimum flow area (throat) in one leg of the system.

In the absence of mass-flow measuring instrumentation in each flow passage of the transition flight exhaust system, the internal performance of the entire exhaust system based on pressure measurements in the turbine section (before the flow splits into separate passages) is of prime importance. A discharge coefficient for the entire exhaust system based on the sum of the minimum flow areas in the two flow passages can be computed. For the present investigation, a discharge coefficient based on the sum of these areas was not completely indicative of the ability of the exhaust system to maintain constant back pressure since the sum of these areas varied as exhaust system geometry changed from cruise to vertical flight. A better representation of the ability of the transitioning exhaust system to maintain a constant back pressure is obtained from an effective throat (flow) area obtained from the product of the discharge coefficient, as presented in the basic data, and the sum of the minimum flow areas. If this product is essentially constant over the range of exhaust system geometries (for a nonafterburning application), then constant back pressure can be maintained.

2D-CD rear nozzle with butterfly door ventral nozzle. The basic internal performance data for six transition flight configurations with partially open (and vectored) 2D-CD rear nozzles and an open butterfly door ventral nozzle (exit vanes at 45°) are presented in figure 29. The rear nozzles were tested with two throat areas, vectored downward 20° or 30°, in long- and short-duct configurations, and with butterfly doors at 45° and 65°. The 30° rear nozzle vector angle was obtained by replacing the downstream 7° duct wedge (fig. 2(a)) with a 17° wedge (W_{17}) so that the duct immediately ahead of the convergent portion of the 20° nozzle was canted downward an additional 10°.

The three configurations with the largest open area in the ventral nozzle system ($\beta = 65°$) had the largest resultant-thrust ratios and the smallest discharge coefficients (fig. 29(a)) over the range of nozzle pressure ratios. As discussed previously for the configuration that had only the butterfly door ventral nozzle open (fig. 18), this resulted from movement of the minimum flow area from the nozzle exit to the butterfly doors when the door angle was changed from 65° to 45°. The large decrease in normal-force ratio because of movement of the minimum area to

the butterfly doors resulted from a lower pressure acting on the downstream side of the doors. The increased discharge coefficient when the flow was choked at the butterfly doors ($\beta = 45°$) indicates the flow-passing qualities of the butterfly doors were better than those of the ventral nozzle exit when the flow was choked there ($\beta = 65°$ or $90°$).

The geometric throat (minimum) areas that were investigated were not always intended to result in on-design settings but were often selected so that the sensitivity of internal performance to incremental geometric changes could be determined. The effects of these variations are discussed in the sections on vertical and cruise flight. However, some on-design throat areas were investigated at the different exhaust system flight conditions and a general idea of how effective throat area would vary with resultant-thrust-vector angle from cruise to vertical flight can be obtained. These data are presented in figure 30 as a summary polar plot showing the variation of effective throat area with resultant-thrust-vector angle for NPR = 3.0. It should be pointed out that the cruise nozzle configurations shown in figure 30 had the equivalent of both the fan and core flow of the engine supplied to them. Conceptually, during transition and vertical flight fan flow is diverted to a forward nozzle (not represented in this investigation) to aid in trimming pitching moments resulting from displacement of the rear and ventral nozzles from the aircraft center of gravity. Therefore, the on-design cruise effective throat areas were quite different in that the rear and ventral nozzles operated only with core flow during transition and vertical flight. It is apparent from figure 30 that effective throat area was considerably larger in transition (both nozzles open) than in vertical flight (ventral nozzle open). Careful scheduling of these areas and the forward nozzle area during transition would therefore be necessary to maintain the proper back pressure on the engine. With the rear nozzle fully closed, it appears that modulation of the ventral nozzle exit area by changing exit vane angle and separately articulating two of the exit vanes to vary the exit area can provide a constant effective throat area. The variation of resultant-thrust ratio as a function of resultant-thrust-vector angle as a configuration transitioned from cruise to vertical flight is shown in figure 31 for NPR = 3.0 and 5.0. With both nozzles partially open for transition flight, there was a significant decrease in resultant-thrust ratio for a given nozzle pressure ratio. This occurred when the butterfly door angle was 45°. Examination of the data of figure 18 (only ventral nozzle open) indicates that the thrust loss occurred in the ventral nozzle system and was the greatest at $\beta = 45°$.

Axisymmetric nozzle with clamshell diverter and butterfly door ventral nozzles. The basic internal performance data for transition flight exhaust system configurations with partially open axisymmetric rear nozzles or ducts and butterfly door or clamshell diverter ventral nozzles (exit vanes at 45°) are presented in figures 32 and 33. The configuration with the butterfly door ventral nozzle was investigated with two rear nozzle throat areas (A_n = 1.71 and 3.28 in^2, see figs. 9(b) and 9(c)). For A_n = 3.28 in^2, the butterfly doors were at 45°, and for A_n = 1.71 in^2, the butterfly doors were at 65°. For diagnostic purposes the ventral nozzle was removed from the nozzle housing and replaced with a solid insert to fair the duct internal surface so that the performance of the two reduced-area (partially open) rear nozzles could be determined.

The configuration with the clamshell diverter ventral nozzle (fig. 5) was investigated with the 15° vectored nozzle fully open so that the throat area for the rear nozzle exhaust system occurred in the duct at the clamshell diverter just aft of the ventral nozzle passage opening. The clamshell diverter, which consisted of two components, was set at two deployments: upper diverter closed and lower diverter at 20° (A_n = 1.92 in^2), and upper diverter closed and lower diverter at 30° (A_n = 2.98 in^2). Cylindrical duct sections of the rear nozzle exhaust system were removed to produce a short-duct version of the aforementioned configurations. In addition, for diagnostic reasons the ventral nozzle exit was blocked and the lower clamshell diverter was removed so that long- and short-duct configurations with only the upper clamshell diverter closed (A_n = 3.14 in^2) were created.

Since the clamshell diverter ventral nozzle concept was not tested over the complete range of cruise to vertical flight with on-design throat areas, the summary data for all the axisymmetric on-design configurations are presented in figures 34 and 35 so that some trends and differences may be inferred. It appears that the butterfly door configuration with $\beta = 45°$ had an effective throat area as large as that of the cruise nozzle configuration (which included fan flow). This would likely cause too low a back pressure for the core-flow-only transition condition and could result in engine overspeed. Some reduction in the rear nozzle throat area would alleviate this problem. In the vertical flight condition, both ventral nozzle concepts had the same effective throat area.

The variation of resultant-thrust ratio with thrust vector angle shown in figure 35 indicates the configuration with the clamshell diverters in the duct had a large loss in resultant-thrust ratio during

transition, especially at NPR = 3.0. Pressures measured in the duct downstream of the upper clamshell diverter indicate a large drag increment because of low pressure on the back of the closed upper clamshell (compare F/F_i in figs. 32 and 33). At NPR = 5.0 this effect was greatly decreased. It appears that at low nozzle pressure ratios solid blockers in the duct can result in large thrust losses.

Concluding Remarks

An investigation of the static performance of ventral and rear nozzle configurations ranging from cruise to vertical flight nozzle internal geometries has been made for nozzle pressure ratios from 1.5 to 6.0. These nozzle and exhaust system concepts represent possible configurations for a single-engine short-takeoff and vertical-landing (STOVL) aircraft. The results of this investigation indicate the following:

1. Clamshell diverters in the duct had significantly higher losses during transition flight than a butterfly door ventral nozzle concept that included flow throttling at the geometric throat of the cruise nozzle.
2. The vertical flight (hover) performance of the ventral nozzles was improved by closing off the flow at the cruise nozzle throat rather than by blocking the main duct flow immediately downstream of the entrance to the ventral nozzle flow passage.
3. Throttling the flow through the ventral nozzle by closing the forward two flow-vectoring exit vanes instead of the aft two exit vanes resulted in higher performance.
4. Ventral nozzle plume-total-pressure decay with distance from the exit was increased significantly when the nozzle exit area was segmented.
5. Ventral nozzles with segmented exit areas had lower thrust performance than unsegmented nozzles because of a suckdown effect on the base areas between the flowing segments.

NASA Langley Research Center
Hampton, VA 23665-5225
July 8, 1991

References

1. Hamilton, D. A.; and Richardson, S. D.: V/STOL Advantages for Ground Attack. AIAA-88-4478, Sept. 1988.
2. Appleyard, George M.: Propulsion/Aerodynamic Integration in ASTOVL Combat Aircraft. *Proceedings of the International Powered Lift Conference*, P-203, Soc. of Automotive Engineers, Inc., 1988, pp. 337–348. (Available as SAE Paper 872333.)
3. Raymer, Daniel P.: The Impact of VTOL on the Conceptual Design Process. AIAA-88-4479, Sept. 1988.
4. Romine, B. M., Jr.; Meyer, B. E.; and Re, R. J.: A Static Investigation of Several STOVL Exhaust System Concepts. AIAA-89-2928, July 1989.
5. Capone, Francis J.: *Static Performance of Five Twin-Engine Nonaxisymmetric Nozzles With Vectoring and Reversing Capability.* NASA TP-1224, 1978.
6. Re, Richard J.; and Leavitt, Laurence D.: *Static Internal Performance Including Thrust Vectoring and Reversing of Two-Dimensional Convergent-Divergent Nozzles.* NASA TP-2253, 1984.
7. Mason, Mary L.; Putnam, Lawrence E.; and Re, Richard J.: *The Effect of Throat Contouring on Two-Dimensional Converging-Diverging Nozzles at Static Conditions.* NASA TP-1704, 1980.

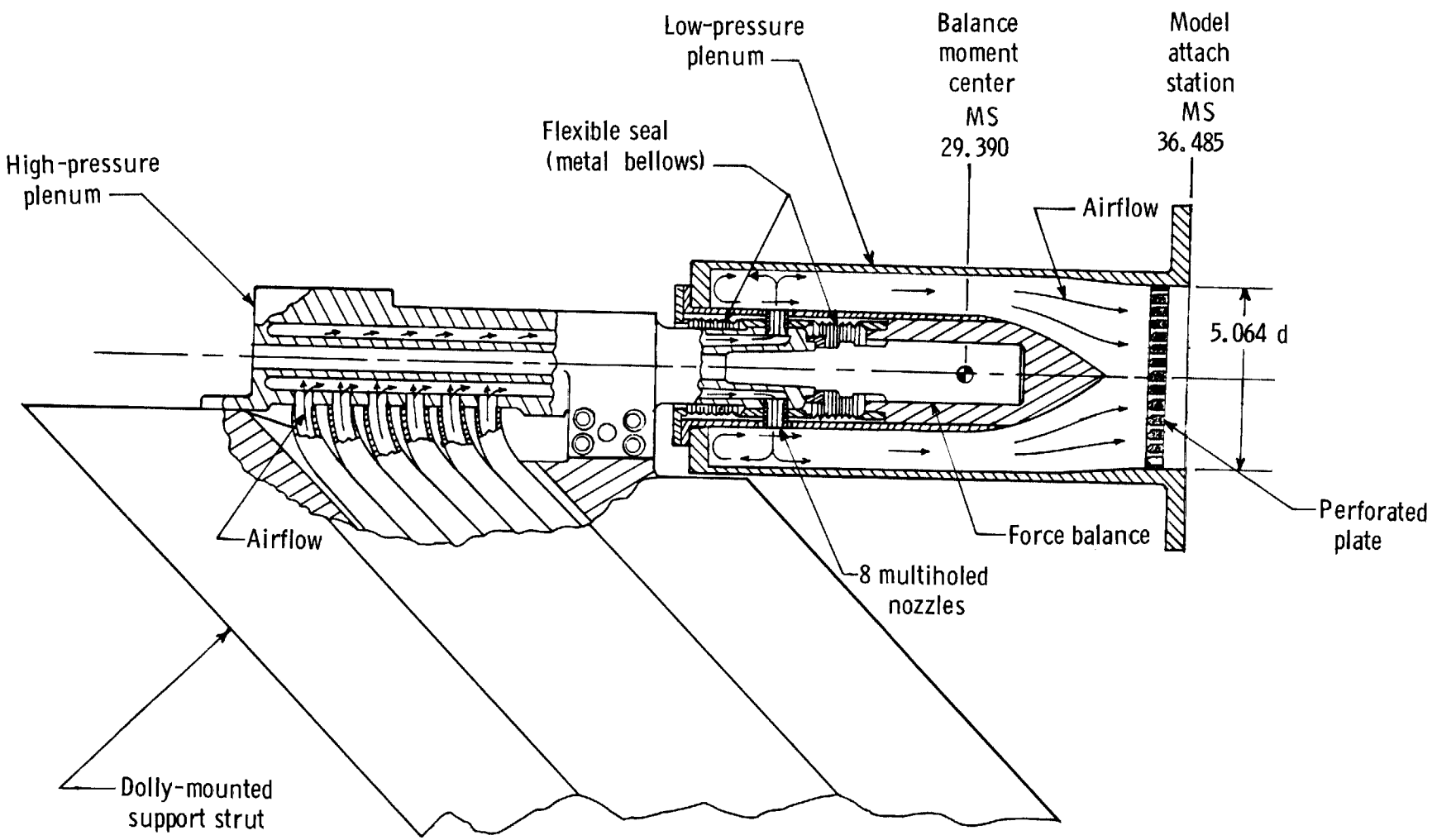

Figure 1. Schematic of propulsion simulation test pod. All dimensions are in inches.

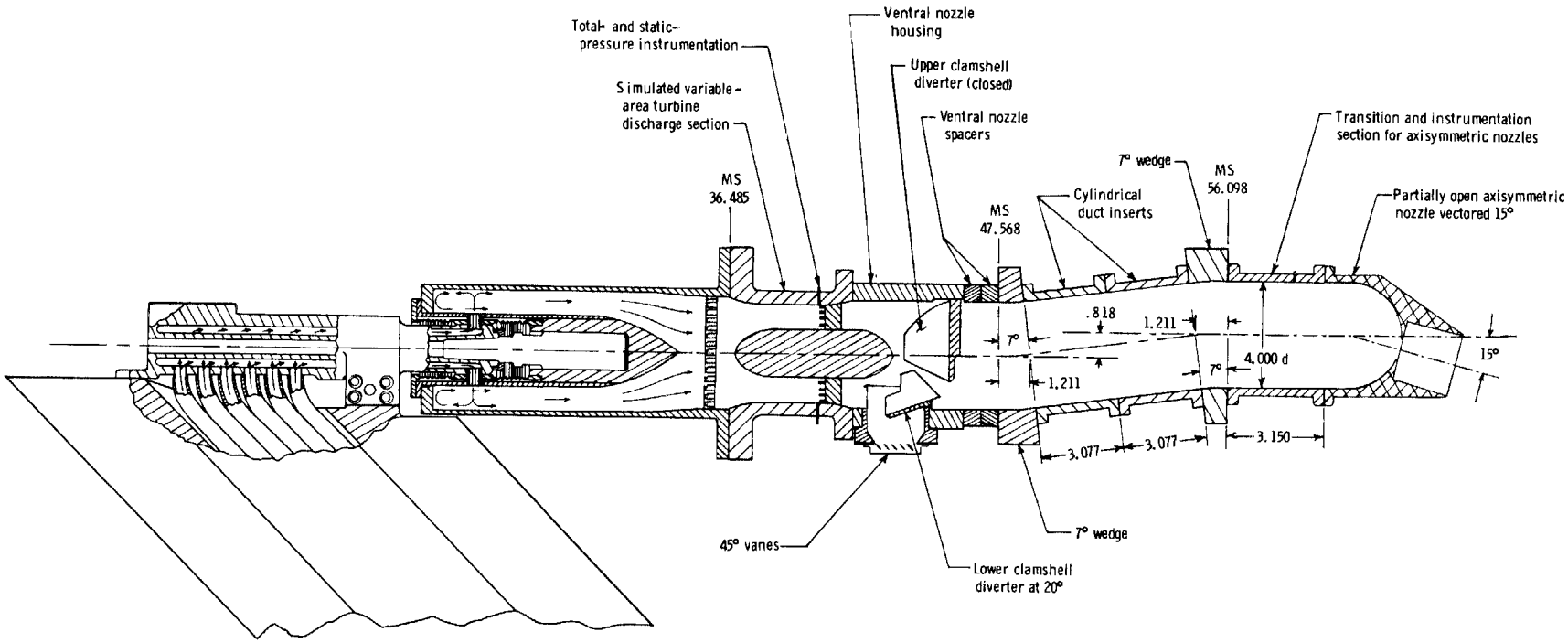

(a) Schematic of long S-shaped duct transition flight configuration with clamshell diverter ventral nozzle and axisymmetric nozzle vectored 15°.

Figure 2. Schematic drawing and photographs of transition flight configurations. All dimensions are in inches unless otherwise indicated.

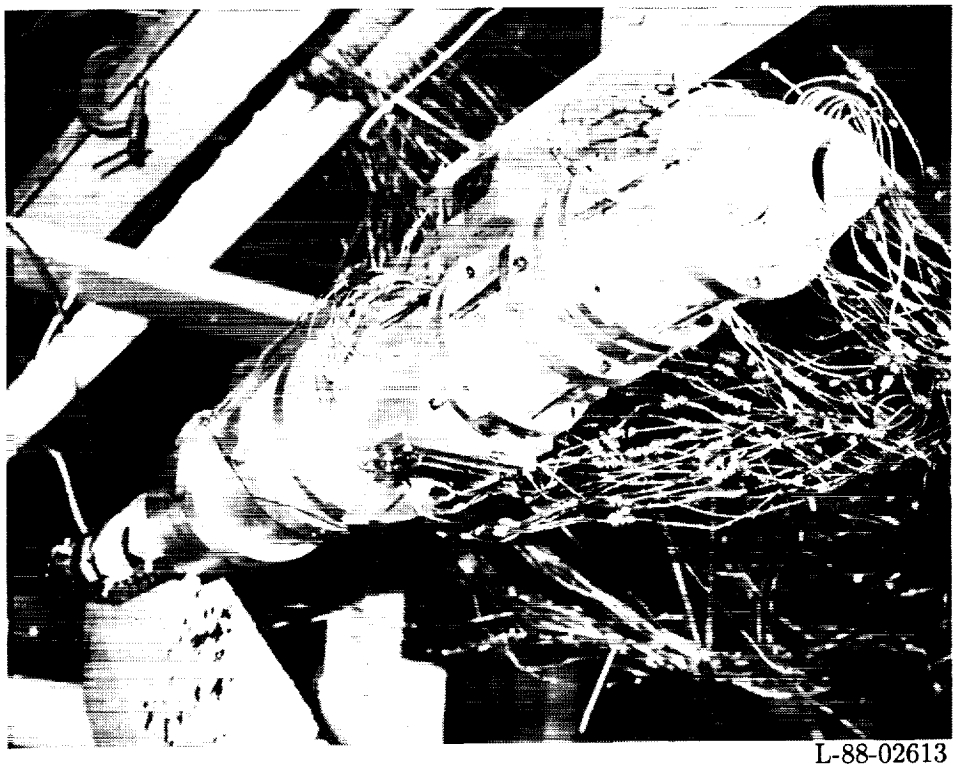

L-88-02613

(b) Photograph of long S-shaped duct transition flight configuration with clamshell diverter ventral nozzle and axisymmetric nozzle vectored 15°.

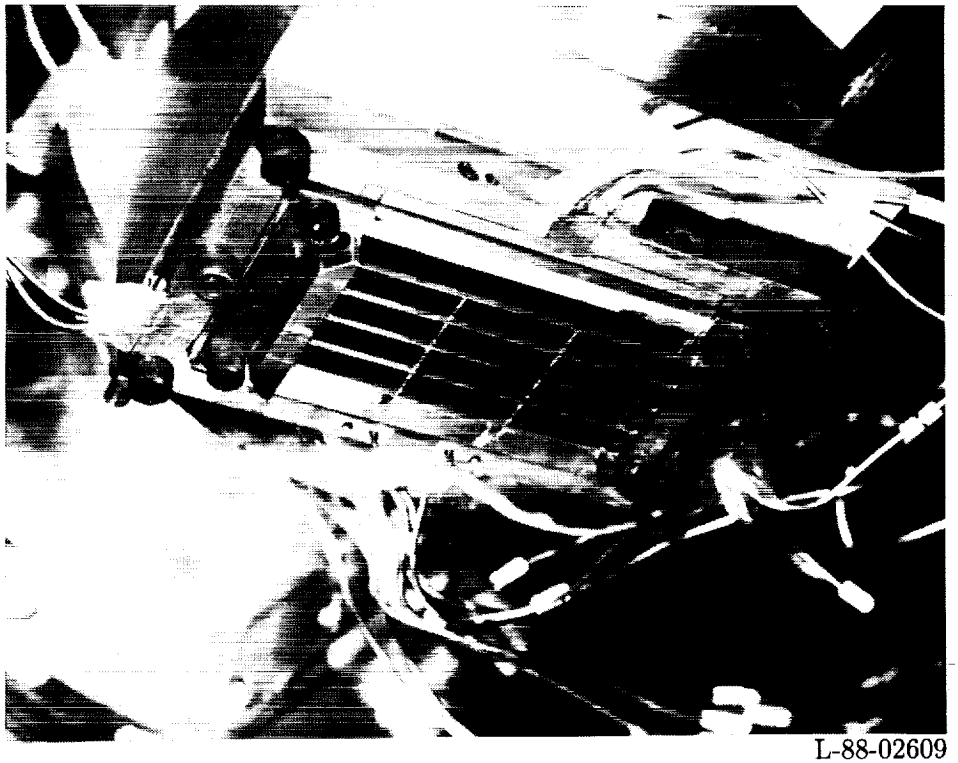

L-88-02609

(c) Ventral nozzle exit vanes at 45°.

Figure 2. Concluded.

Internal contour of variable area flow sections		
	Fan plus core flow	Core flow only
x	d	d
0.000	4.000	4.000
.100	3.910	3.673
.300	3.849	3.450
.500	3.811	3.311
.700	3.783	3.209
.900	3.762	3.133
1.100	3.746	3.075
1.300	3.734	3.032
1.500	3.726	2.993
1.700	3.722	2.986
1.900	3.720	2.980
4.006	3.720	2.980
4.290	-	2.980

Centerbody contour without extension	
x	d
0.183	0.000
.283	.566
.483	.954
.683	1.196
.883	1.372
1.083	1.504
1.283	1.606
1.483	1.680
1.683	1.730
1.883	1.760
2.083	1.770
4.040	1.770
4.240	1.751
4.440	1.692
4.640	1.588
4.840	1.431
5.040	1.200
5.240	.833
5.400	0.0

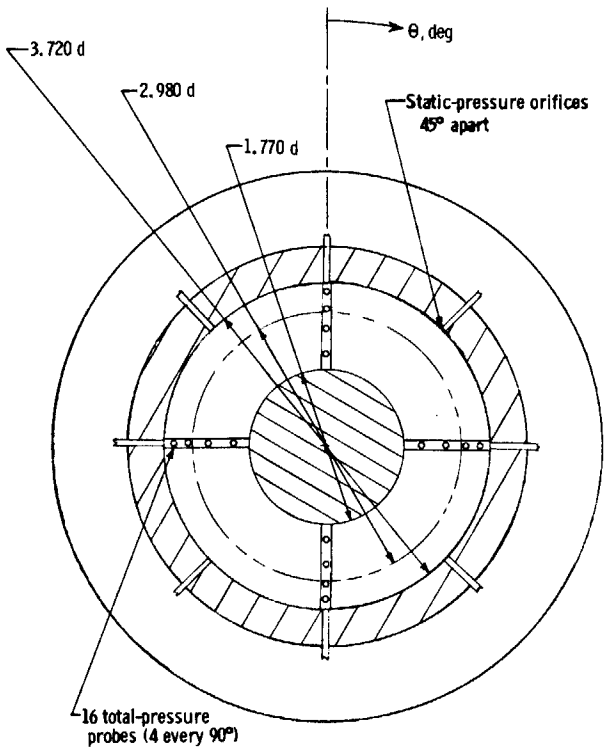

Section A - A

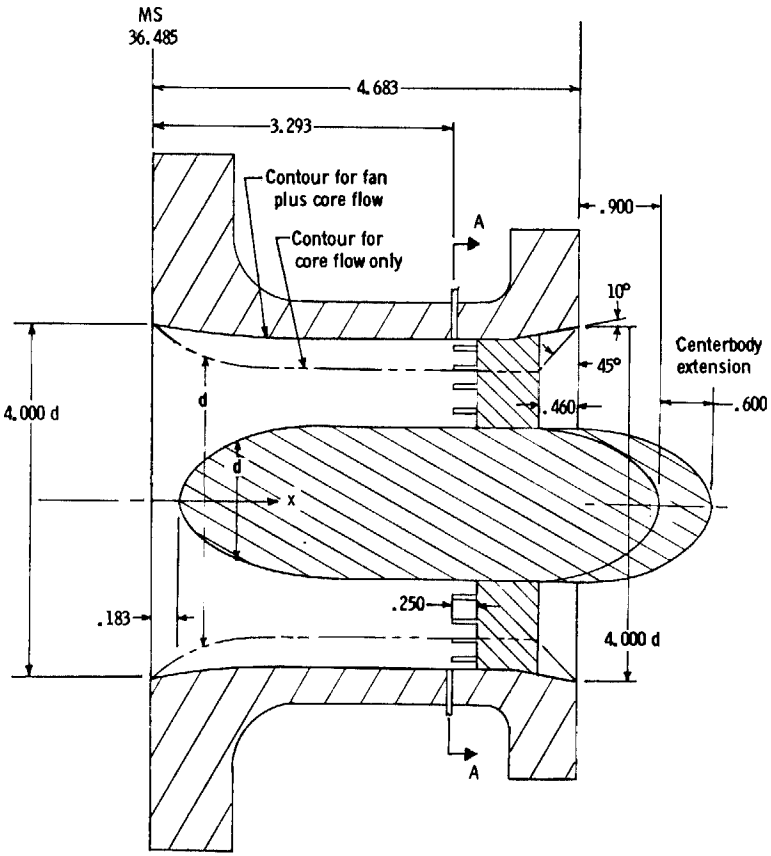

Figure 3. Two simulated turbine discharge sections and centerbody lengths. All dimensions are in inches unless otherwise indicated.

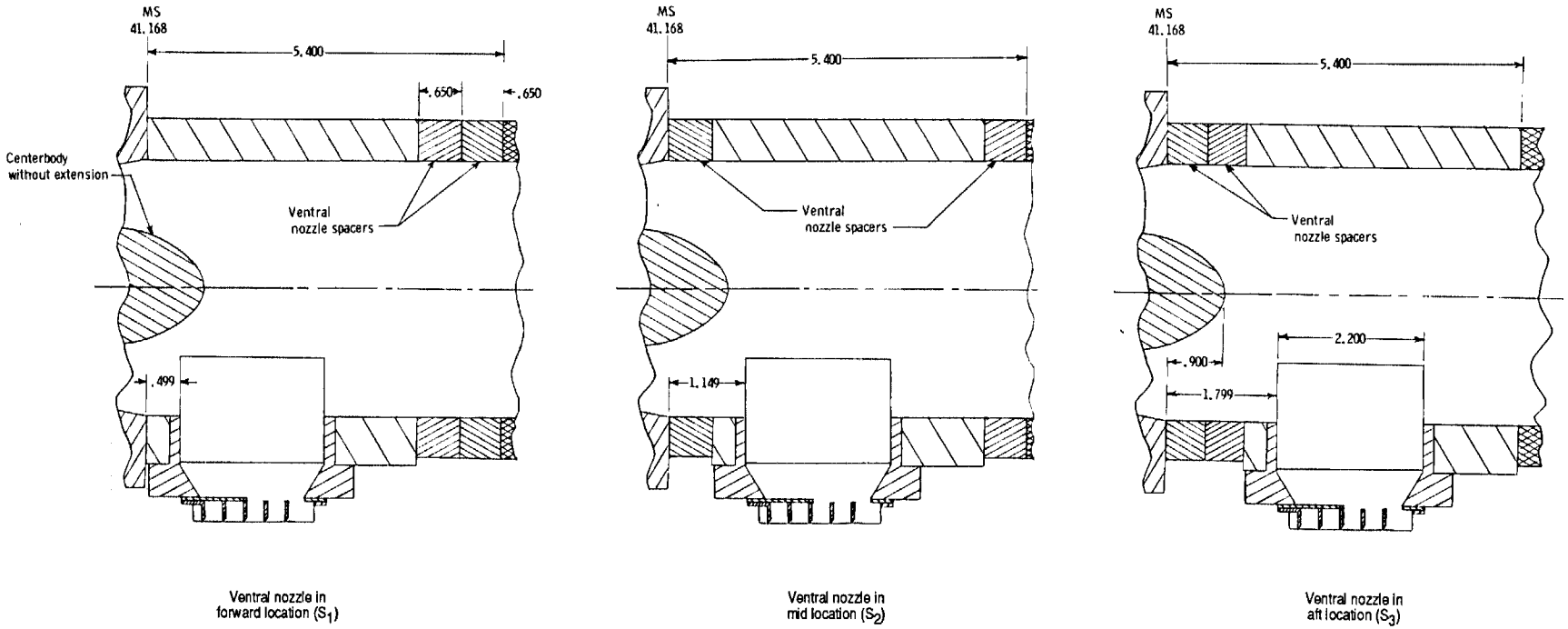

Figure 4. Butterfly door ventral nozzle in three axial locations relative to variable-area turbine discharge section. All dimensions are in inches unless otherwise indicated.

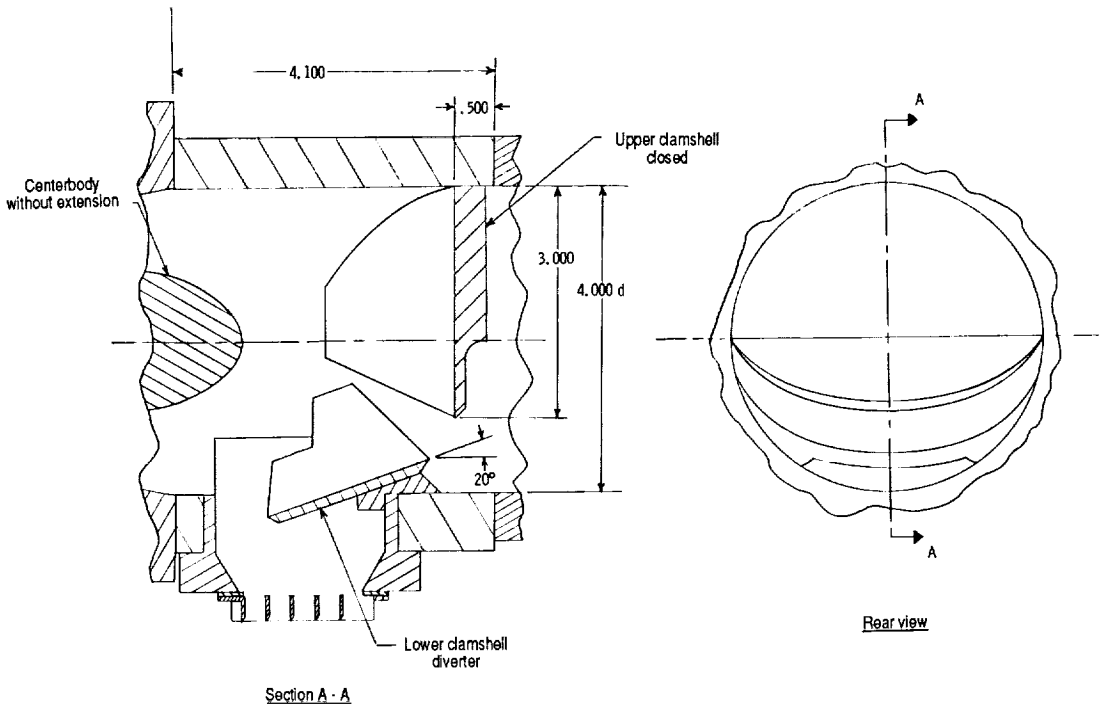

(a) Installed diverter with lower clamshell at 20° deployment.

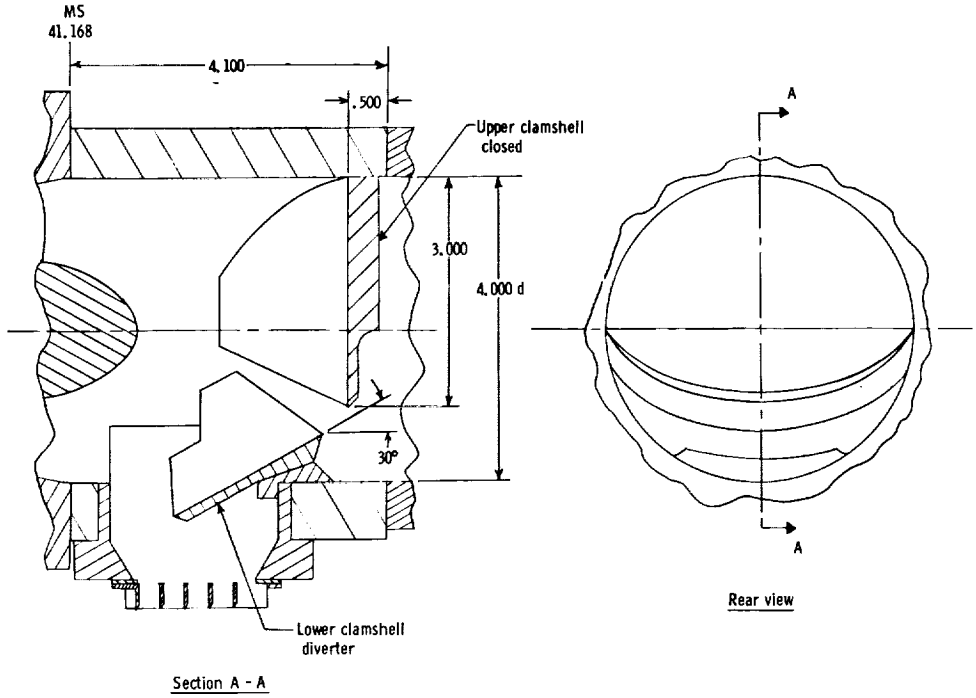

(b) Installed diverter with lower clamshell at 30° deployment.

Figure 5. Clamshell flow diverter components and installed diverter at three deployments. All dimensions are in inches unless otherwise indicated.

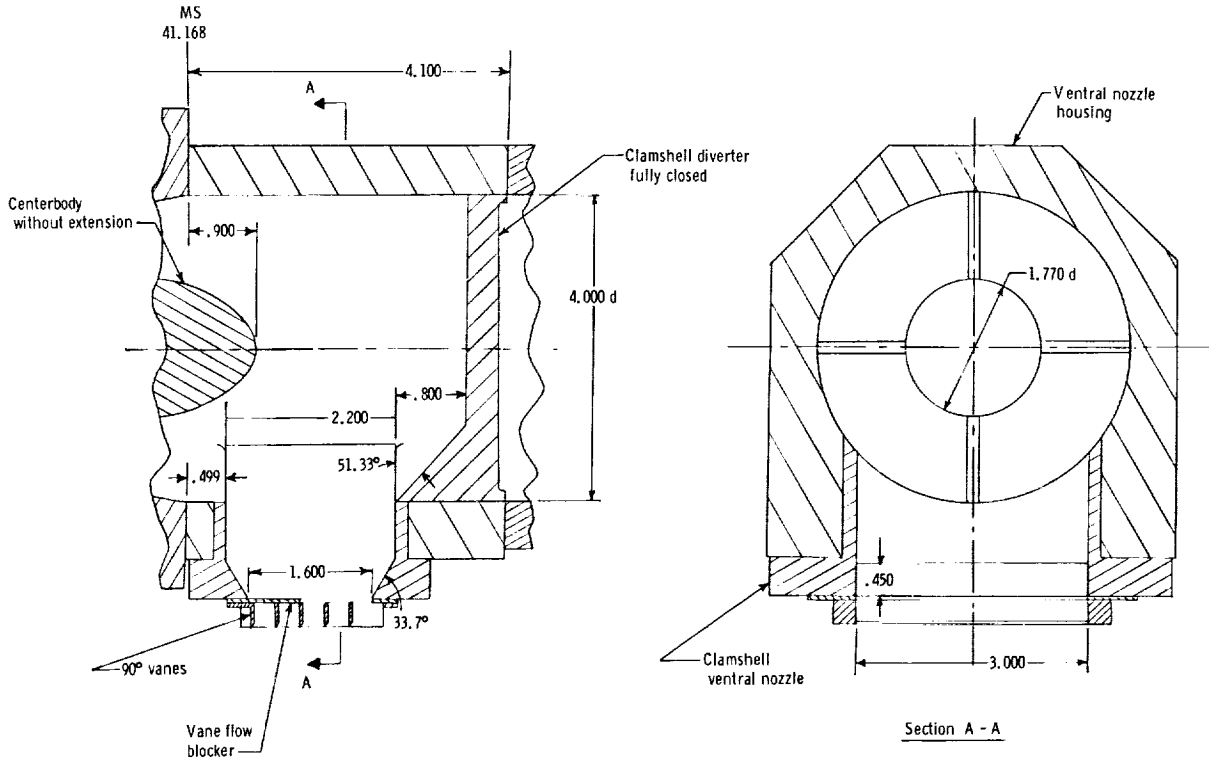

(c) Ventral nozzle with clamshell diverter fully closed.

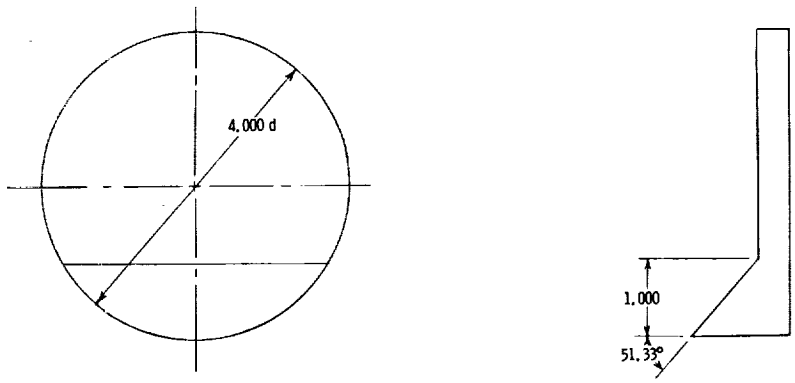

(d) Clamshell diverter for fully closed duct.

Figure 5. Continued.

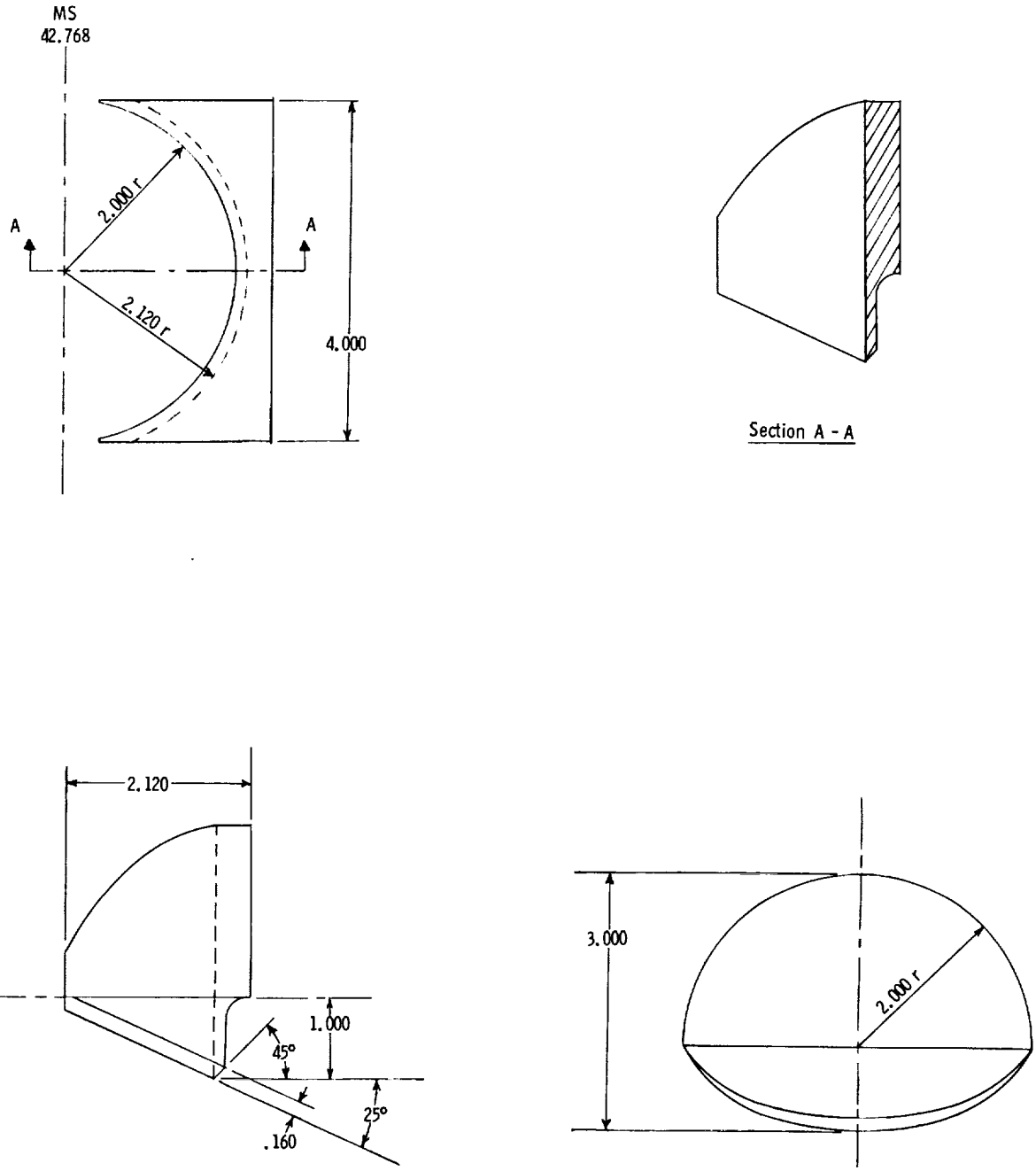

(e) Upper clamshell diverter.

Figure 5. Continued.

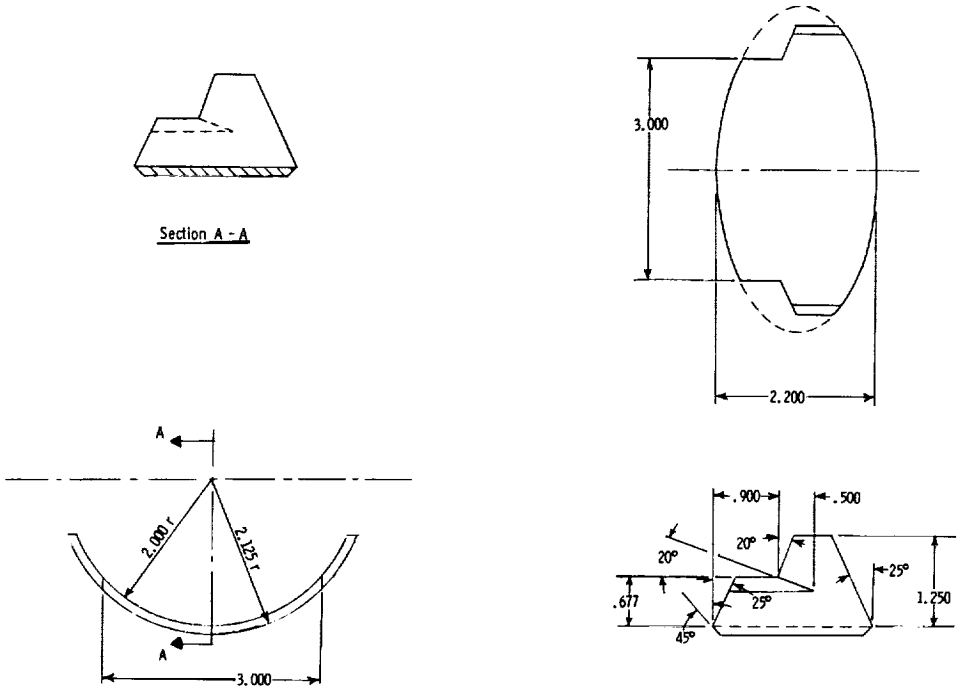

(f) 20° lower clamshell diverter.

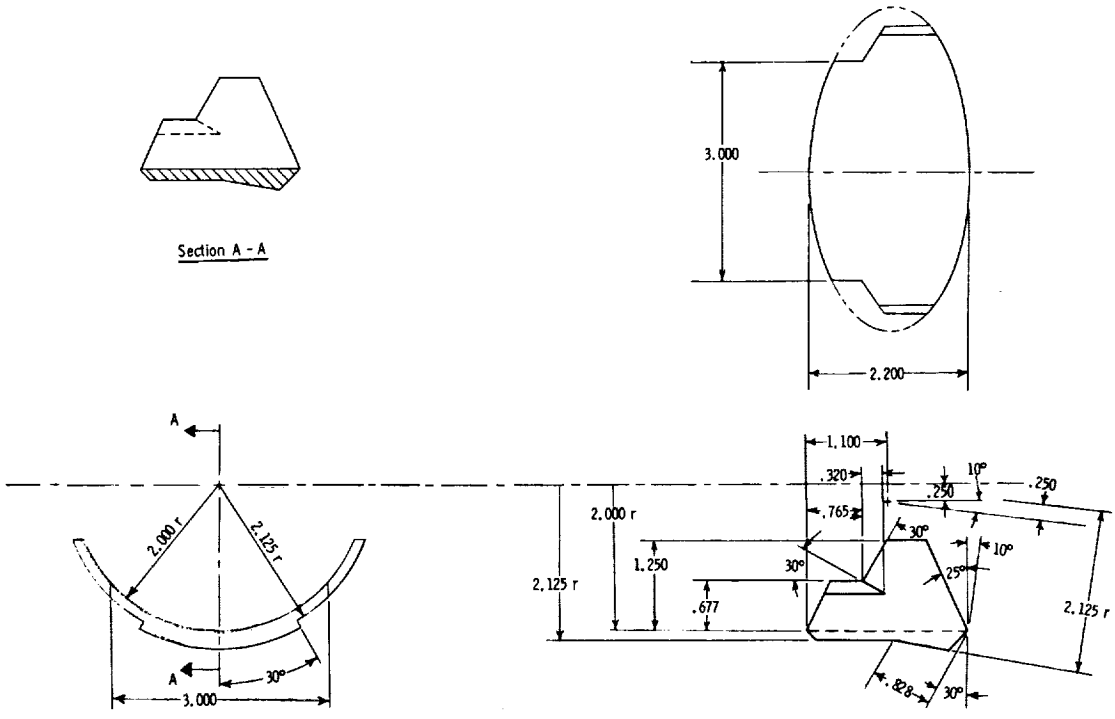

(g) 30° lower clamshell diverter.

Figure 5. Concluded.

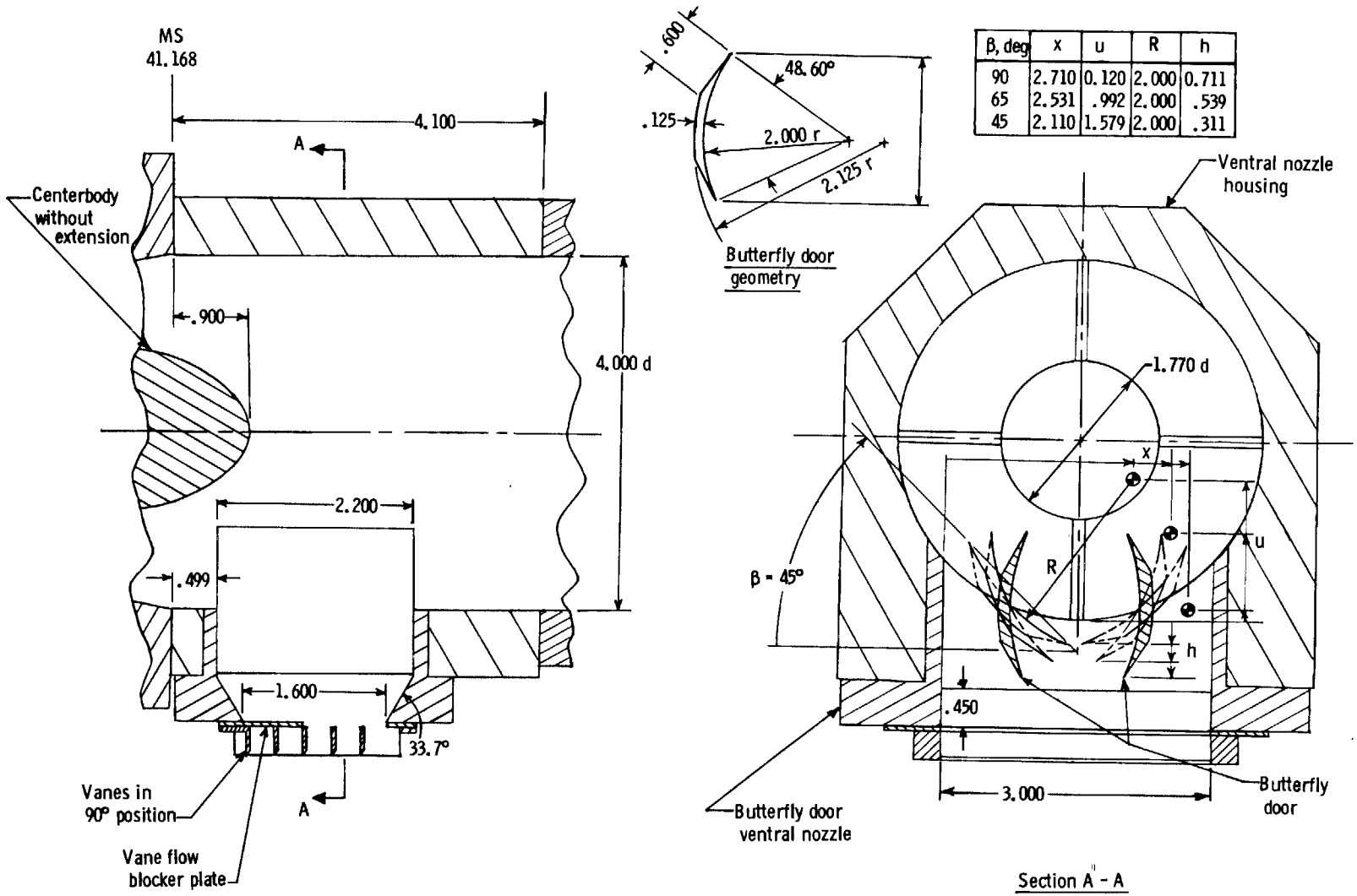

Figure 6. Butterfly door ventral nozzle and butterfly doors. All dimensions are in inches unless otherwise indicated.

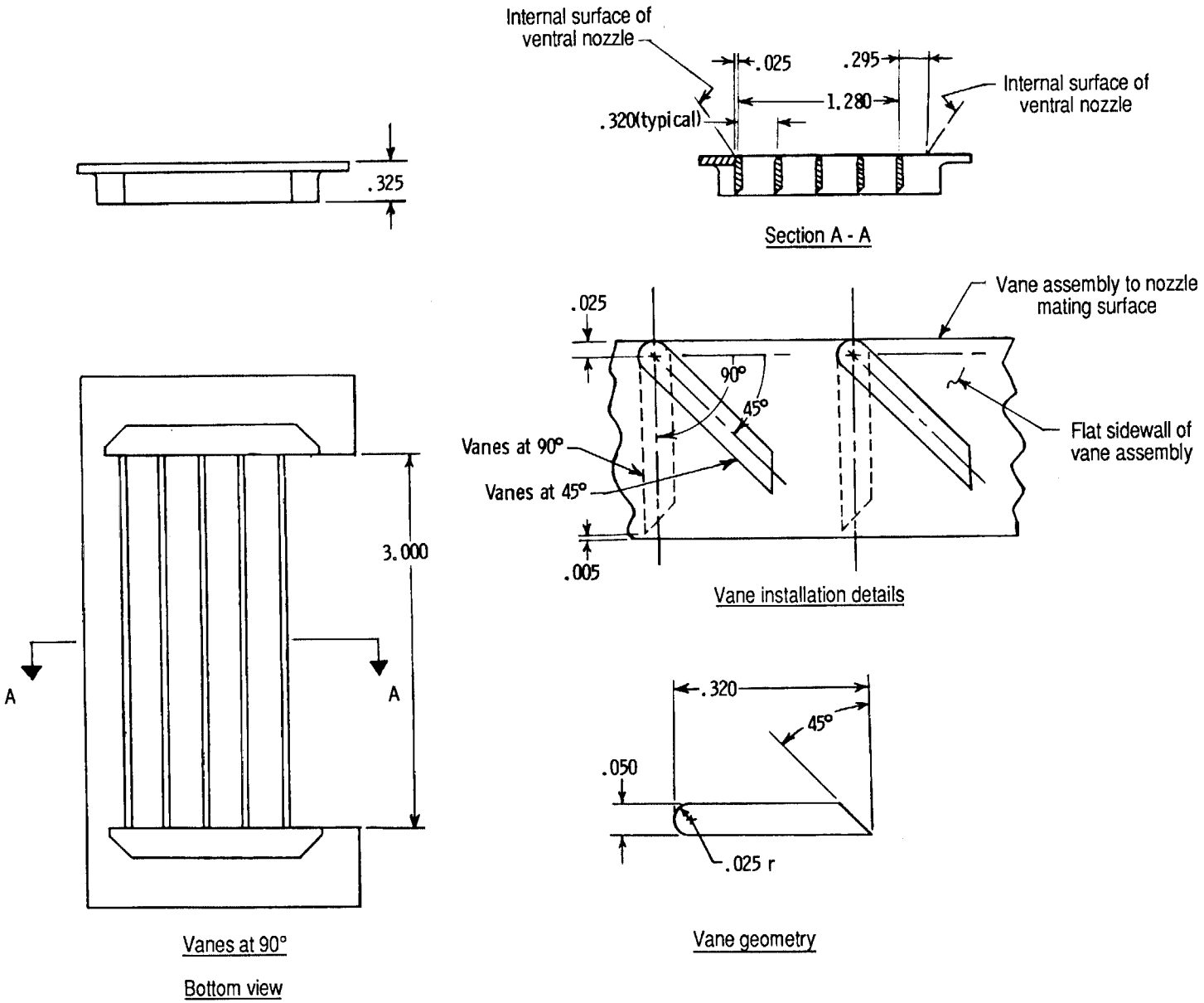

Figure 7. Ventral nozzle exit vane geometry and assembly details. All dimensions are in inches unless otherwise indicated.

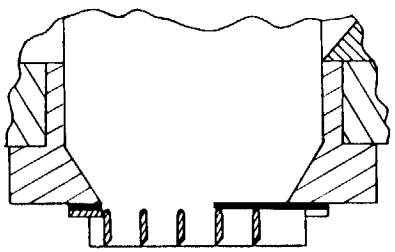

Blocker B_1
Aft two openings blocked

$A_V = 2.43$ in.^{2}

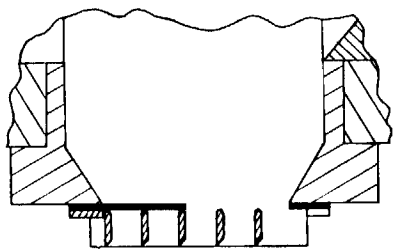

Blocker B_2
Forward two openings blocked

$A_V = 2.43$ in.^{2}

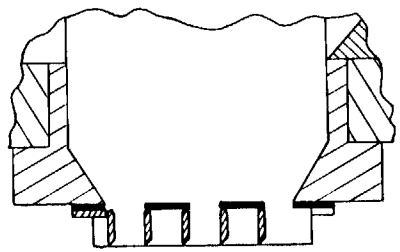

Blocker B_3
Alternate openings blocked

$A_V = 2.43$ in.^{2}

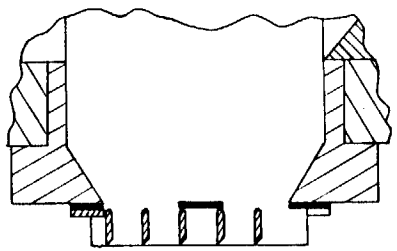

Blocker B_4
Center opening blocked

$A_V = 3.24$ in.^{2}

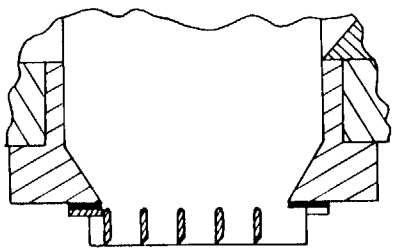

Blocker B_0
All open

$A_V = 4.05$ in.^{2}

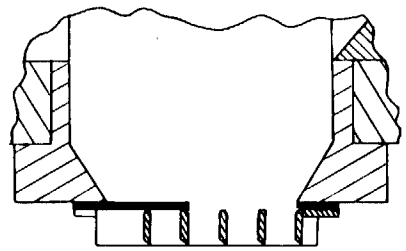

Blocker B_2
Forward two openings blocked
(exit vane assembly reversed)

$A_V = 2.43$ in.^{2}

Figure 8. Side sections of clamshell diverter ventral nozzle with 90° nozzle exit vanes and six-vane blocker configurations.

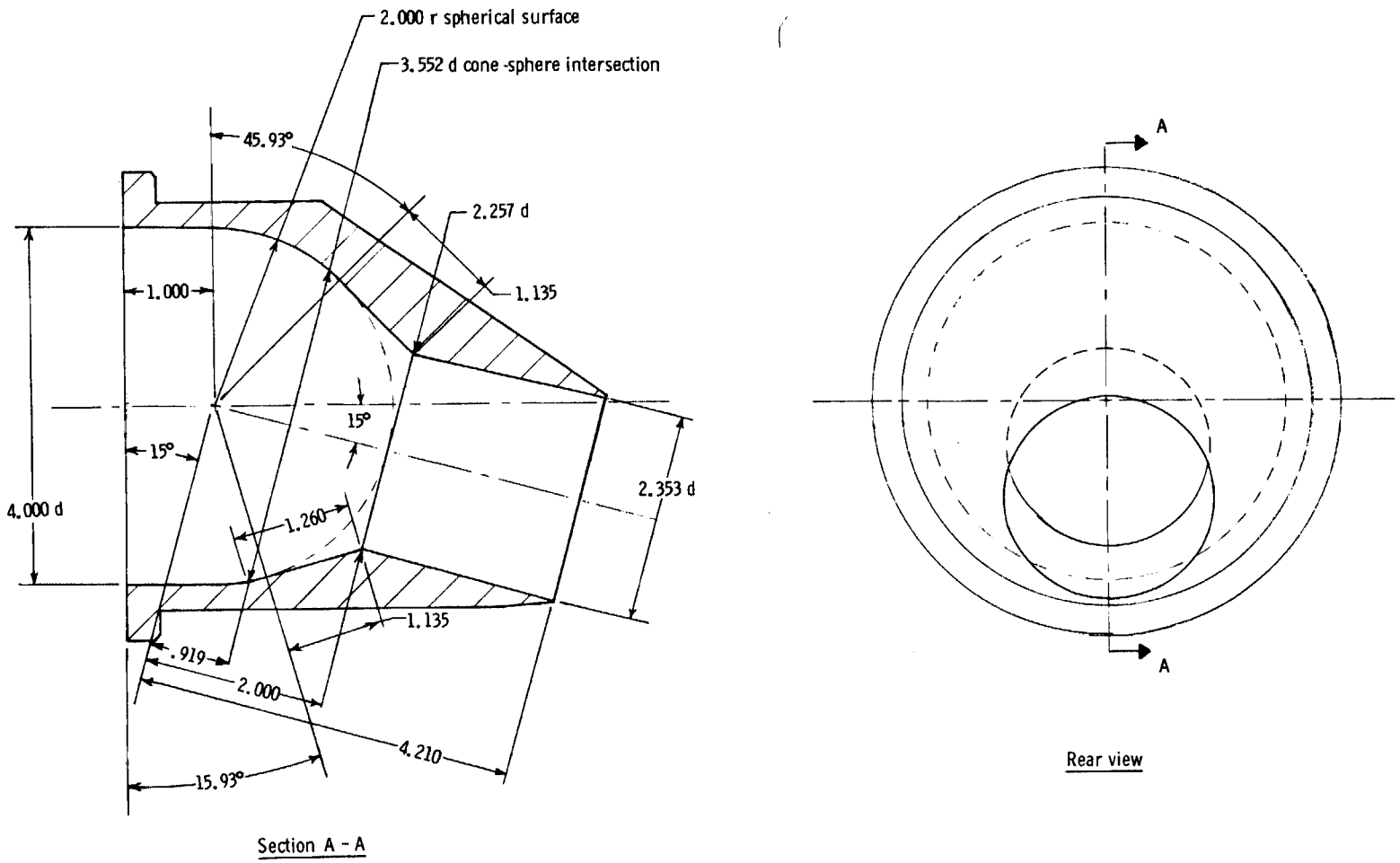

(a) Fully open axisymmetric nozzle vectored 15°; $A_n = 4.00$ in^2.

Figure 9. Axisymmetric rear nozzles. All dimensions are in inches unless otherwise indicated.

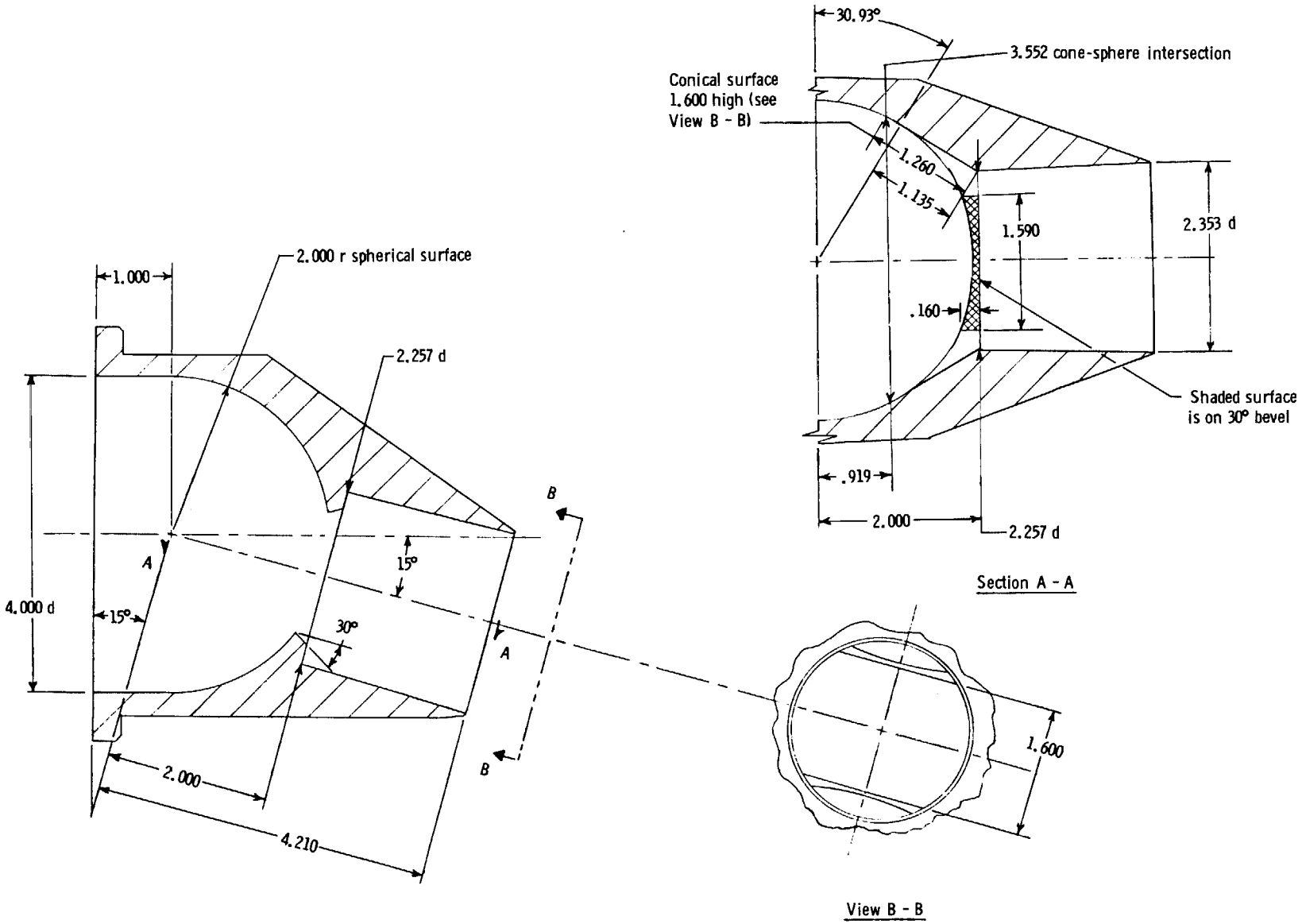

(b) Partially open axisymmetric nozzle vectored 15°; $A_n = 3.28$ in^2.

Figure 9. Continued.

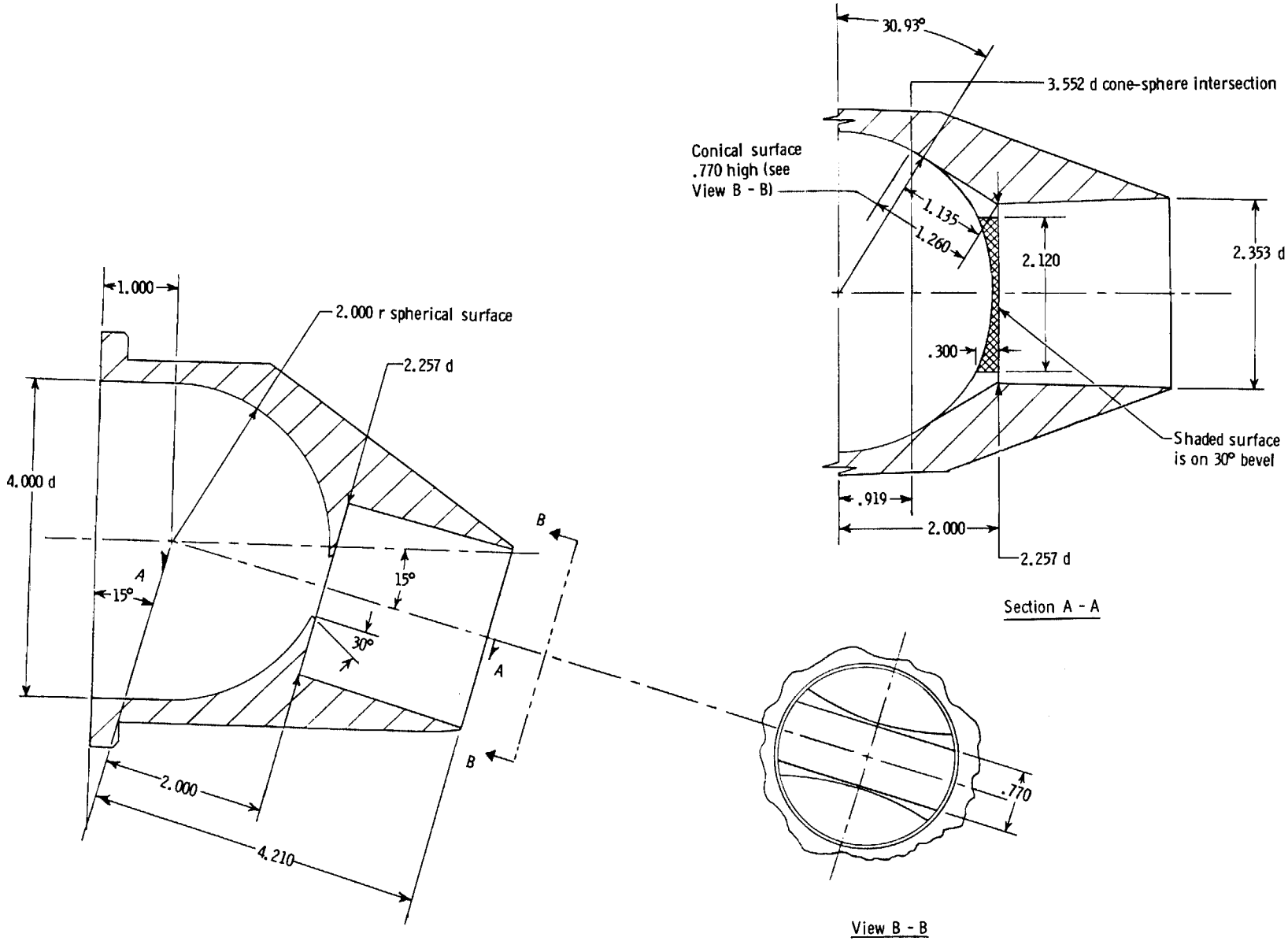

(c) Partially open axisymmetric nozzle vectored 15°; $A_n = 1.71$ in^2.

Figure 9. Concluded.

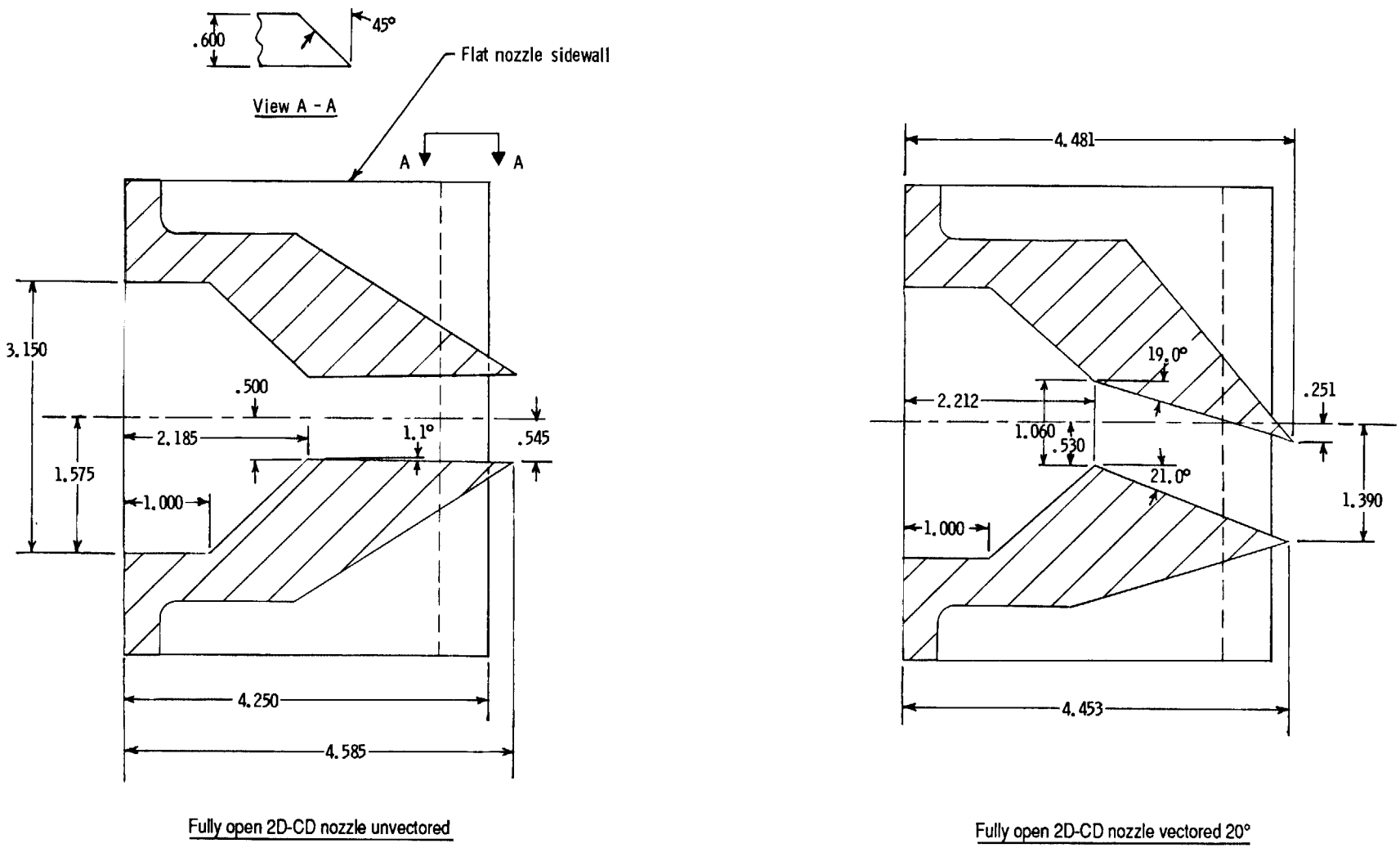

(a) Fully open 2D-CD nozzles unvectored and vectored 20°; $A_n = 4.00$ in^2.

Figure 10. Two-dimensional convergent-divergent rear nozzles. All dimensions are in inches unless otherwise indicated.

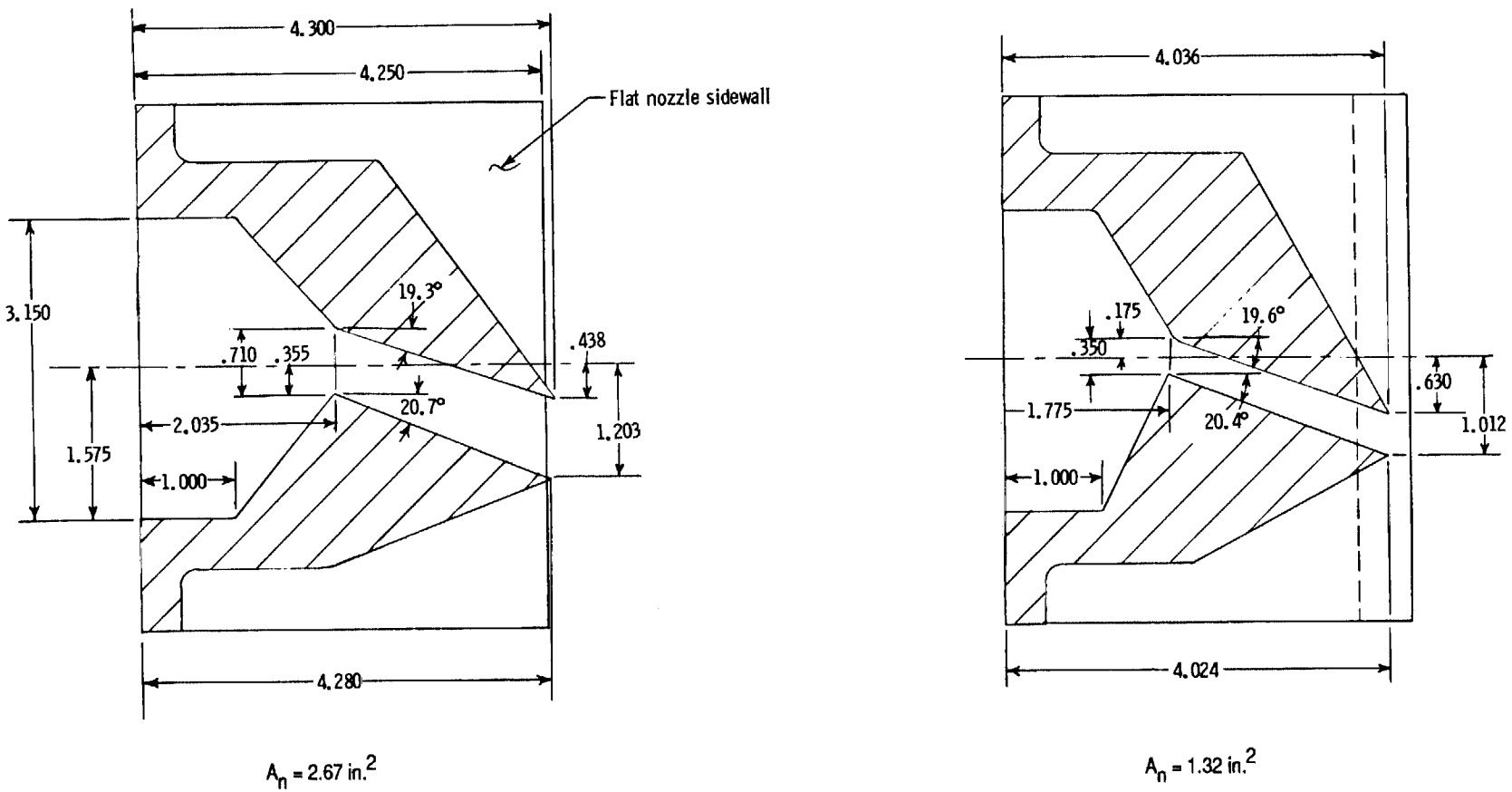

(b) Partially open 2D-CD nozzles vectored 20°.

Figure 10. Concluded.

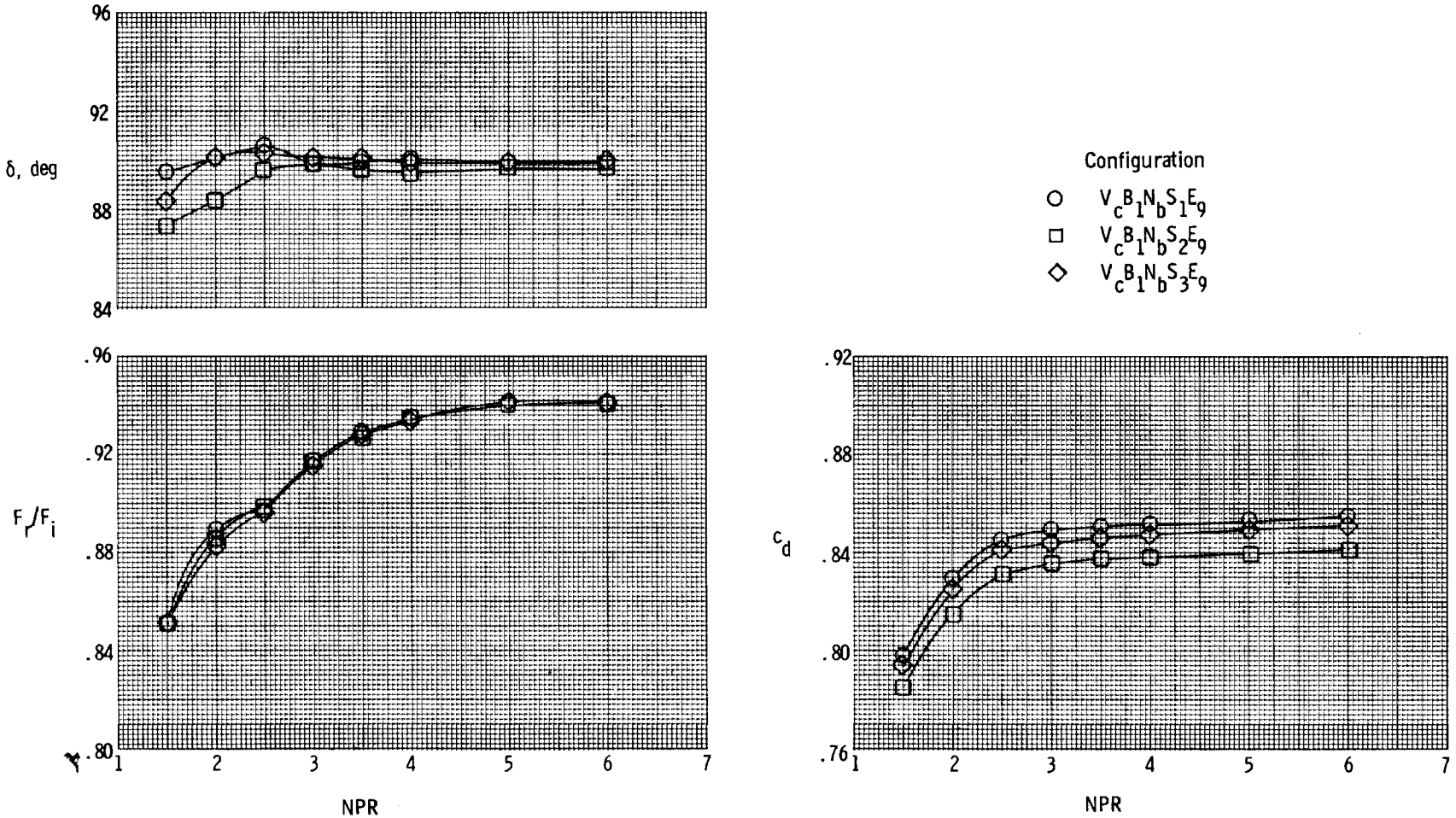

(a) Resultant-thrust-vector angle, resultant-thrust ratio, and discharge coefficient.

Figure 11. Effect of ventral nozzle axial location relative to variable-area turbine section on internal performance characteristics in hover with ventral nozzle butterfly doors at 90° and exit vanes at 90°.

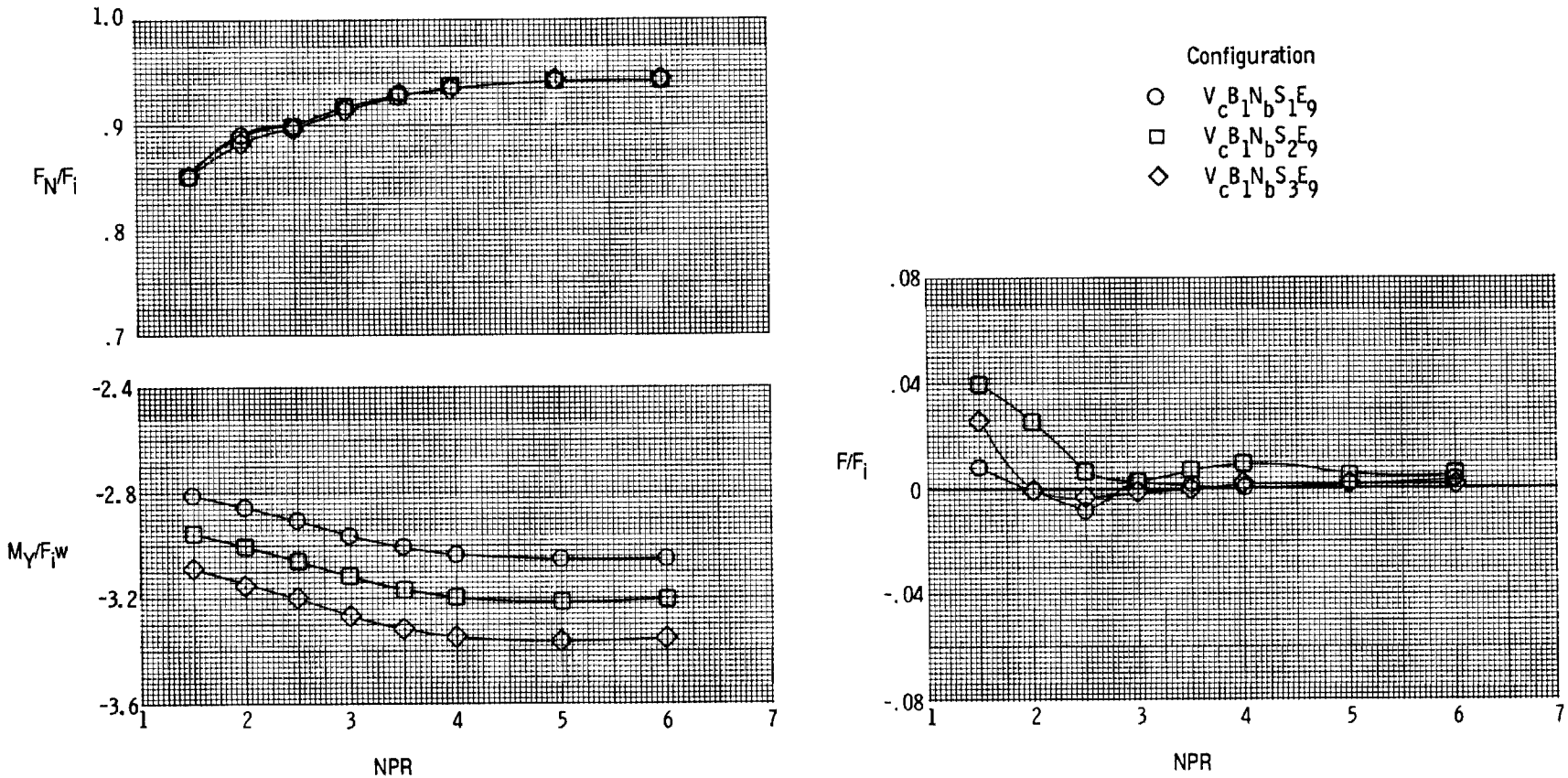

(b) Normal-force ratio, pitching-moment ratio, and thrust ratio.

Figure 11. Concluded.

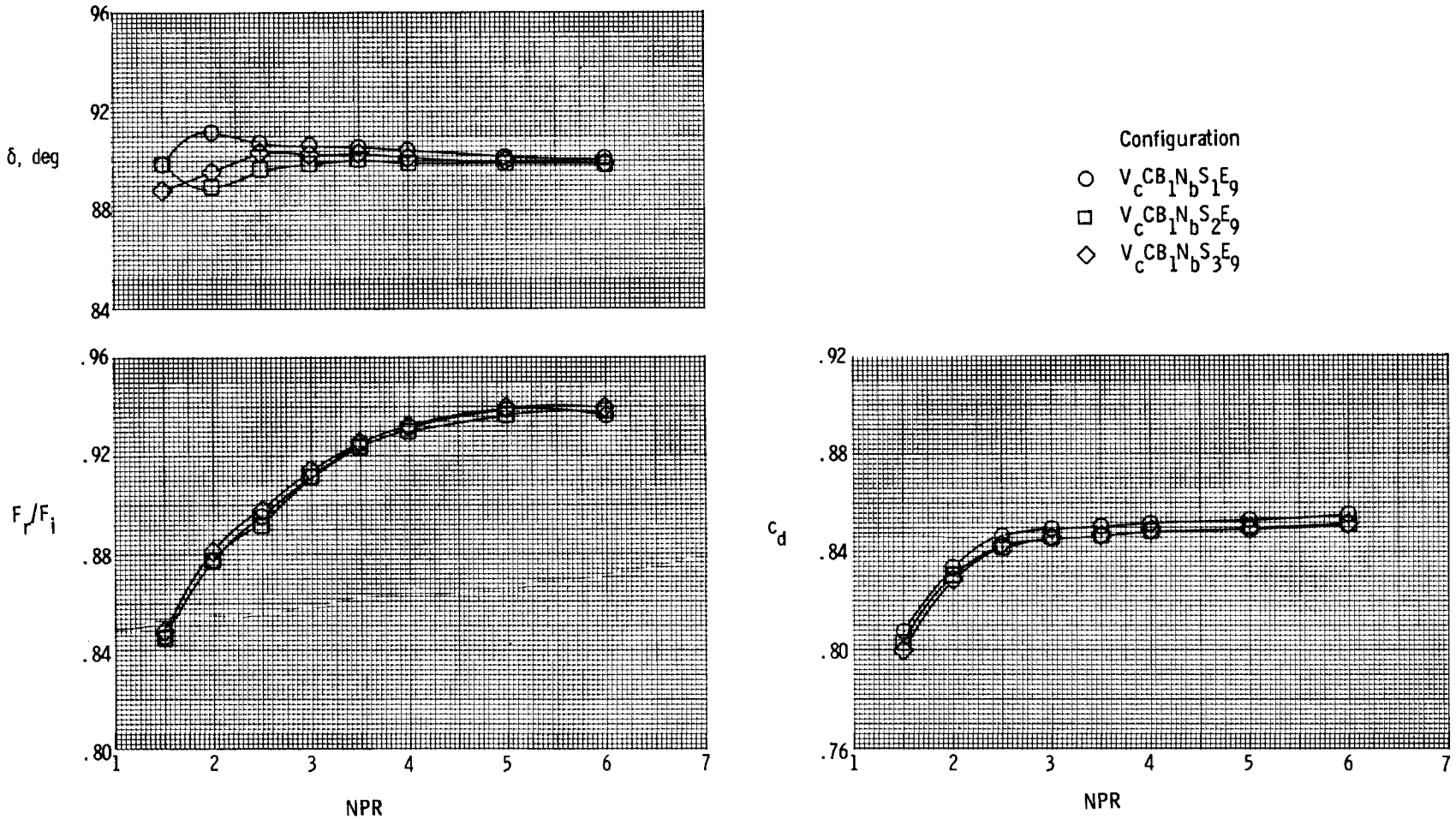

(a) Resultant-thrust-vector angle, resultant-thrust ratio, and discharge coefficient.

Figure 12. Effect of ventral nozzle axial location relative to variable-area turbine section with centerbody extended on internal performance characteristics in hover with ventral nozzle butterfly doors at 90° and exit vanes at 90°.

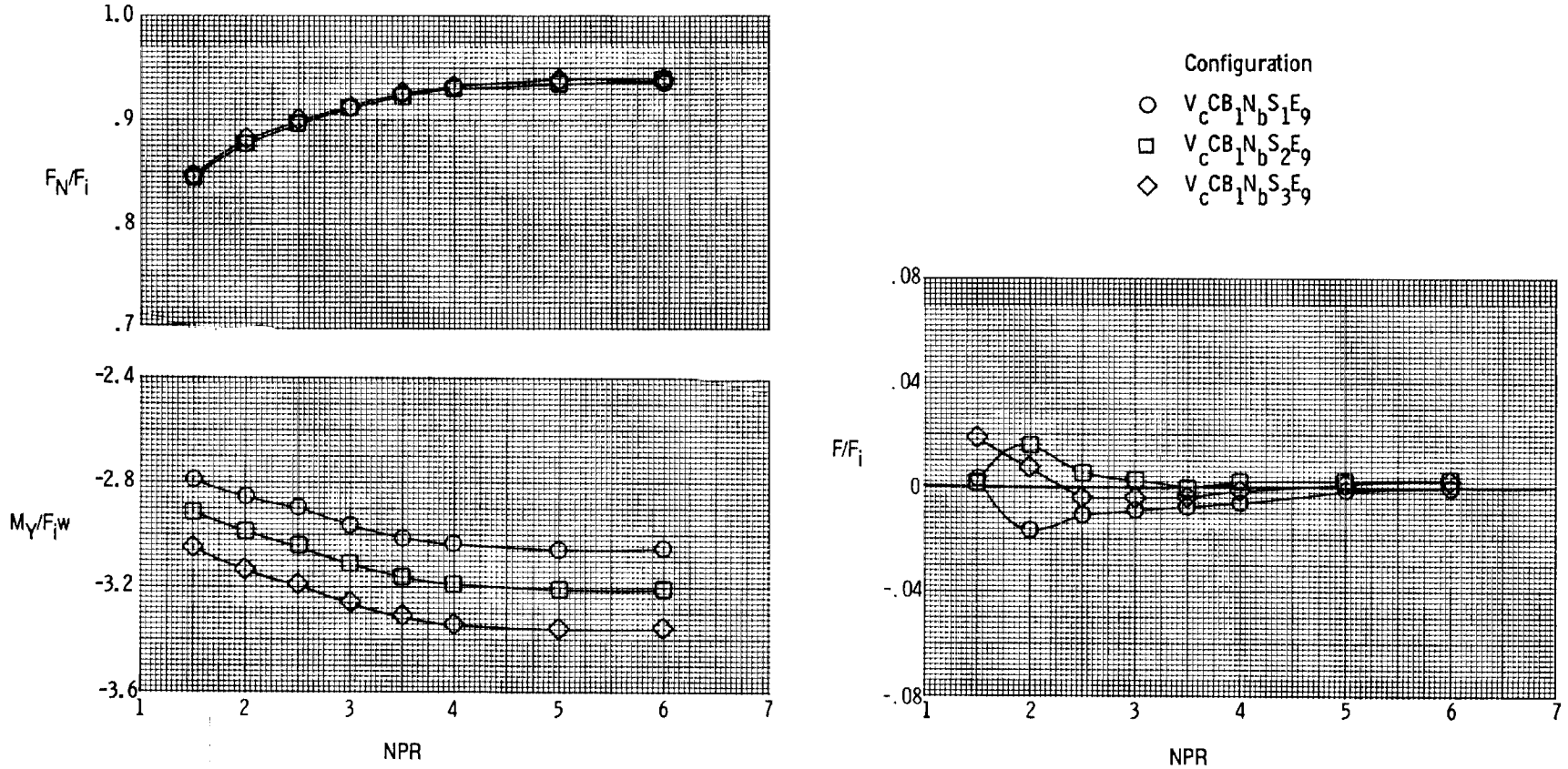

(b) Normal-force ratio, pitching-moment ratio, and thrust ratio.

Figure 12. Concluded.

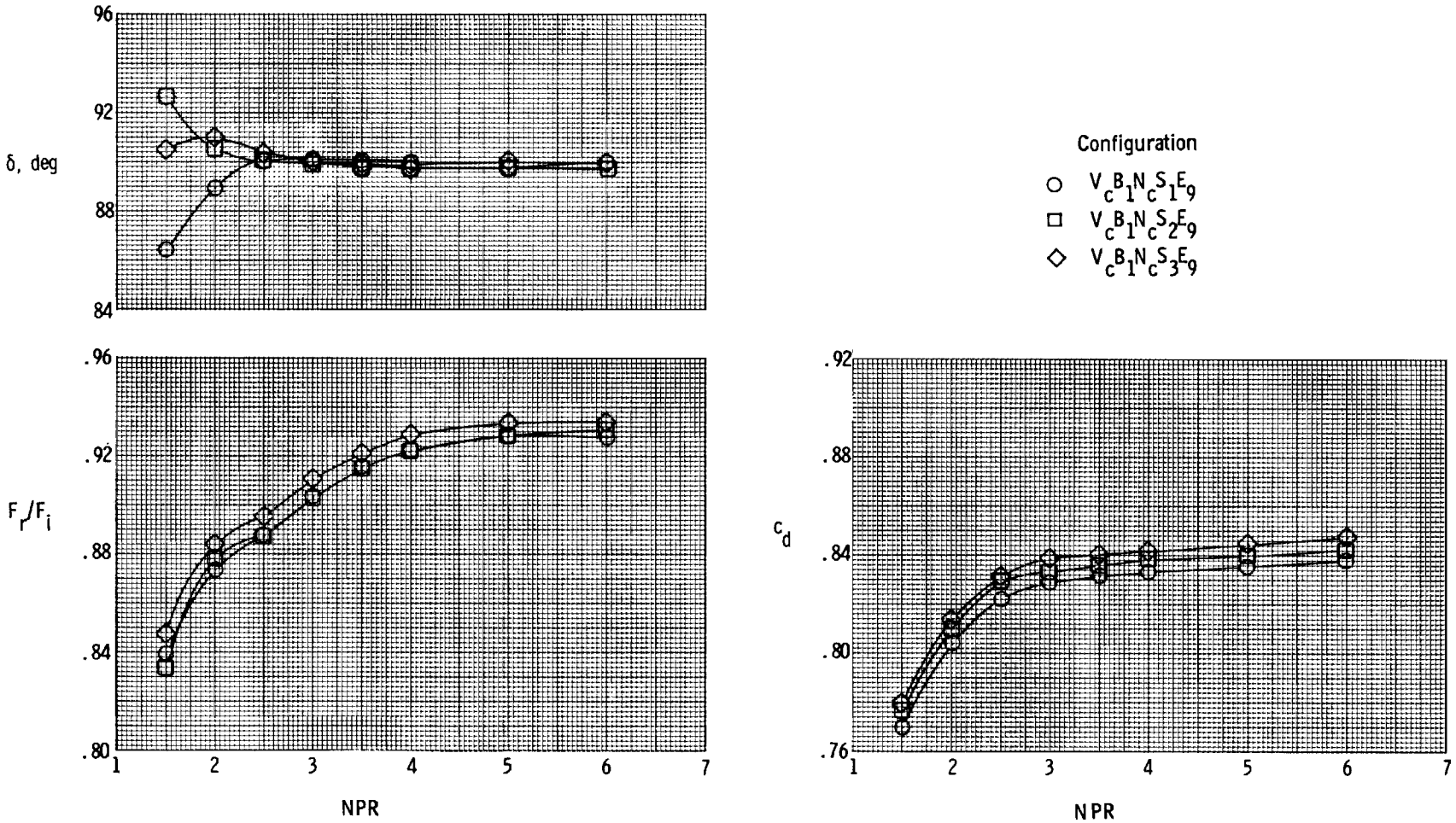

(a) Resultant-thrust-vector angle, resultant-thrust ratio, and discharge coefficient.

Figure 13. Effect of ventral nozzle axial location relative to variable-area turbine section on internal performance characteristics in hover with clamshell diverters closed and exit vanes at 90°.

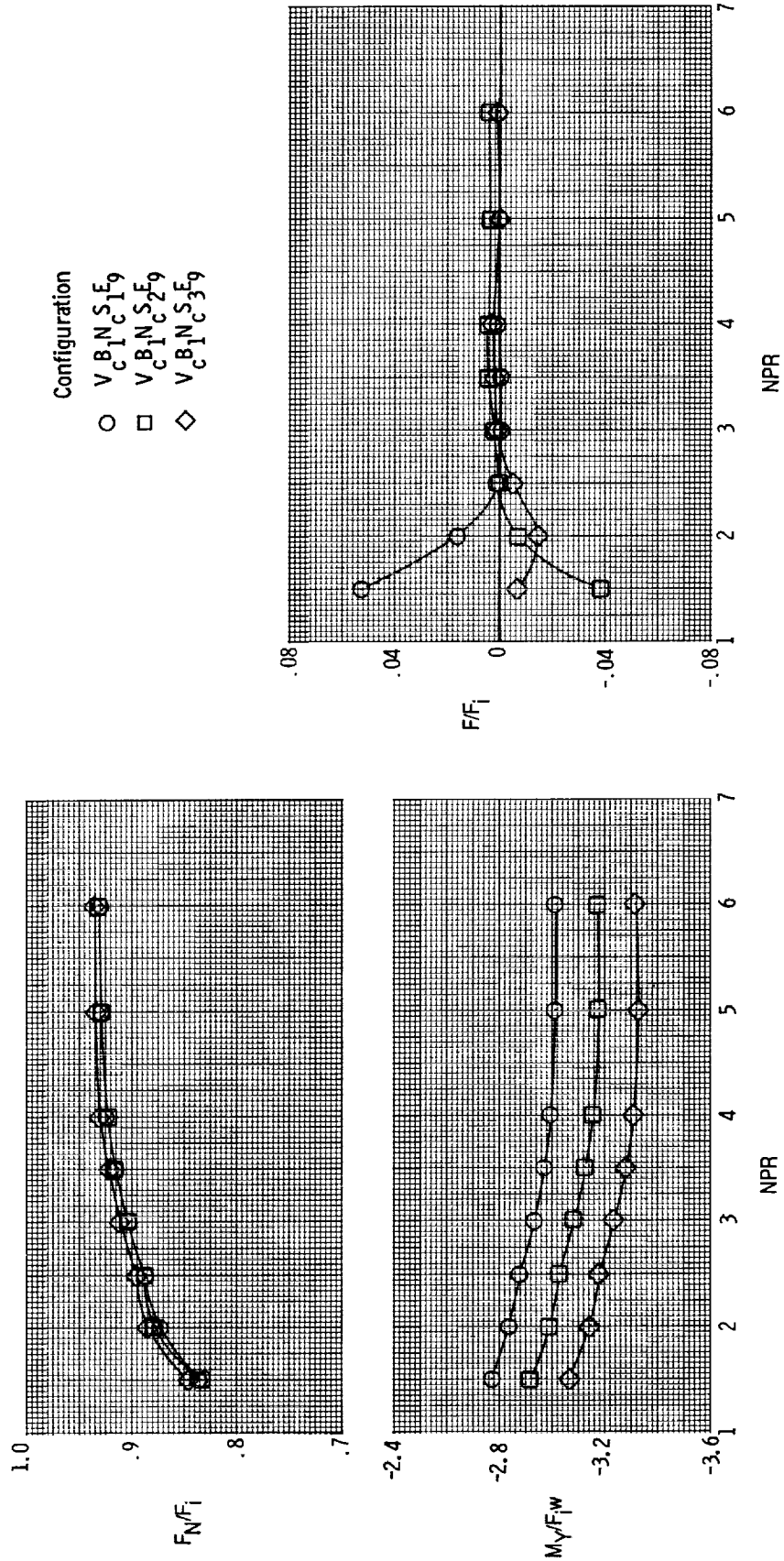

(b) Normal-force ratio, pitching-moment ratio, and thrust ratio.

Figure 13. Concluded.

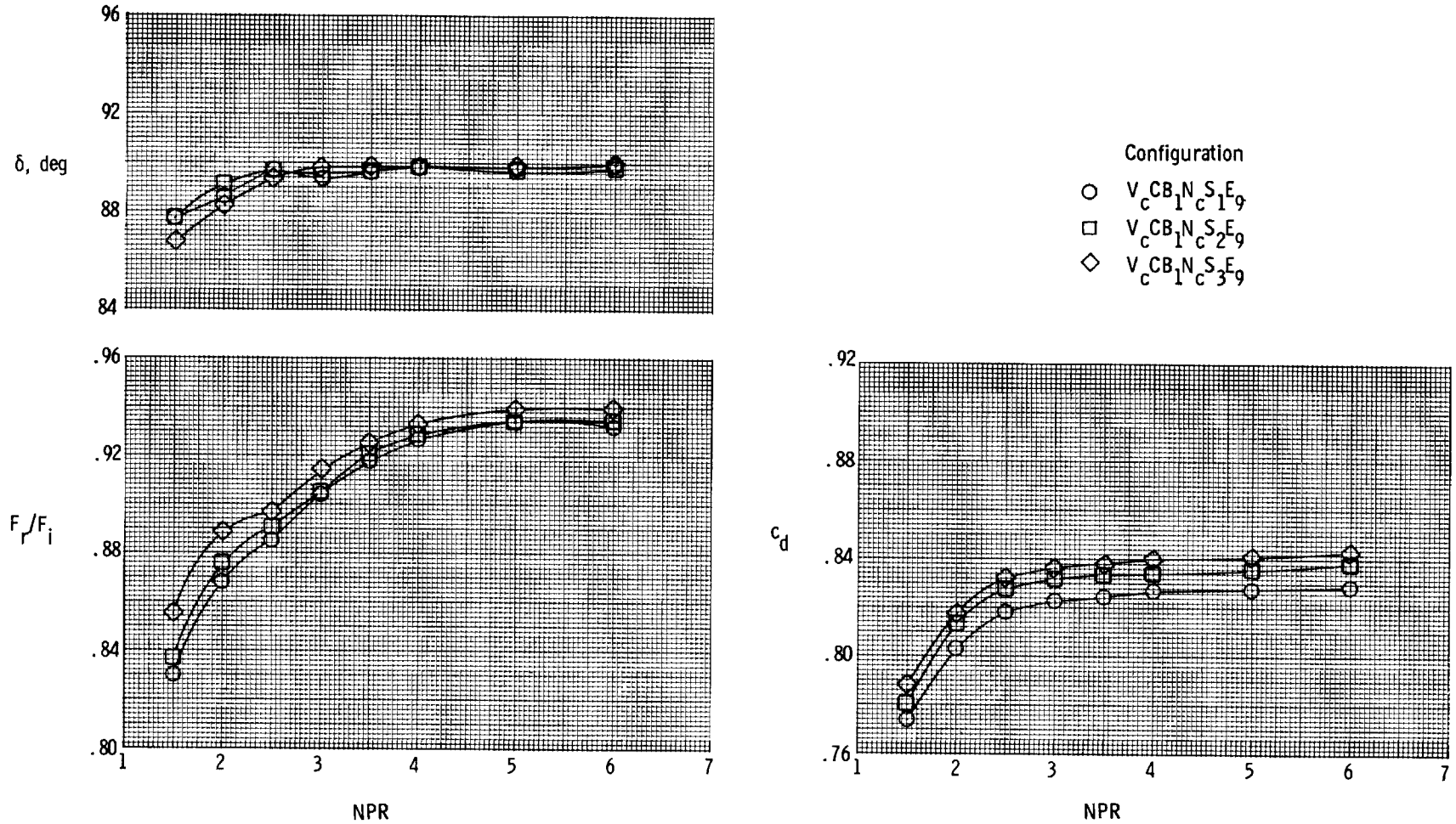

(a) Resultant-thrust-vector angle, resultant-thrust ratio, and discharge coefficient.

Figure 14. Effect of ventral nozzle axial location relative to variable-area turbine section with centerbody extended on internal performance characteristics in hover with clamshell diverters closed and exit vanes at 90°.

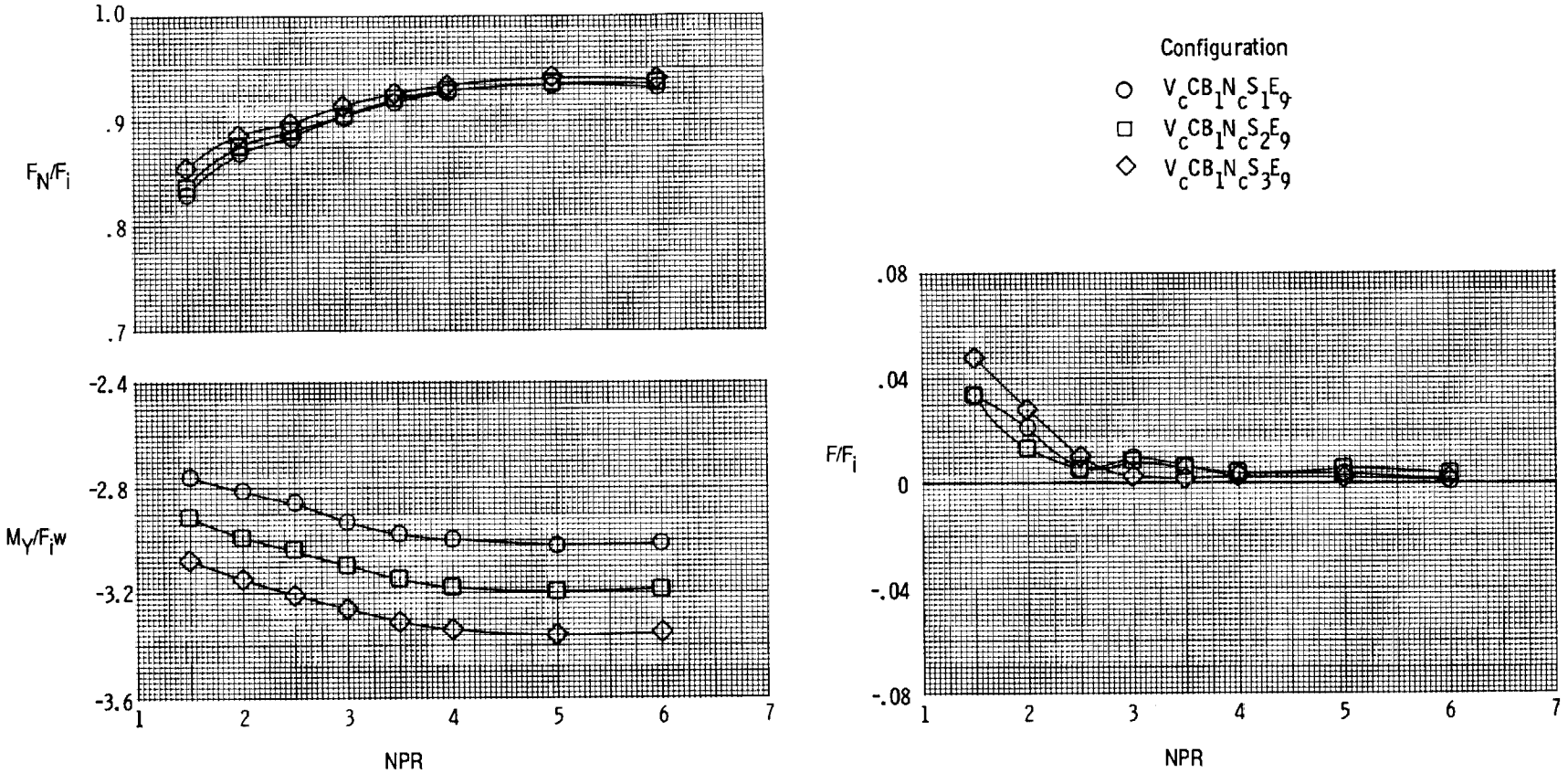

(b) Normal-force ratio, pitching-moment ratio, and thrust ratio.

Figure 14. Concluded.

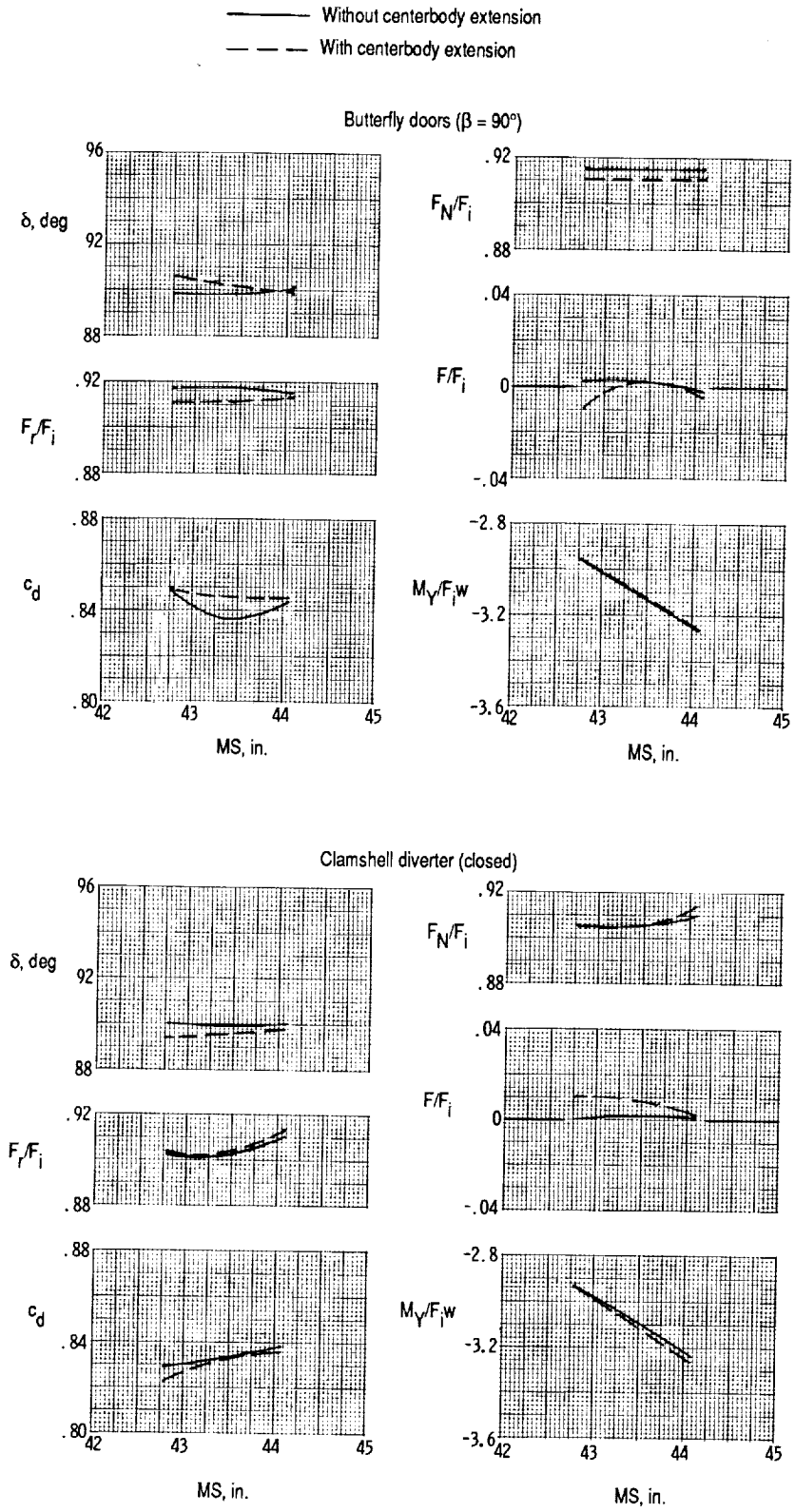

Figure 15. Effect of ventral nozzle location with and without variable-area turbine section centerbody extension on ventral nozzle internal performance for butterfly door and clamshell diverter configurations at NPR = 3.0.

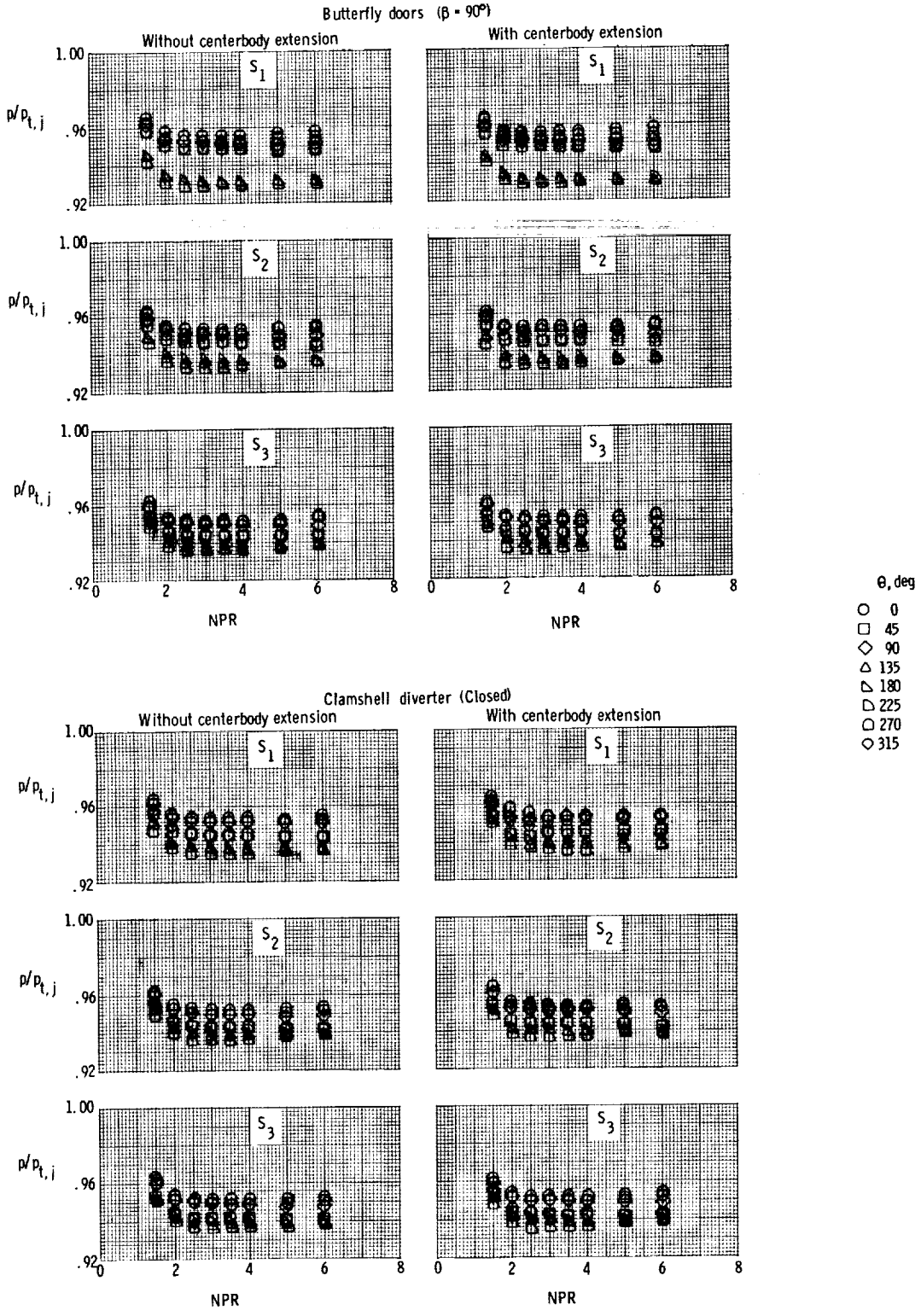

Figure 16. Wall static-pressure ratio in variable-area turbine section as function of NPR for butterfly door and clamshell diverter ventral nozzles with and without centerbody extension.

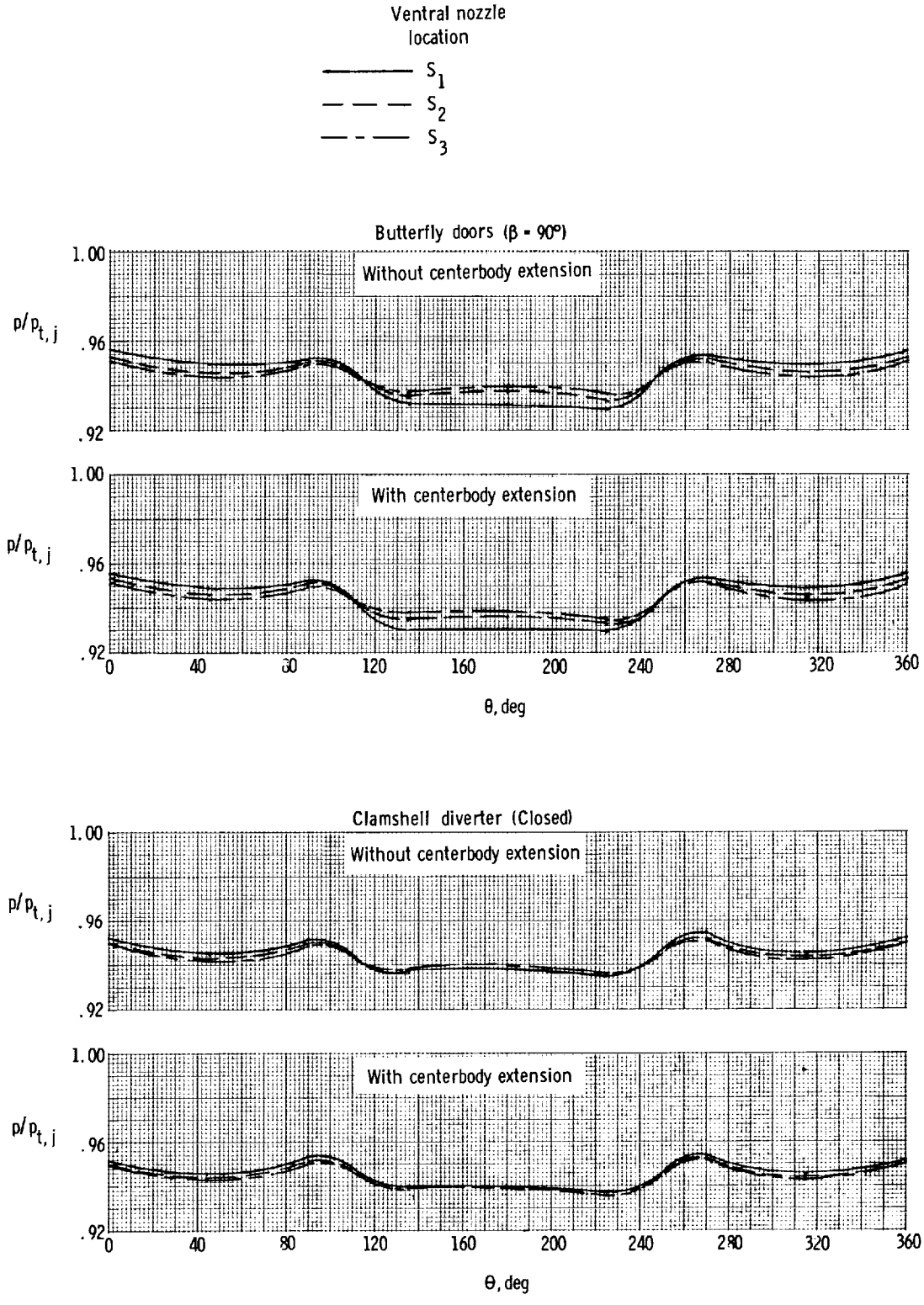

Figure 17. Circumferential variation of wall static-pressure ratio in variable-area turbine section for butterfly door and clamshell diverter ventral nozzles with and without centerbody extension.

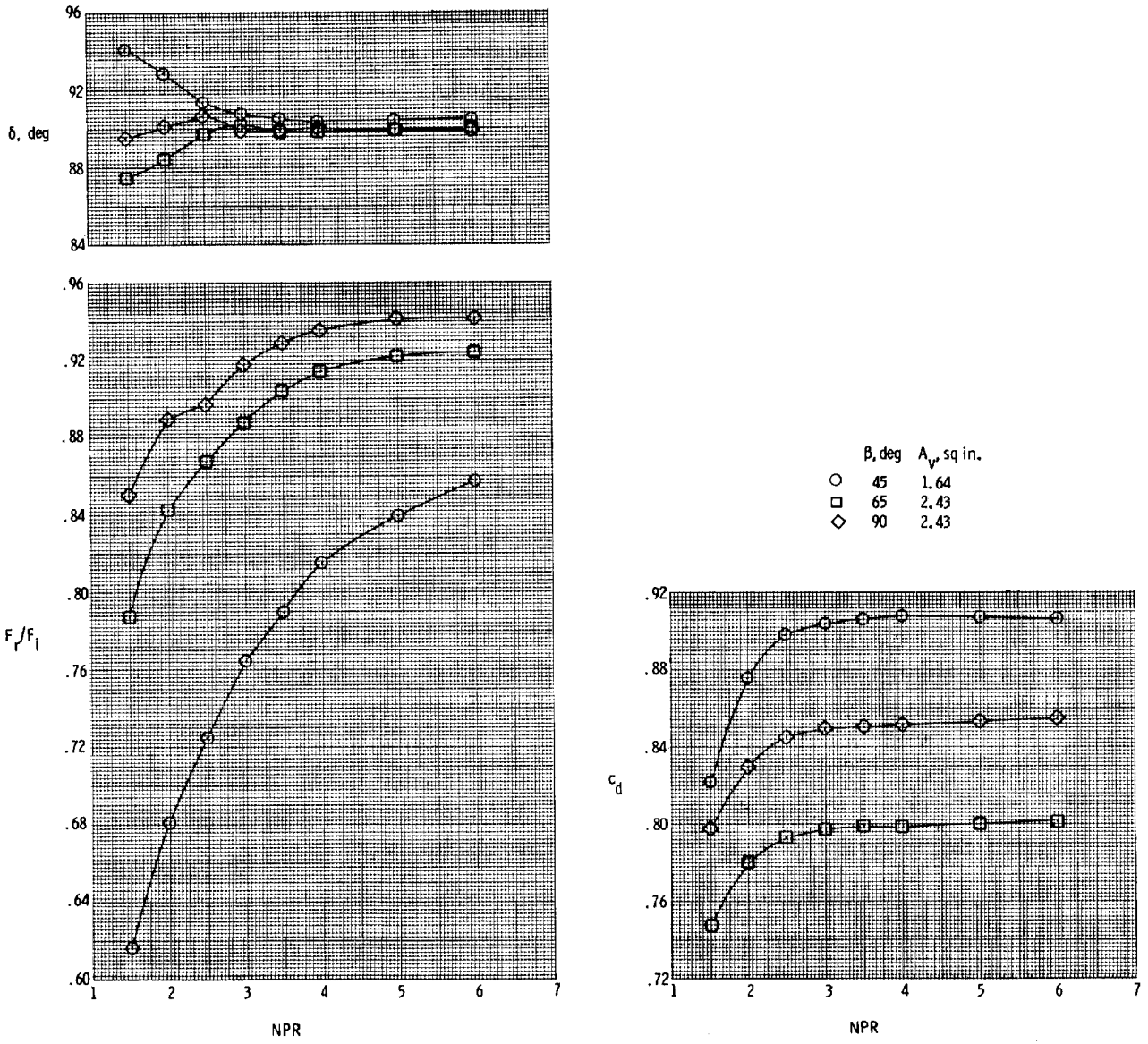

(a) Resultant-thrust-vector angle, resultant-thrust ratio, and discharge coefficient.

Figure 18. Effect of ventral nozzle butterfly door angle on internal performance characteristics of hover configuration $V_cB_1N_bS_1E_9$. $\phi = 90°$.

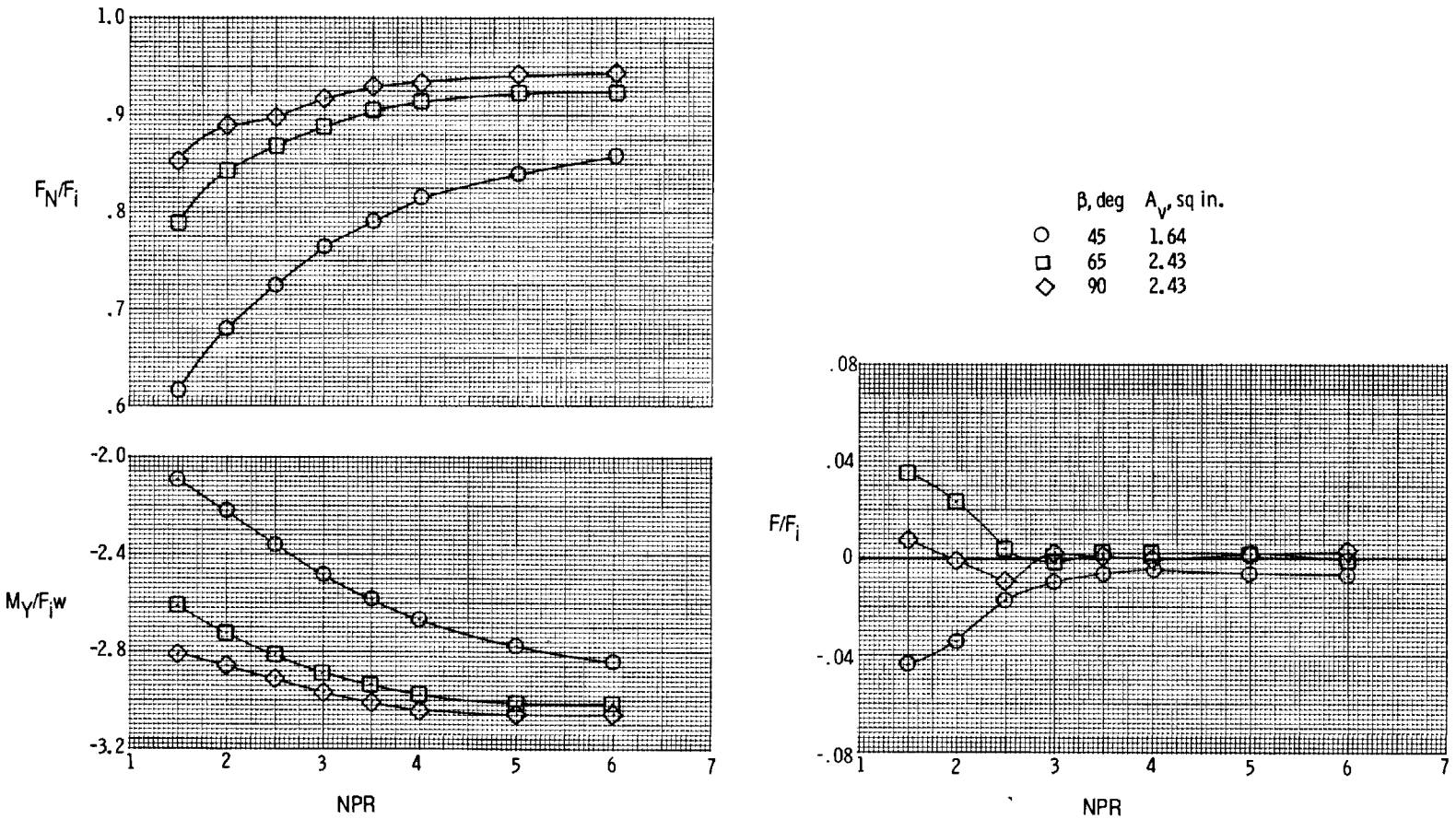

(b) Normal-force ratio, pitching-moment ratio, and thrust ratio.

Figure 18. Concluded.

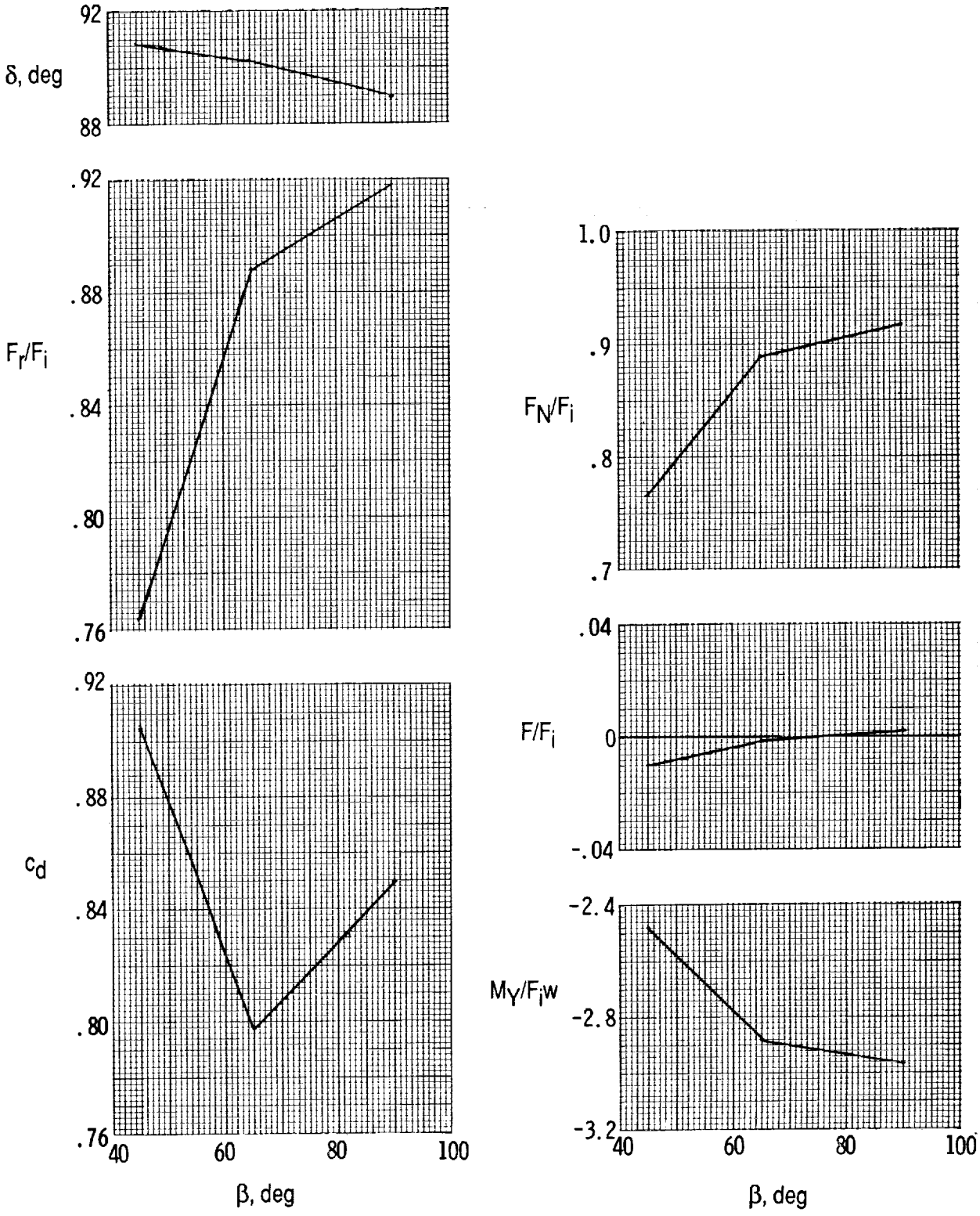

Figure 19. Effect of butterfly door angle on nozzle internal performance at NPR = 3.0 for configuration $V_cB_1N_bS_1E_9$. $\phi = 90°$.

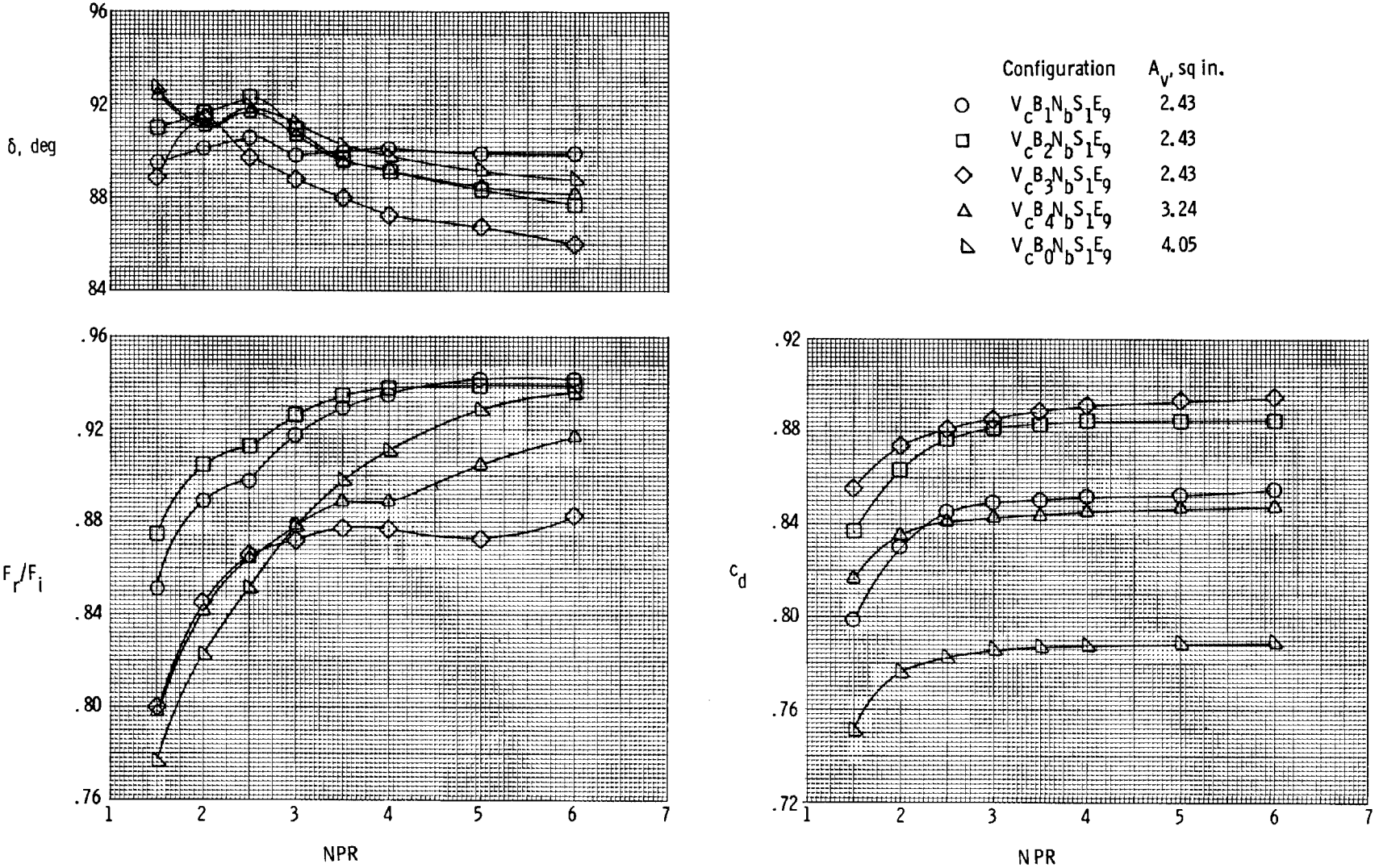

(a) Resultant-thrust-vector angle, resultant-thrust ratio, and discharge coefficient.

Figure 20. Effect of ventral nozzle open-area changes on internal performance characteristics in hover with butterfly doors at 90° and exit vanes at 90°.

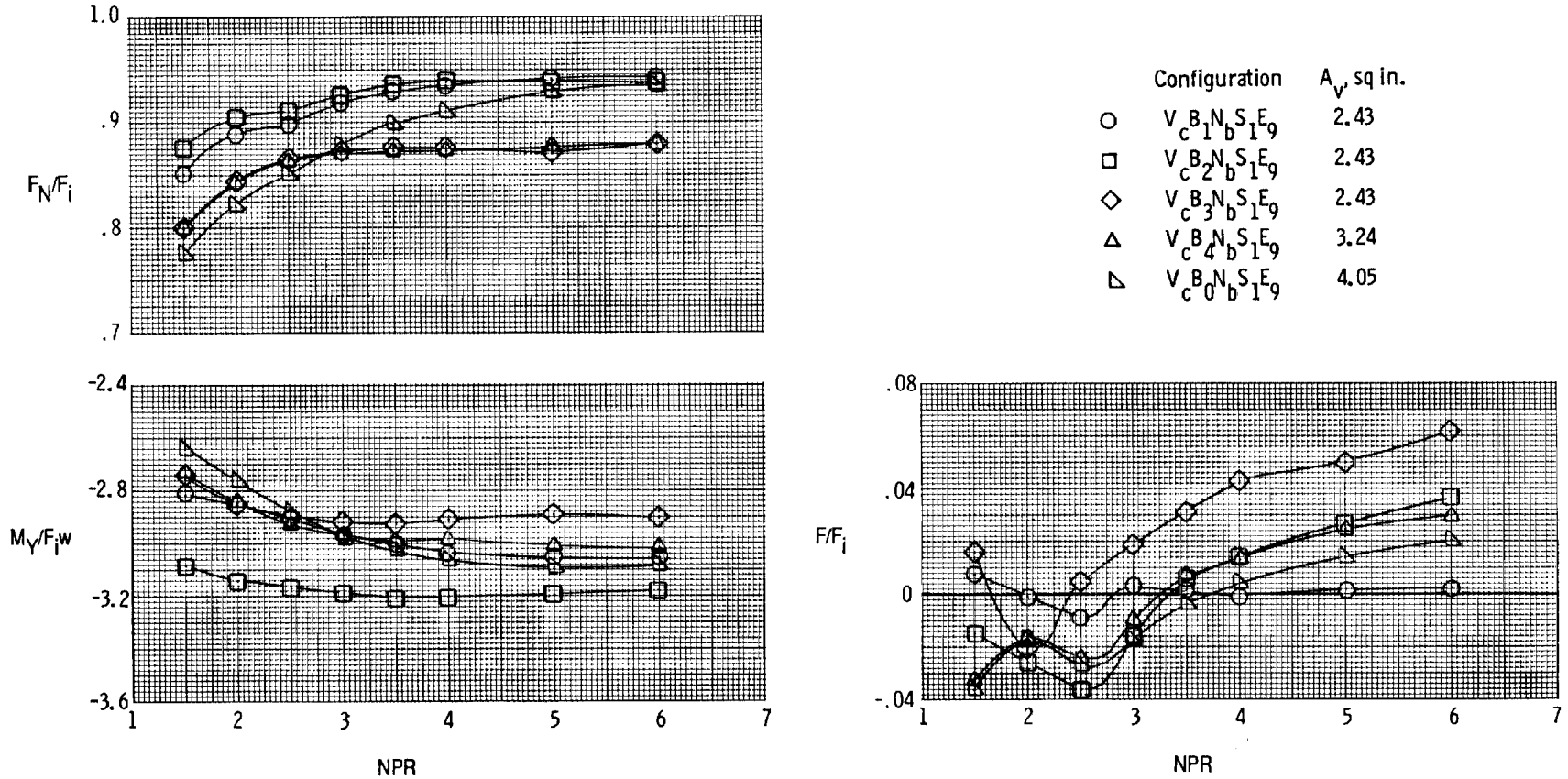

(b) Normal-force ratio, pitching-moment ratio, and thrust ratio.

Figure 20. Concluded.

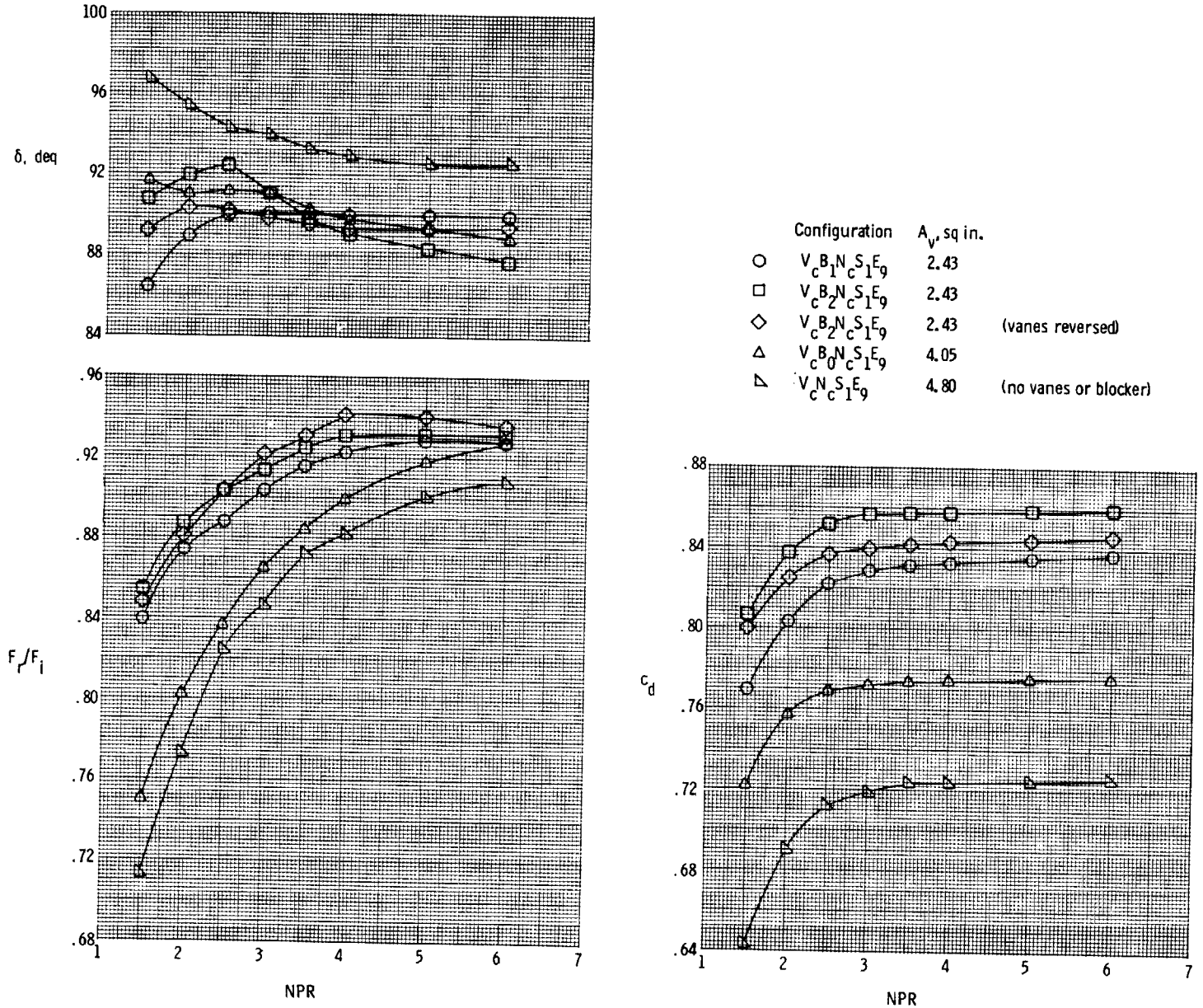

(a) Resultant-thrust-vector angle, resultant-thrust ratio, and discharge coefficient.

Figure 21. Effect of ventral nozzle area and vane openings on internal performance characteristics in hover with clamshell diverters closed. $\phi = 90°$.

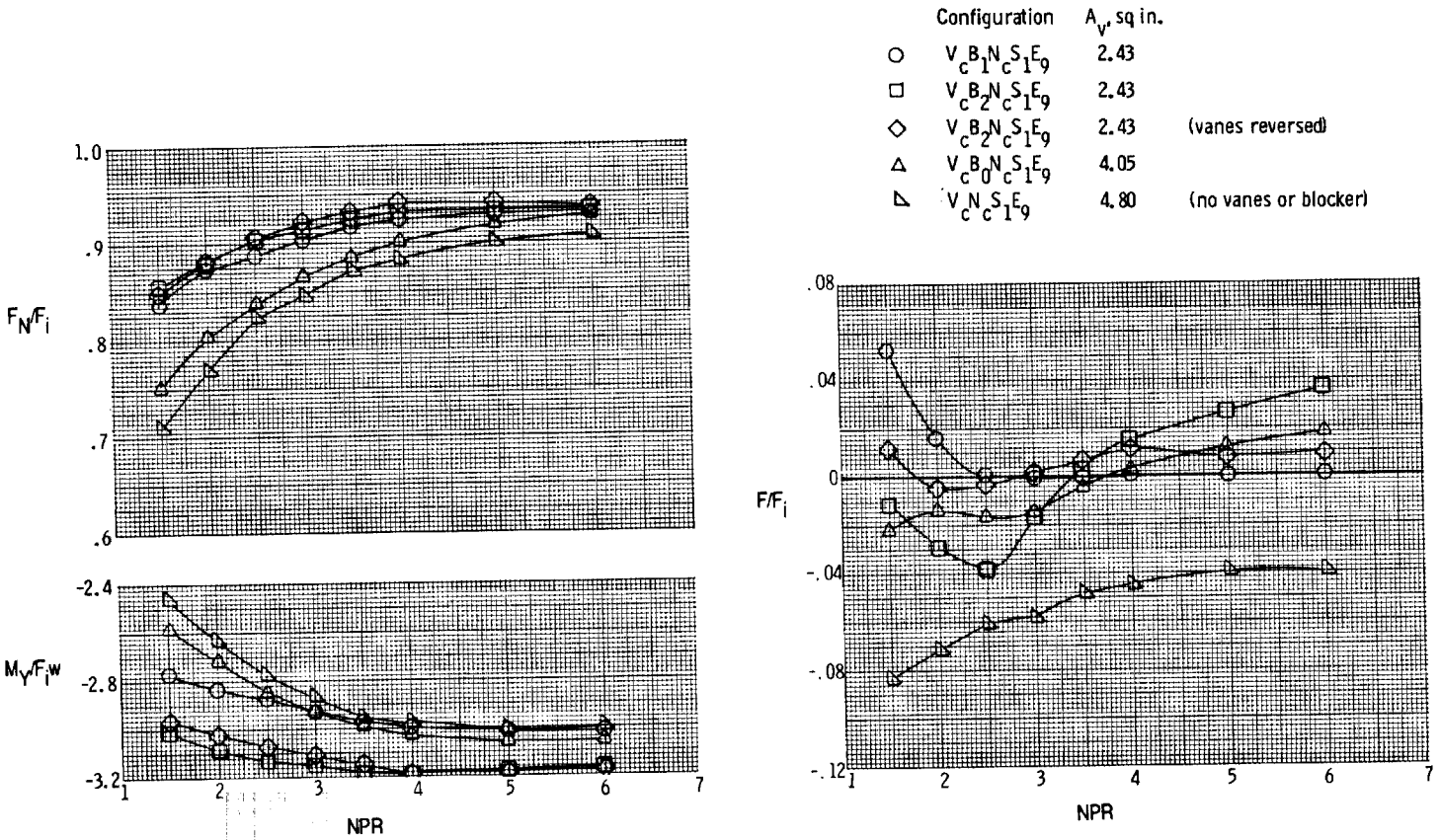

(b) Normal-force ratio, pitching-moment ratio, and thrust ratio.

Figure 21. Concluded.

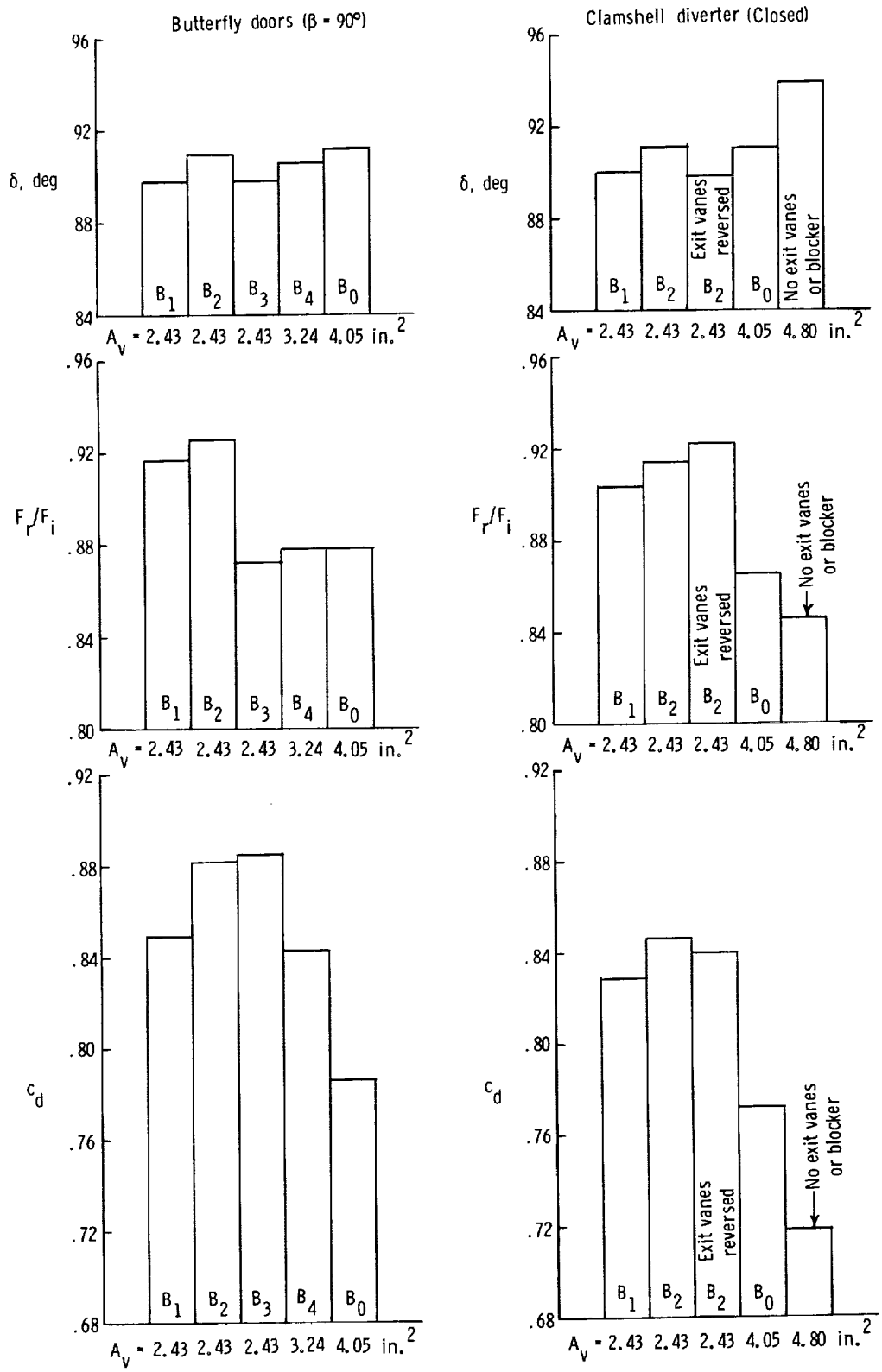

Figure 22. Butterfly door and clamshell diverter ventral nozzle internal performance with various nozzle exit blockers at NPR = 3.0 and nozzle exit vanes at 90°.

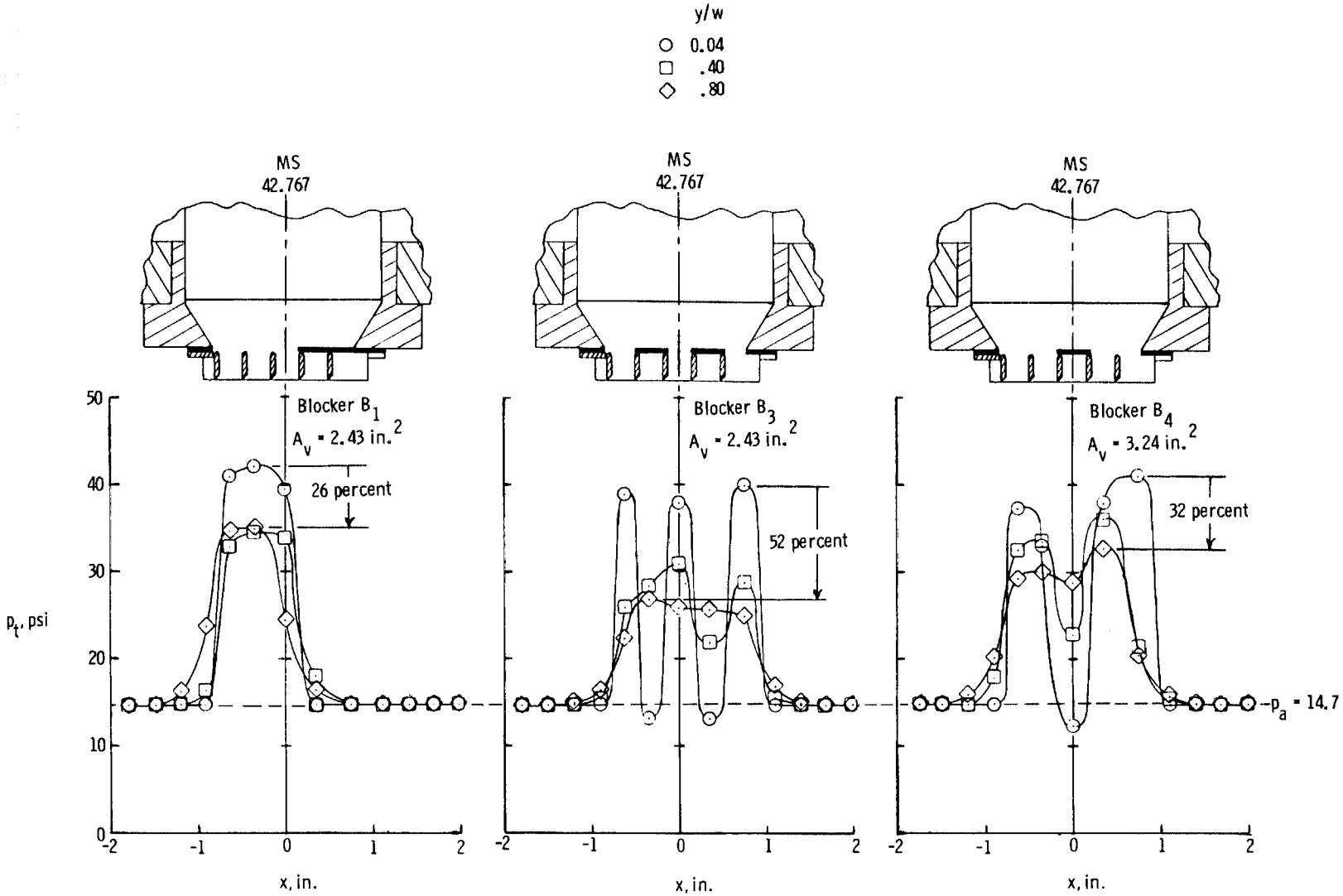

Figure 23. Effect of ventral nozzle exit segmentation on plume-total-pressure decay for butterfly door ($\beta = 90°$) ventral nozzle at NPR = 3.0.

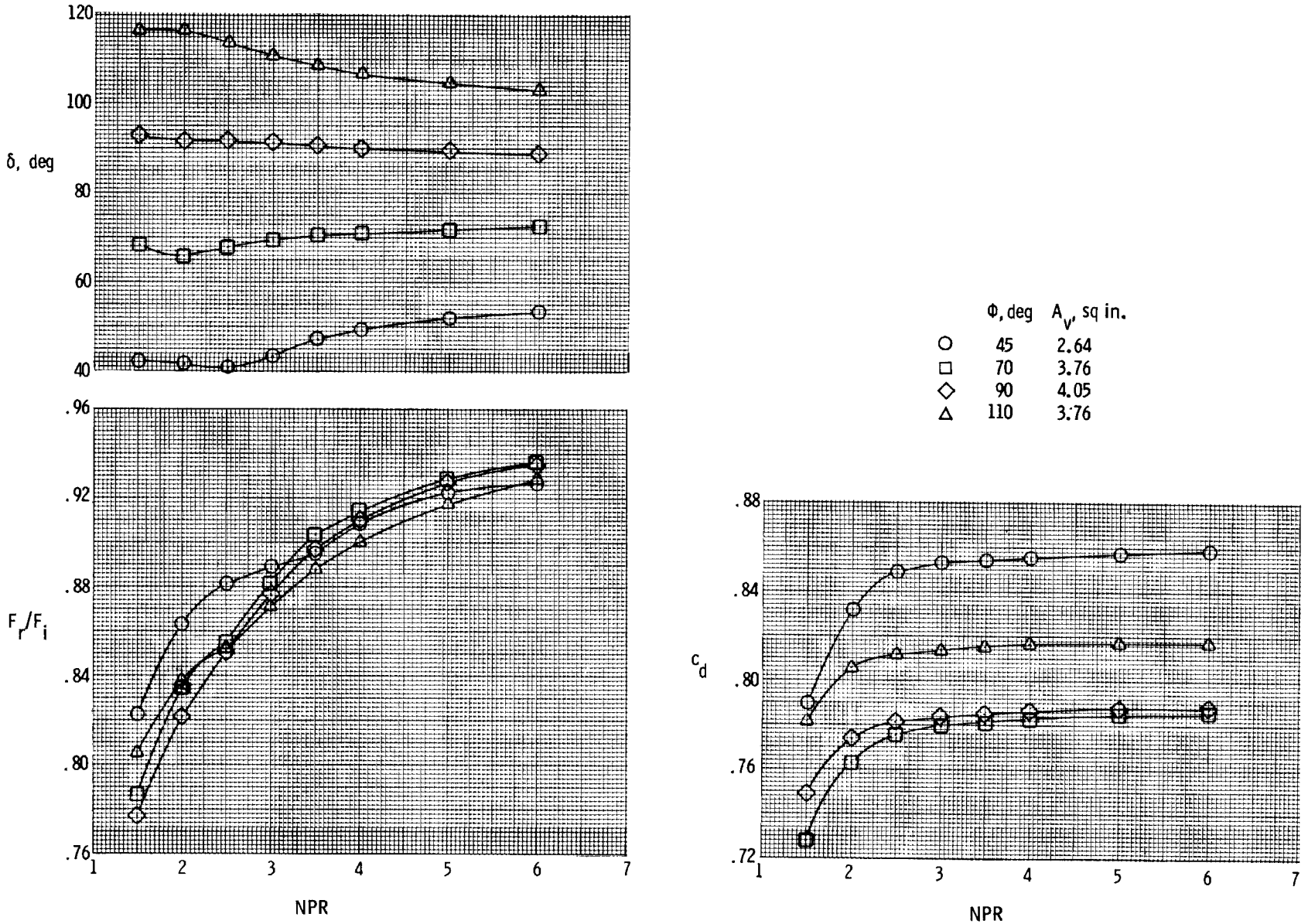

(a) Resultant-thrust-vector angle, resultant-thrust ratio, and discharge coefficient.

Figure 24. Effect of ventral nozzle exit vane angle on internal performance characteristics of butterfly door ventral nozzle ($\beta = 90°$) for hover configuration $V_cB_0N_bS_1W_7D_2W_7E_9$.

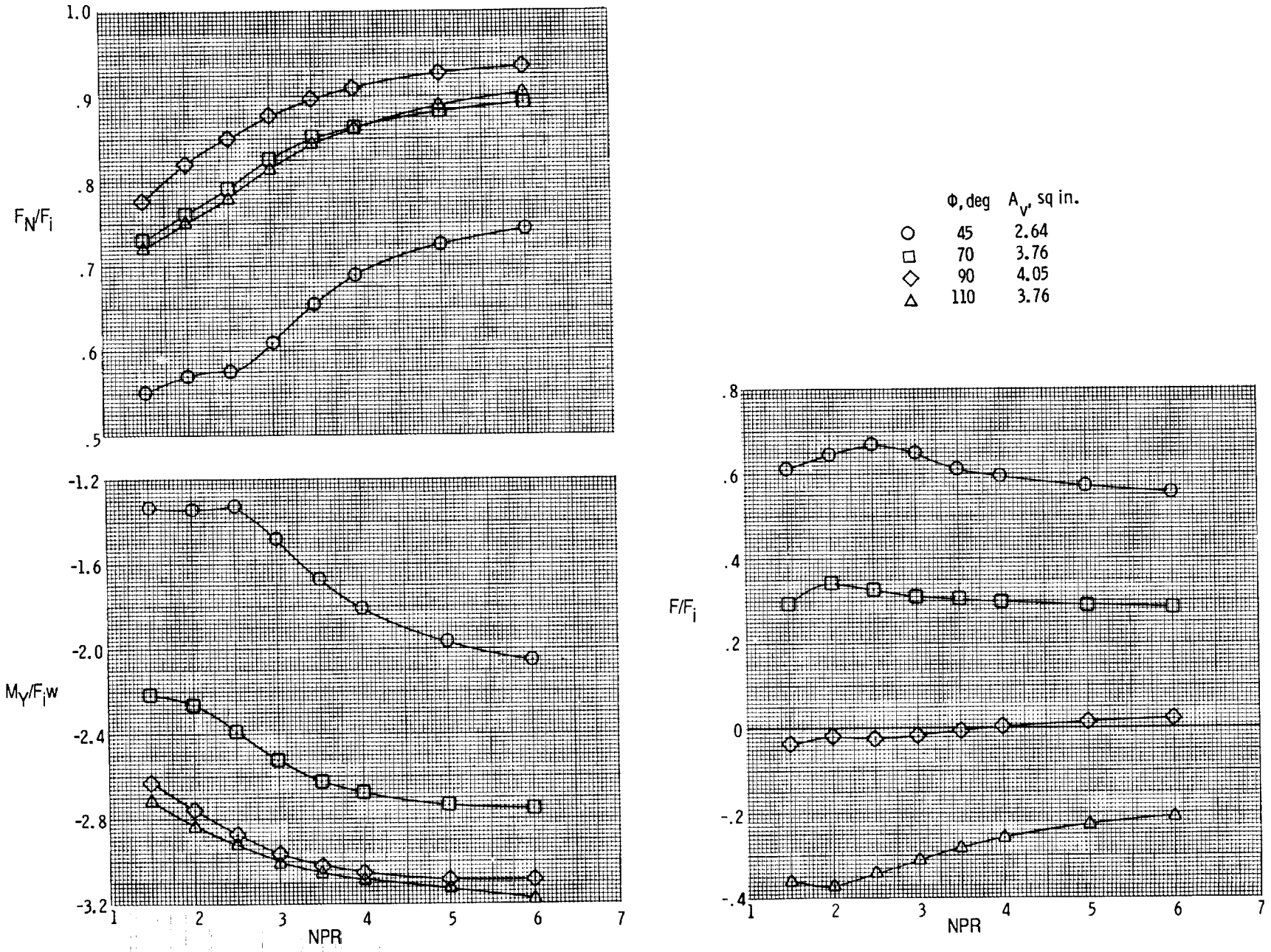

(b) Normal-force ratio, pitching-moment ratio, and thrust ratio.

Figure 24. Concluded.

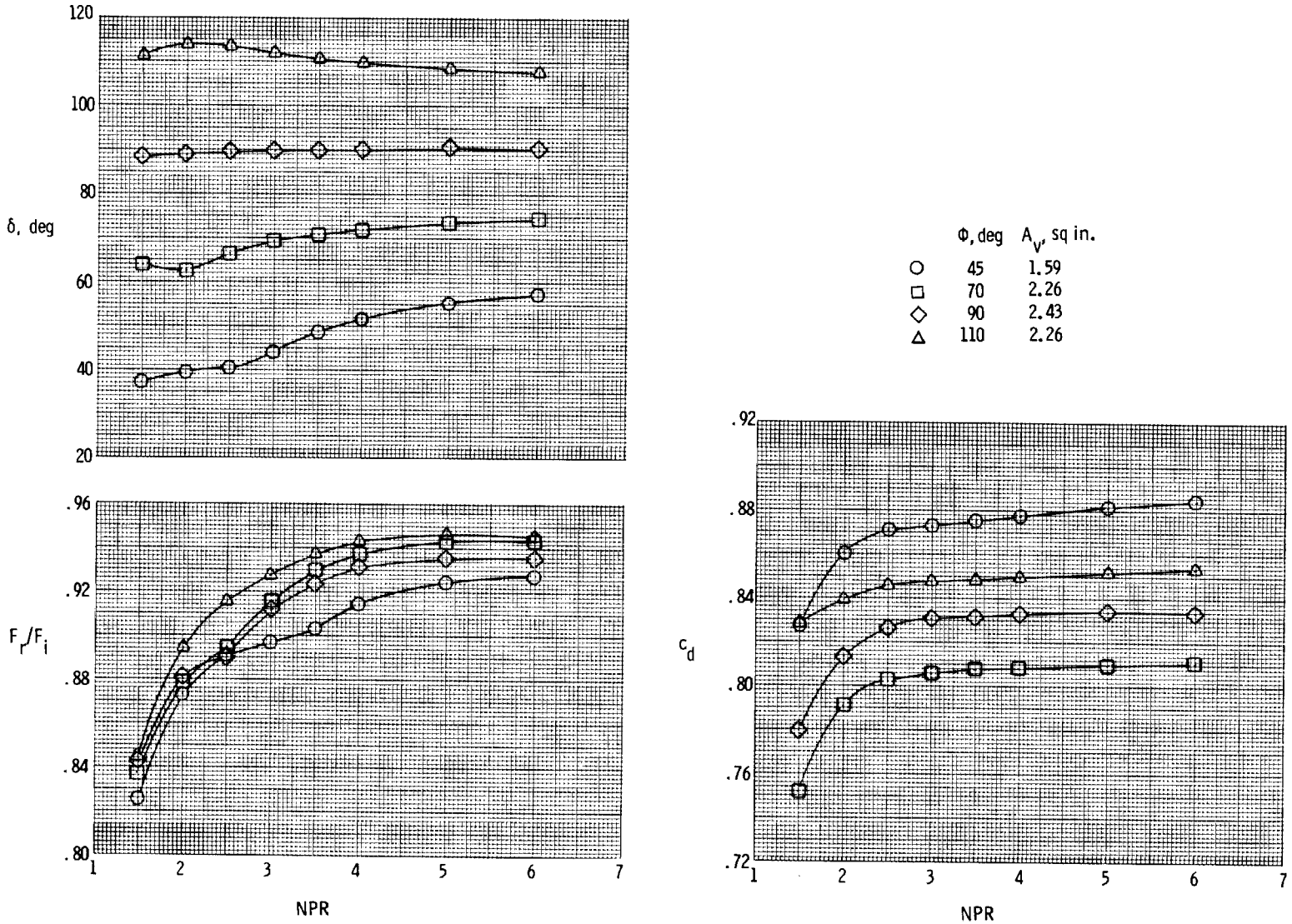

(a) Resultant-thrust-vector angle, resultant-thrust ratio, and discharge coefficient.

Figure 25. Effect of ventral nozzle exit vane angle on internal performance characteristics of clamshell diverter ventral nozzle (clamshells closed) for hover configuration $V_cB_1N_cS_1E_9$.

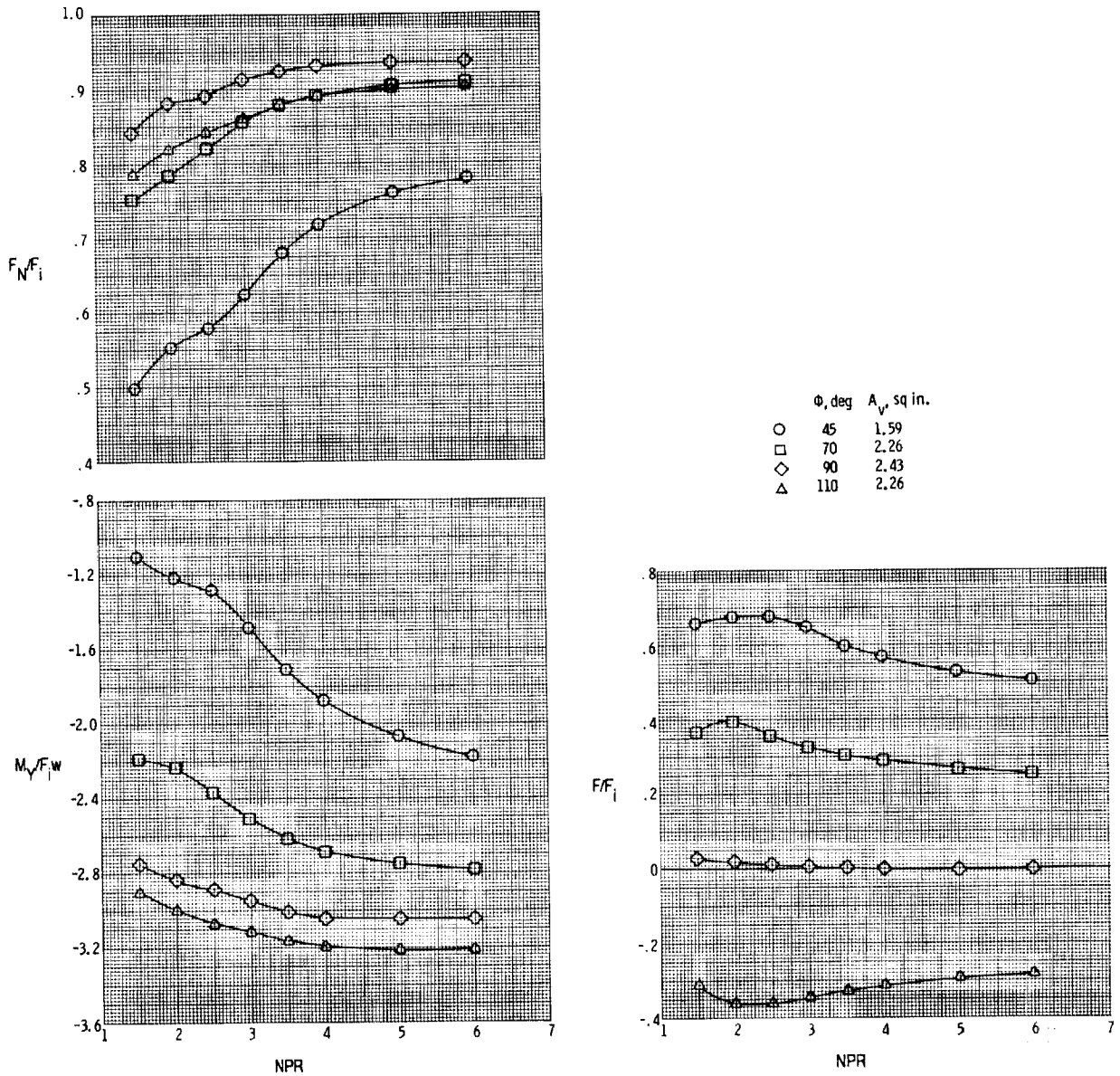

(b) Normal-force ratio, pitching-moment ratio, and thrust ratio.

Figure 25. Concluded.

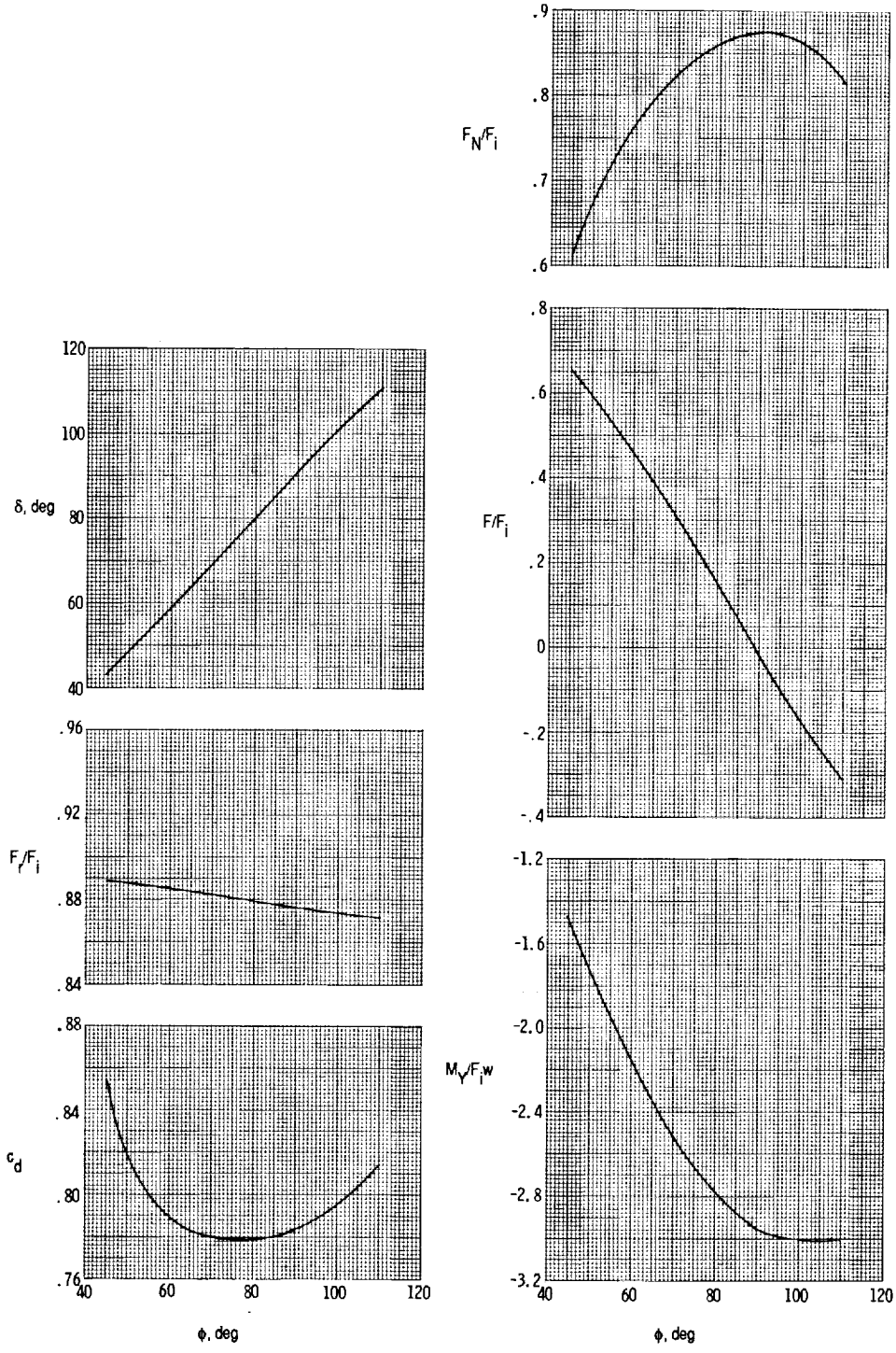

(a) Configuration with butterfly door ventral nozzle ($V_cB_0N_bS_1W_7D_2W_7E_9$).

Figure 26. Variation of ventral nozzle internal performance with geometric exit vane angle for butterfly door and clamshell diverter ventral nozzles at NPR = 3.0.

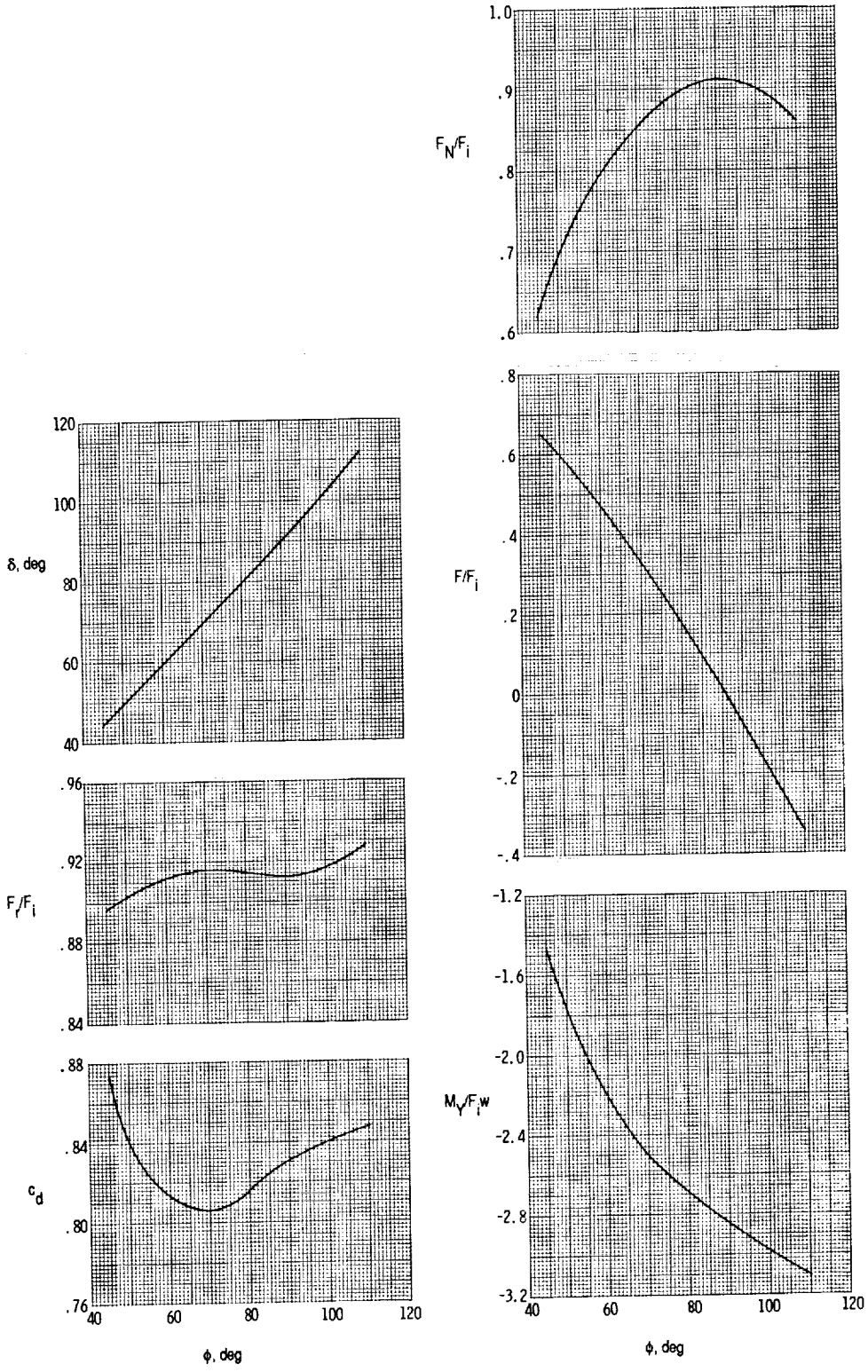

(b) Configuration with clamshell diverter ventral nozzle ($V_cB_1N_cS_1E_9$).

Figure 26. Concluded.

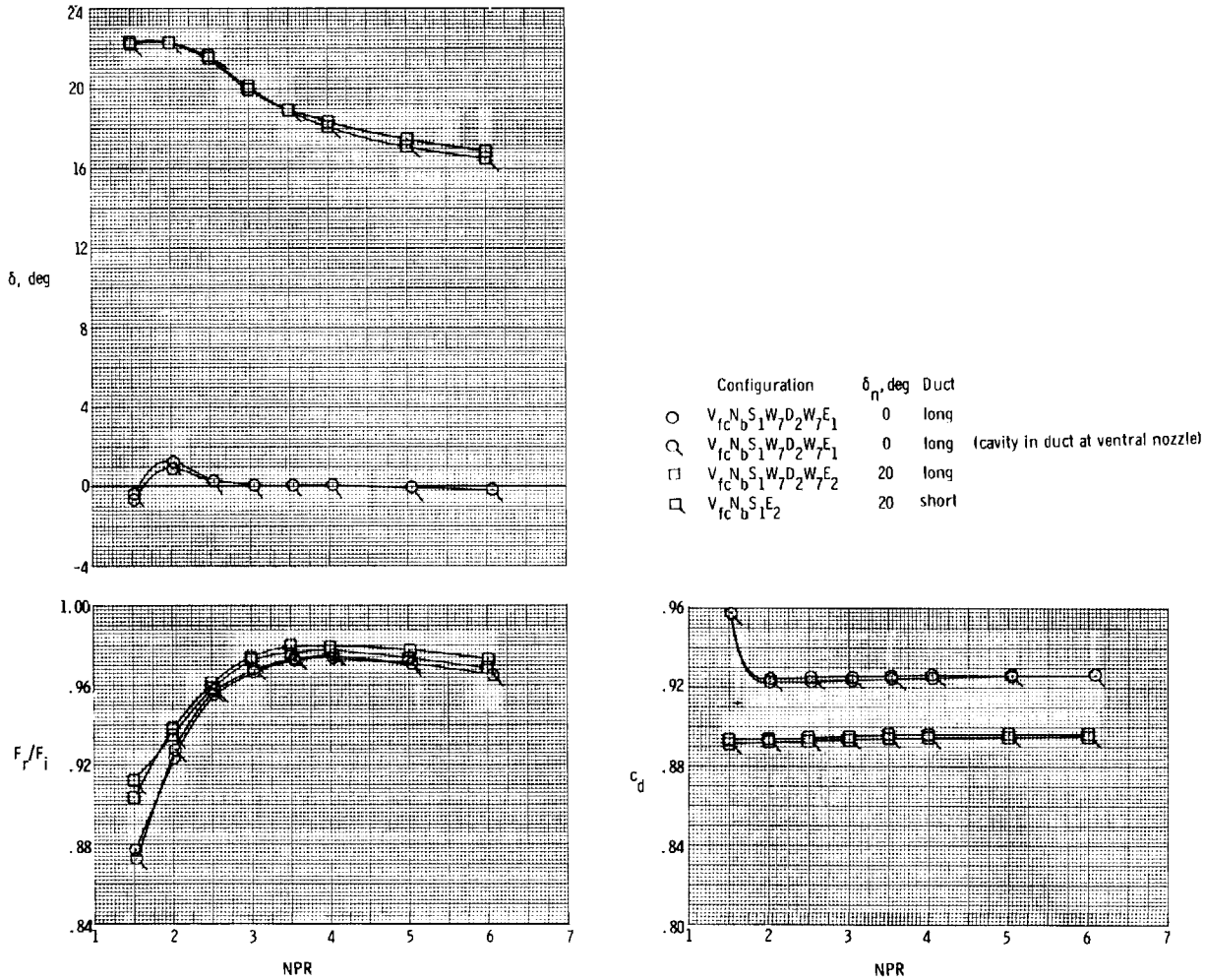

(a) Resultant-thrust-vector angle, resultant-thrust ratio, and discharge coefficient.

Figure 27. Internal performance characteristics of vectored ($\delta_n = 20°$) and unvectored 2D-CD rear nozzle configurations with cruise throat area ($A_n = 4.00$ in^2).

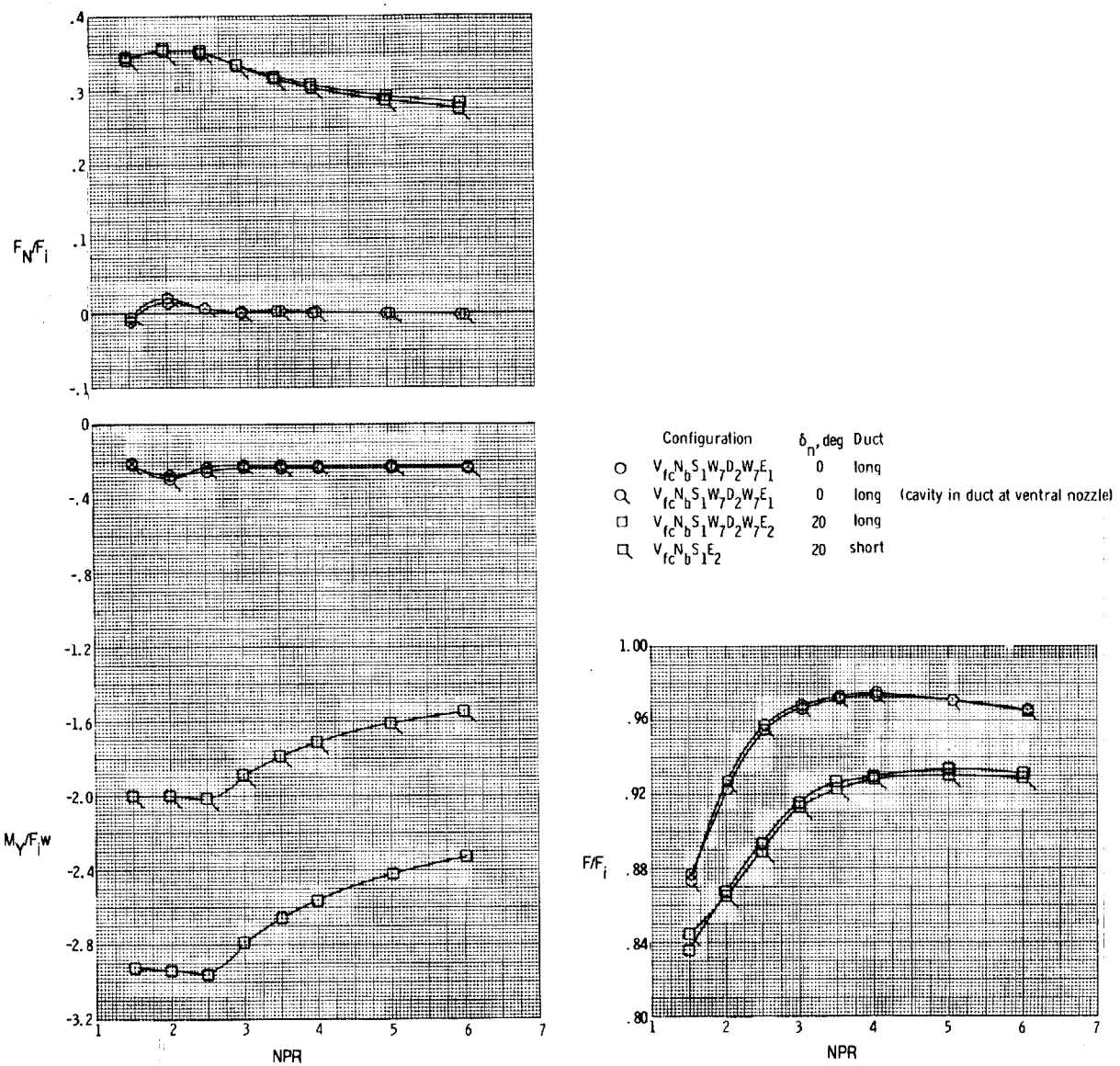

(b) Normal-force ratio, pitching-moment ratio, and thrust ratio.

Figure 27. Concluded.

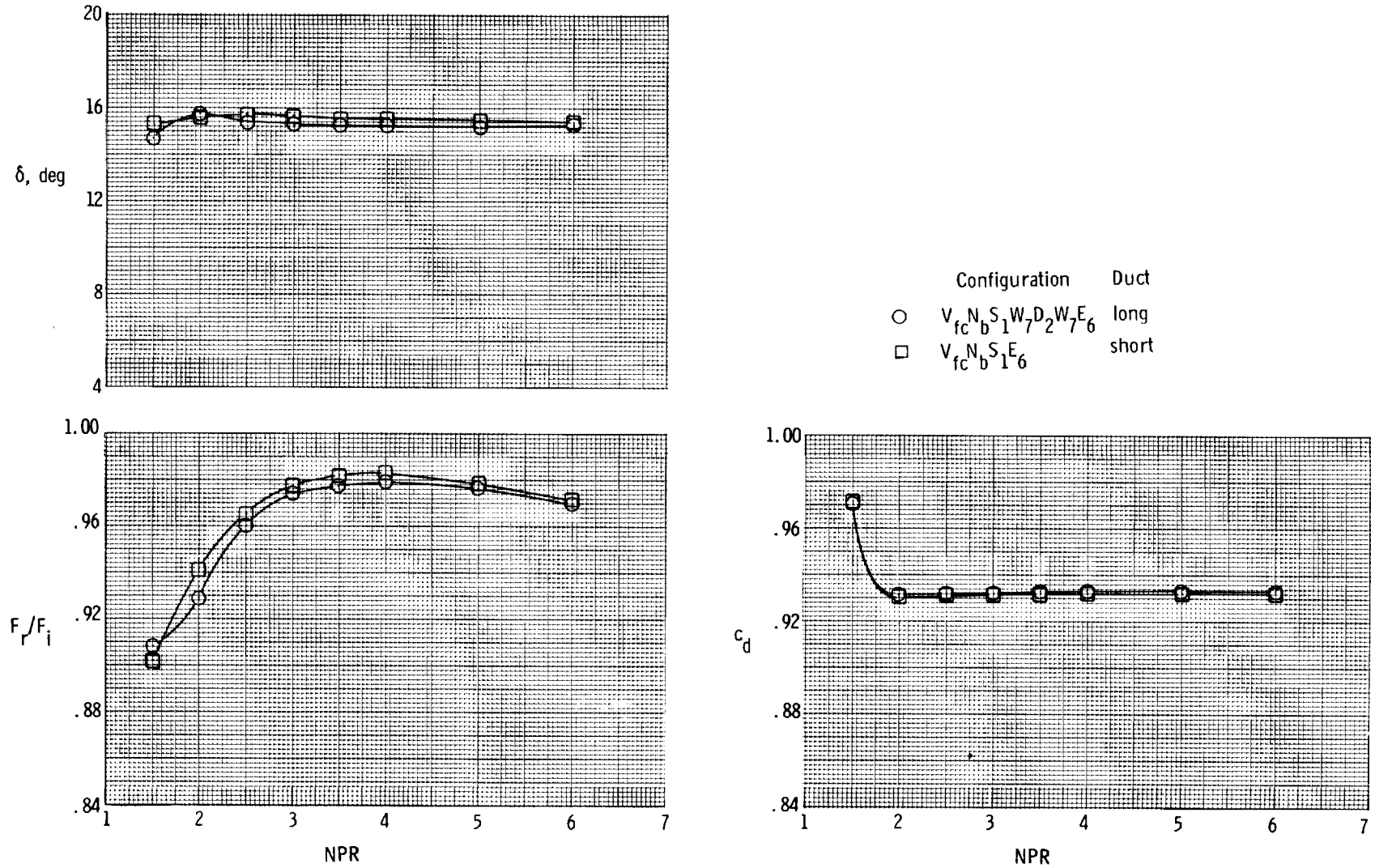

(a) Resultant-thrust-vector angle, resultant-thrust ratio, and discharge coefficient.

Figure 28. Internal performance characteristics of vectored ($\delta_n = 15°$) long and short axisymmetric rear nozzle configurations with cruise throat area ($A_n = 4.00$ in^2).

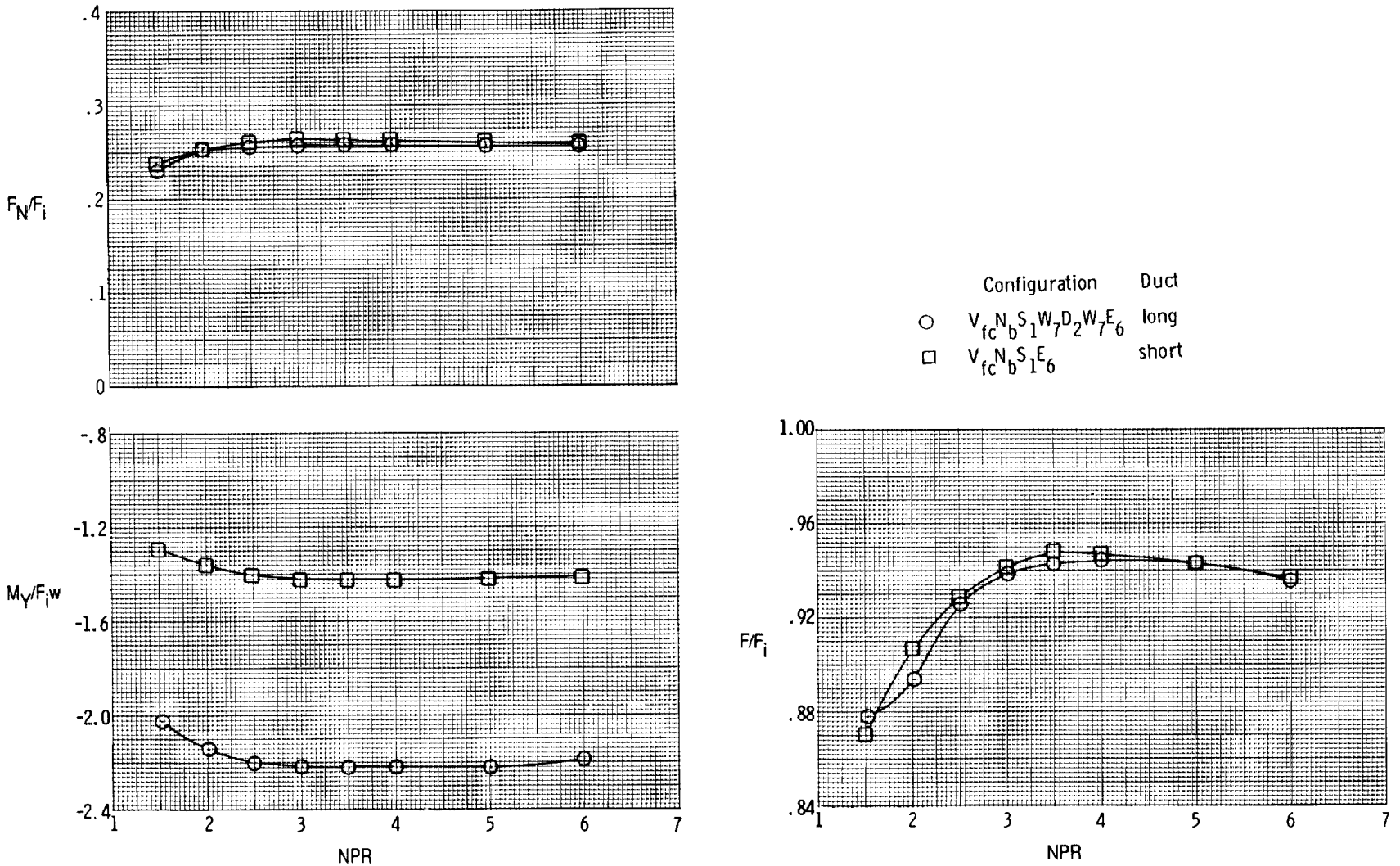

(b) Normal-force ratio, pitching-moment ratio, and thrust ratio.

Figure 28. Concluded.

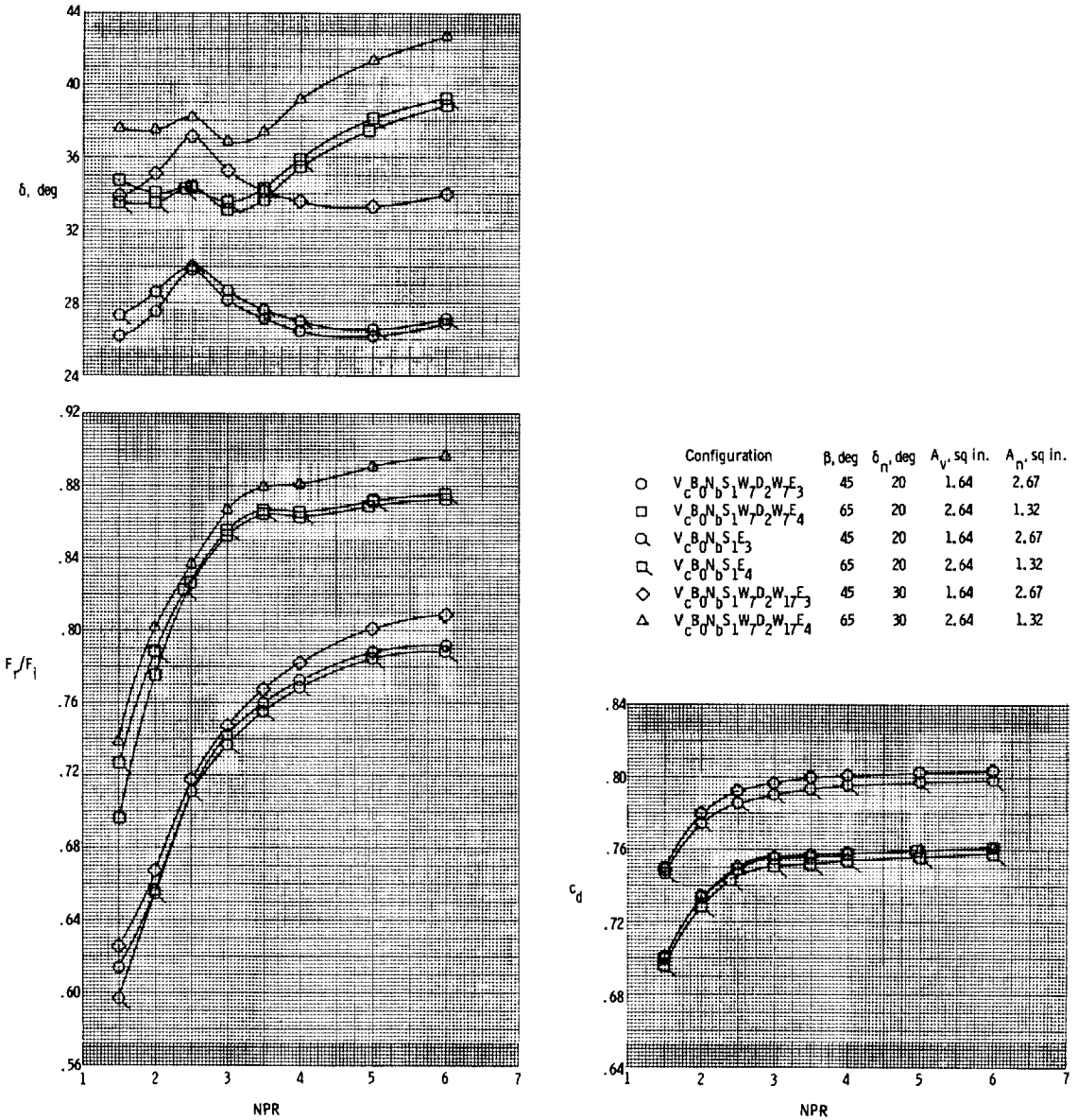

(a) Resultant-thrust-vector angle, resultant-thrust ratio, and discharge coefficient.

Figure 29. Effect of ventral nozzle butterfly door angle and 2D-CD rear nozzle open area and vector angle on internal performance characteristics of long- and short-duct transition configurations. ($\phi = 45°$).

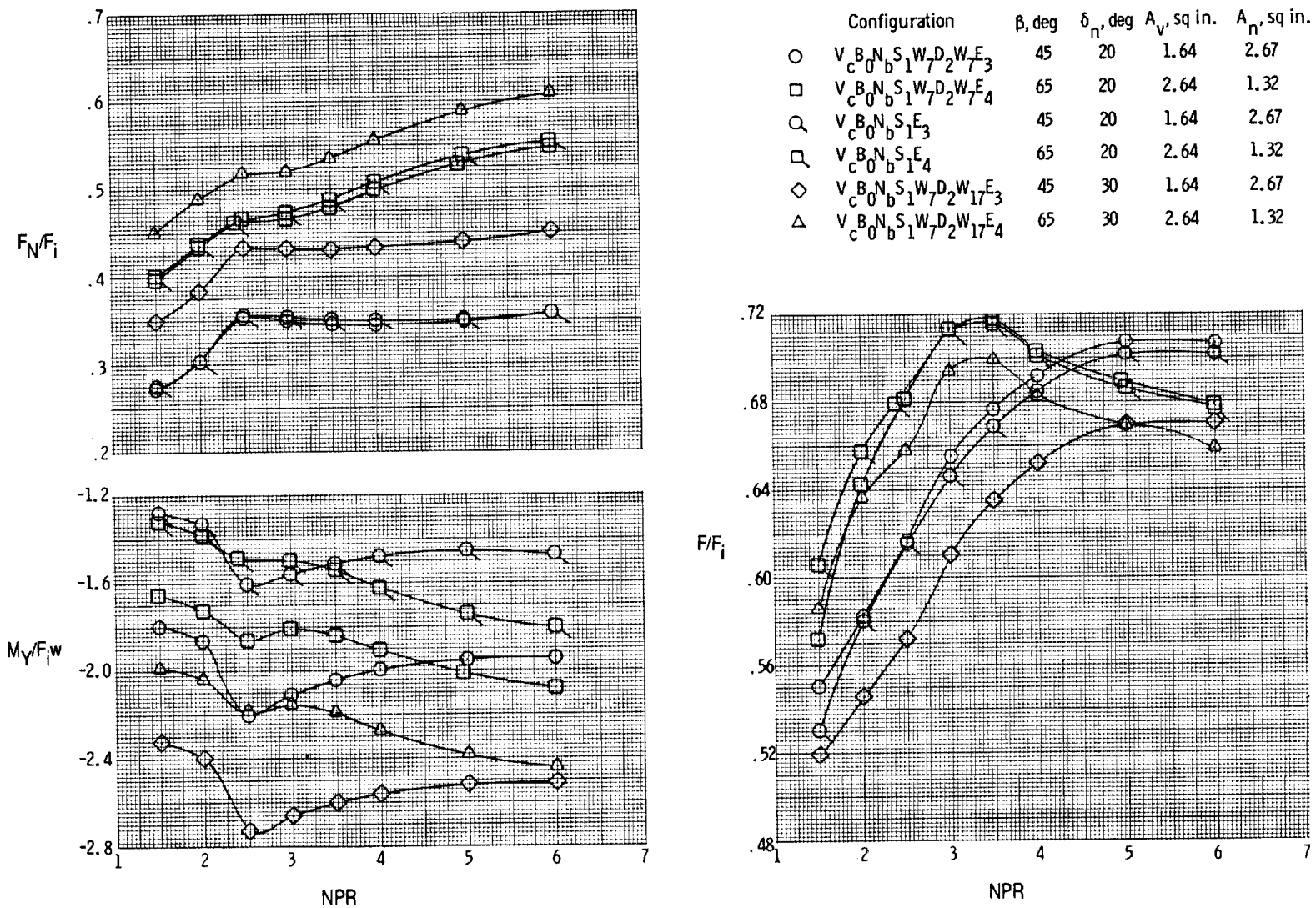

(b) Normal-force ratio, pitching-moment ratio, and thrust ratio.

Figure 29. Concluded.

	Configuration	δ_n, deg	ϕ, deg	A_n, sq in.	A_v, sq in.	β, deg	Flight regime
○	$V_{fc}N_bS_1W_7D_2W_7E_1$	0	–	4.00	–	–	Cruise
□	$V_{fc}N_bS_1W_7D_2W_7E_2$	20	–	4.00	–	–	Cruise
◇	$V_cB_0N_bS_1W_7D_2W_7E_3$	20	45	2.67	1.64	45	Transition
△	$V_cB_0N_bS_1W_7D_2W_7E_4$	20	45	1.32	2.64	65	Transition
▷	$V_cB_0N_bS_1W_7D_2W_{17}E_3$	30	45	2.67	1.64	45	Transition
▷	$V_cB_0N_bS_1W_7D_2W_{17}E_4$	30	45	1.32	2.64	65	Transition
⬠	$V_cB_0N_bS_1W_7D_2W_7E_9$	–	45	–	2.64	90	Vertical
◇	$V_cB_1N_bS_1E_9$	–	90	–	2.43	90	Vertical
◇	$V_cB_2N_bS_1E_9$	–	90	–	2.43	90	Vertical
⬠	$V_cB_3N_bS_1E_9$	–	90	–	2.43	90	Vertical

(Shaded symbols indicate geometric throat area (A_t) for each of the above configurations)

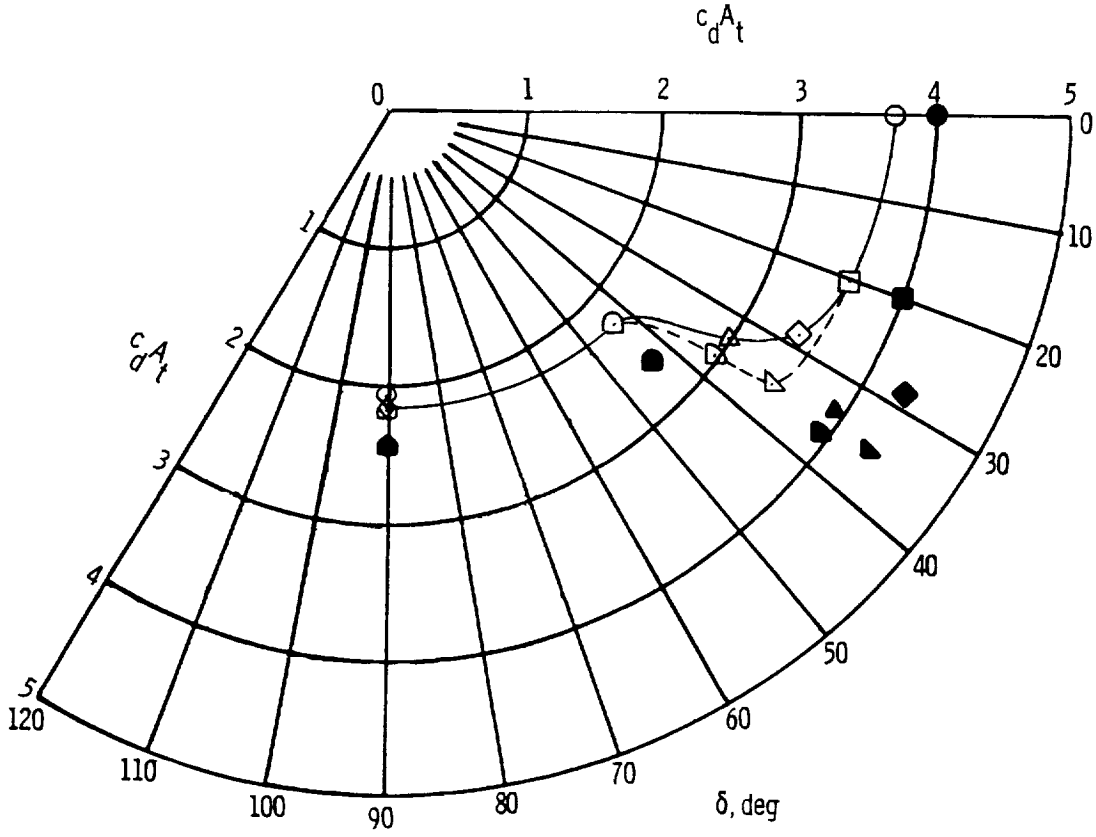

Figure 30. Variation of effective throat area c_dA_t with resultant-thrust-vector angle from cruise to vertical flight for 2D-CD rear nozzle configurations with butterfly door ventral nozzle at NPR = 3.0. Dashed line indicates extrapolation and fairing of data for 30° rear nozzle through transition range.

	Configuration	δ_n, deg	ϕ, deg	A_n, sq in.	A_v, sq in.	β, deg	Flight regime
○	$V_{fc}N_bS_1W_7D_2W_7E_1$	0	–	4.00	–	–	Cruise
□	$V_{fc}N_bS_1W_7D_2W_7E_2$	20	–	4.00	–	–	Cruise
◇	$V_cB_0N_bS_1W_7D_2W_7E_3$	20	45	2.67	1.64	45	Transition
△	$V_cB_0N_bS_1W_7D_2W_7E_4$	20	45	1.32	2.64	65	Transition
▱	$V_cB_0N_bS_1W_7D_2W_{17}E_3$	30	45	2.67	1.64	45	Transition
▱	$V_cB_0N_bS_1W_7D_2W_{17}E_4$	30	45	1.32	2.64	65	Transition
⬠	$V_cB_0N_bS_1W_7D_2W_7E_9$	–	45	–	2.64	90	Vertical
◇	$V_cB_1N_bS_1E_9$	–	90	–	2.43	90	Vertical
◇	$V_cB_2N_bS_1E_9$	–	90	–	2.43	90	Vertical
⬠	$V_cB_3N_bS_1E_9$	–	90	–	2.43	90	Vertical

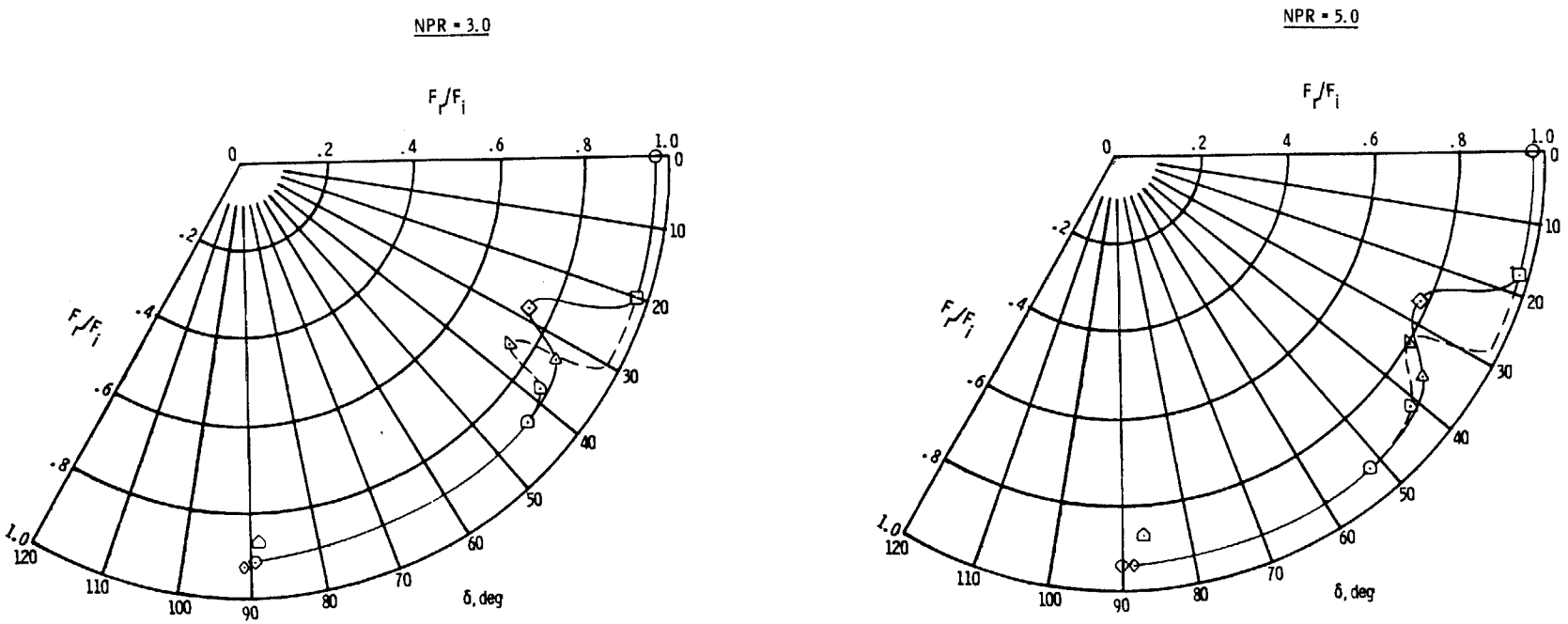

Figure 31. Variation of resultant-thrust ratio with resultant-thrust-vector angle from cruise to vertical flight for 2D-CD rear nozzle configurations with butterfly door ventral nozzle at two nozzle pressure ratios. Dashed line indicates extrapolation and fairing of data for 30° rear nozzle through transition range.

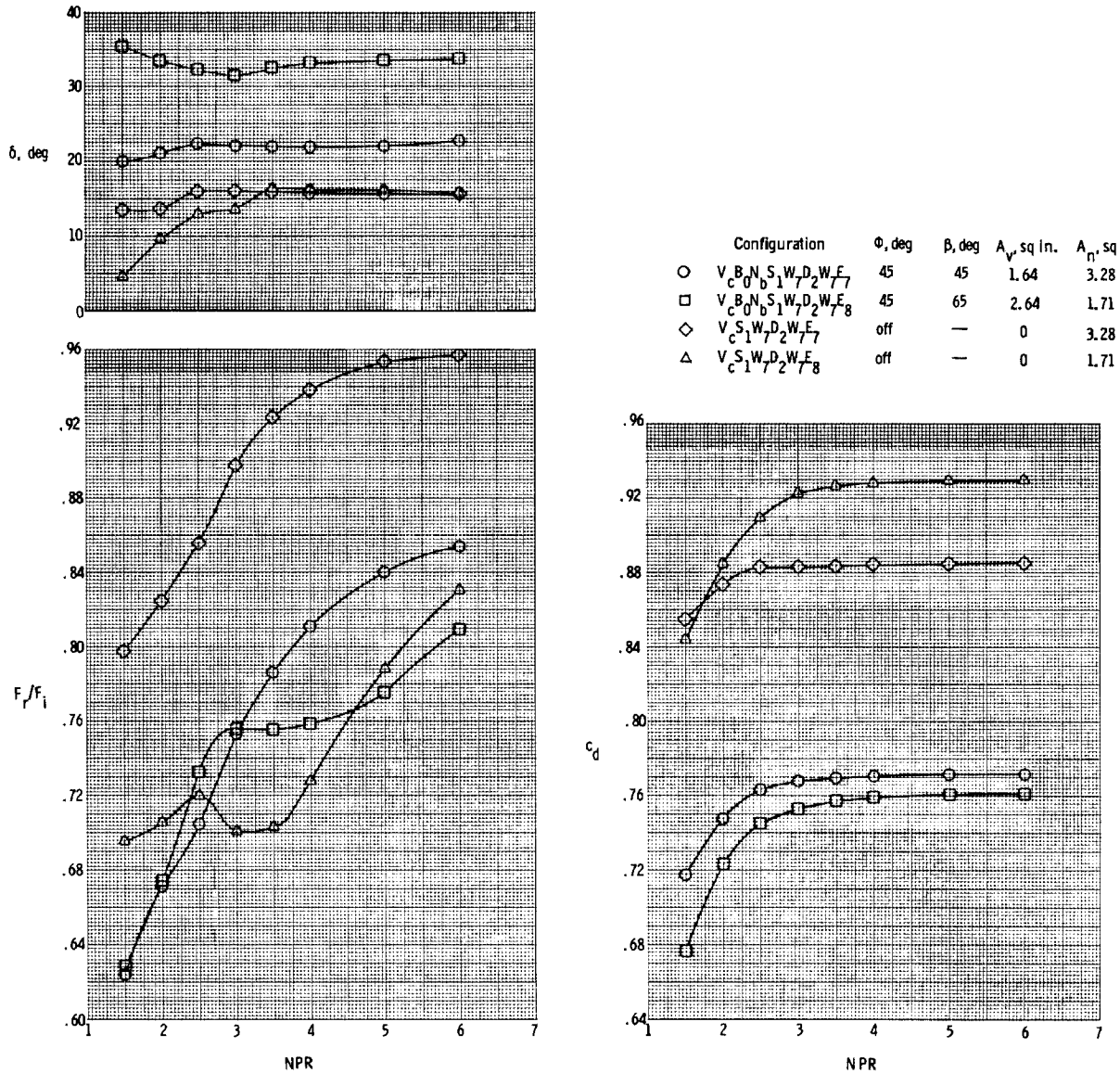

(a) Resultant-thrust-vector angle, resultant-thrust ratio, and discharge coefficient.

Figure 32. Effect of ventral nozzle butterfly door angle and axisymmetric rear nozzle open area on internal performance characteristics of long-duct transition configuration. $\phi = 45°$.

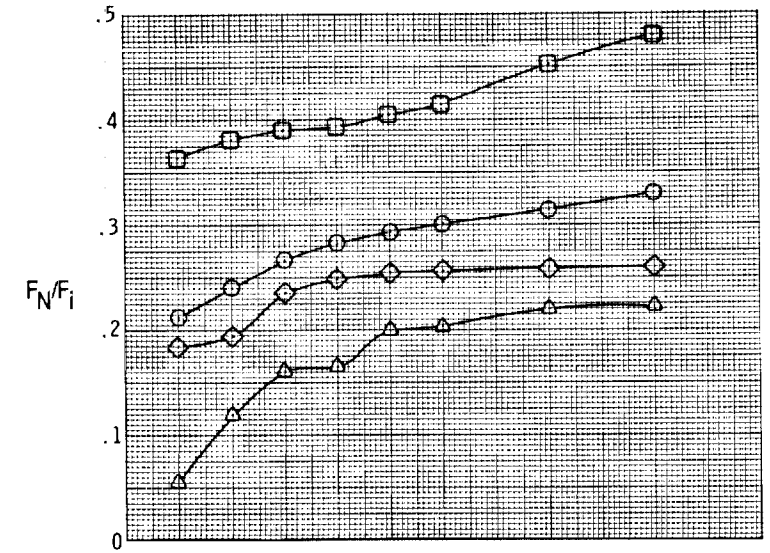

Configuration	Φ, deg	β, deg	A_v, sq in.	A_n, sq in.
○ $V_cB_0N_bS_1W_7D_2W_7E_7$	45	45	1.64	3.28
□ $V_cB_0N_bS_1W_7D_2W_7E_8$	45	65	2.64	1.71
◇ $V_cS_1W_7D_2W_7E_7$	off	—	0	3.28
△ $V_cS_1W_7D_2W_7E_8$	off	—	0	1.71

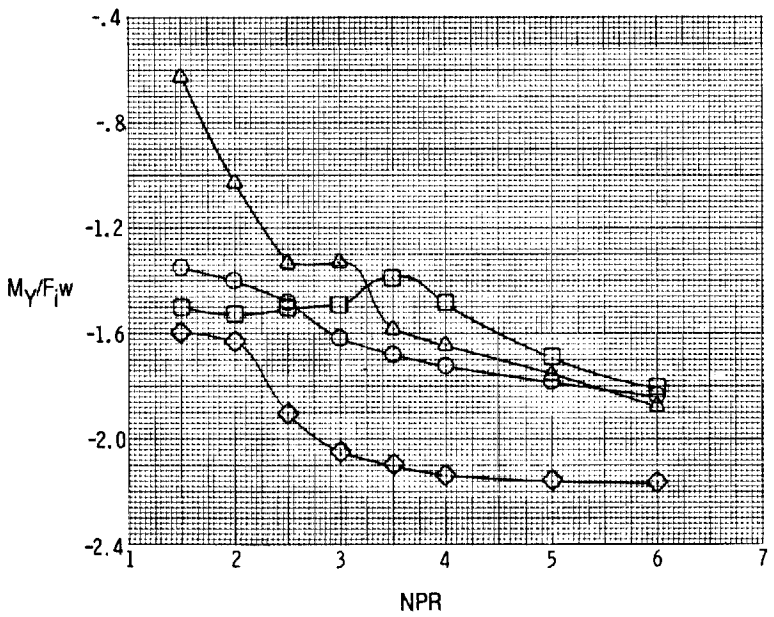

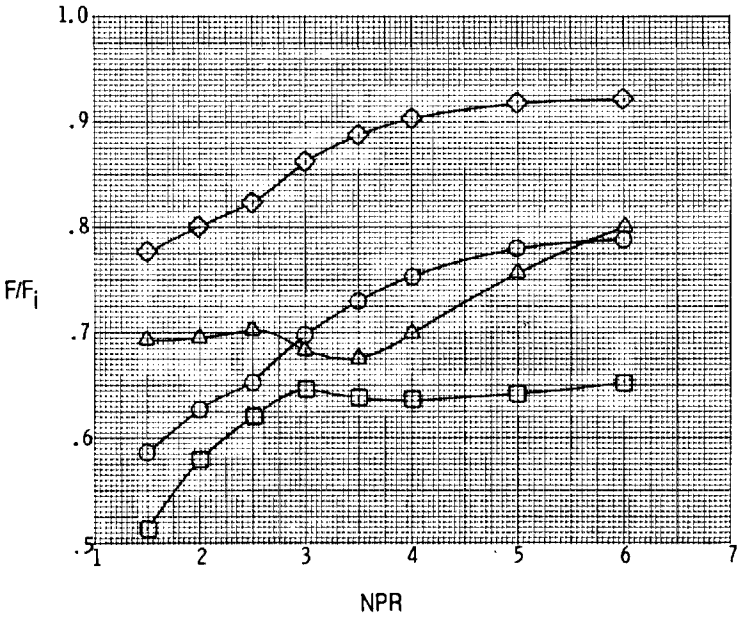

(b) Normal-force ratio, pitching-moment ratio, and thrust ratio.

Figure 32. Concluded.

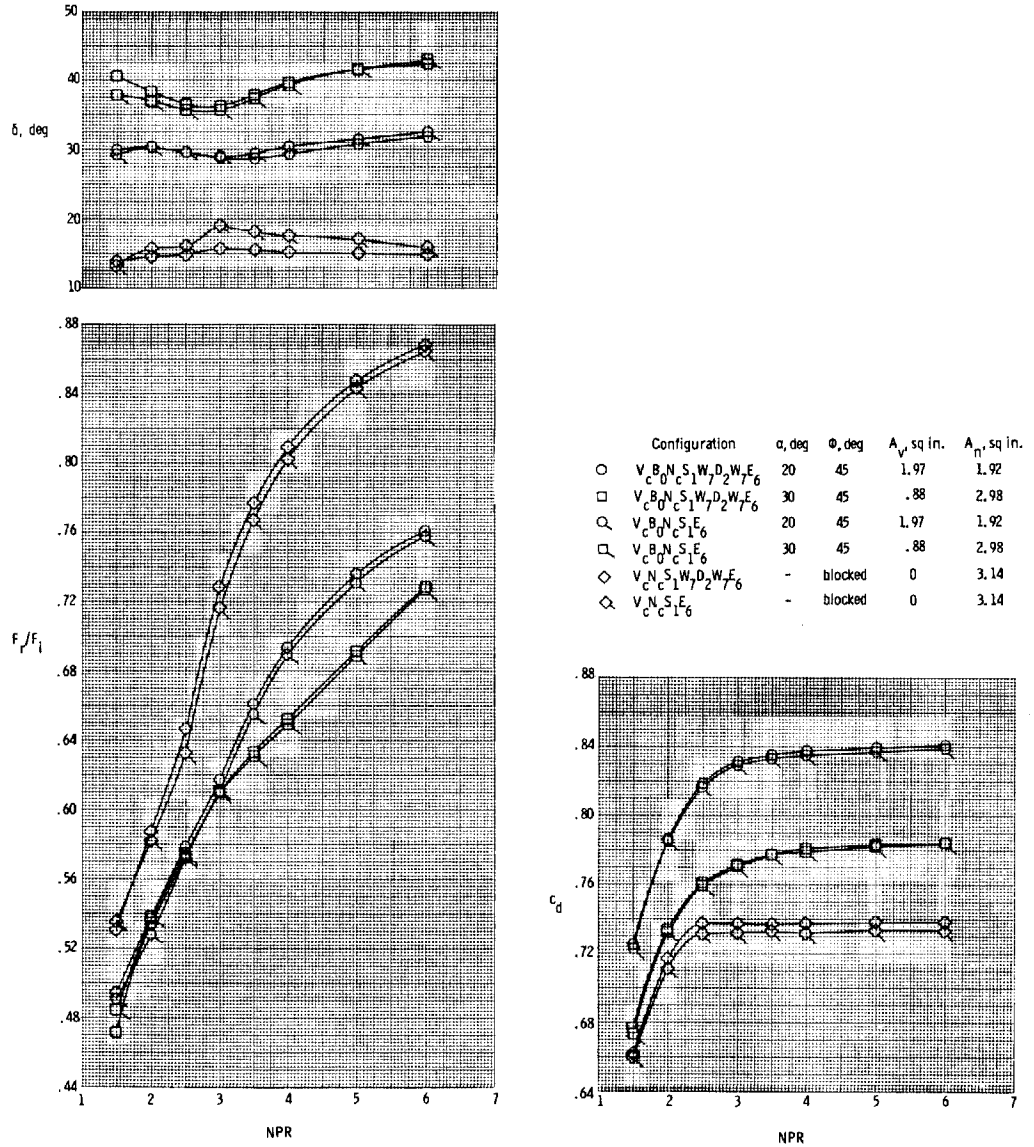

(a) Resultant-thrust-vector angle, resultant-thrust ratio, and discharge coefficient.

Figure 33. Effect of lower clamshell diverter angle (upper diverter closed) and blocked ventral nozzle on internal performance characteristics of the axisymmetric rear nozzle long- and short-duct transition configurations. $\delta_n = 15°$.

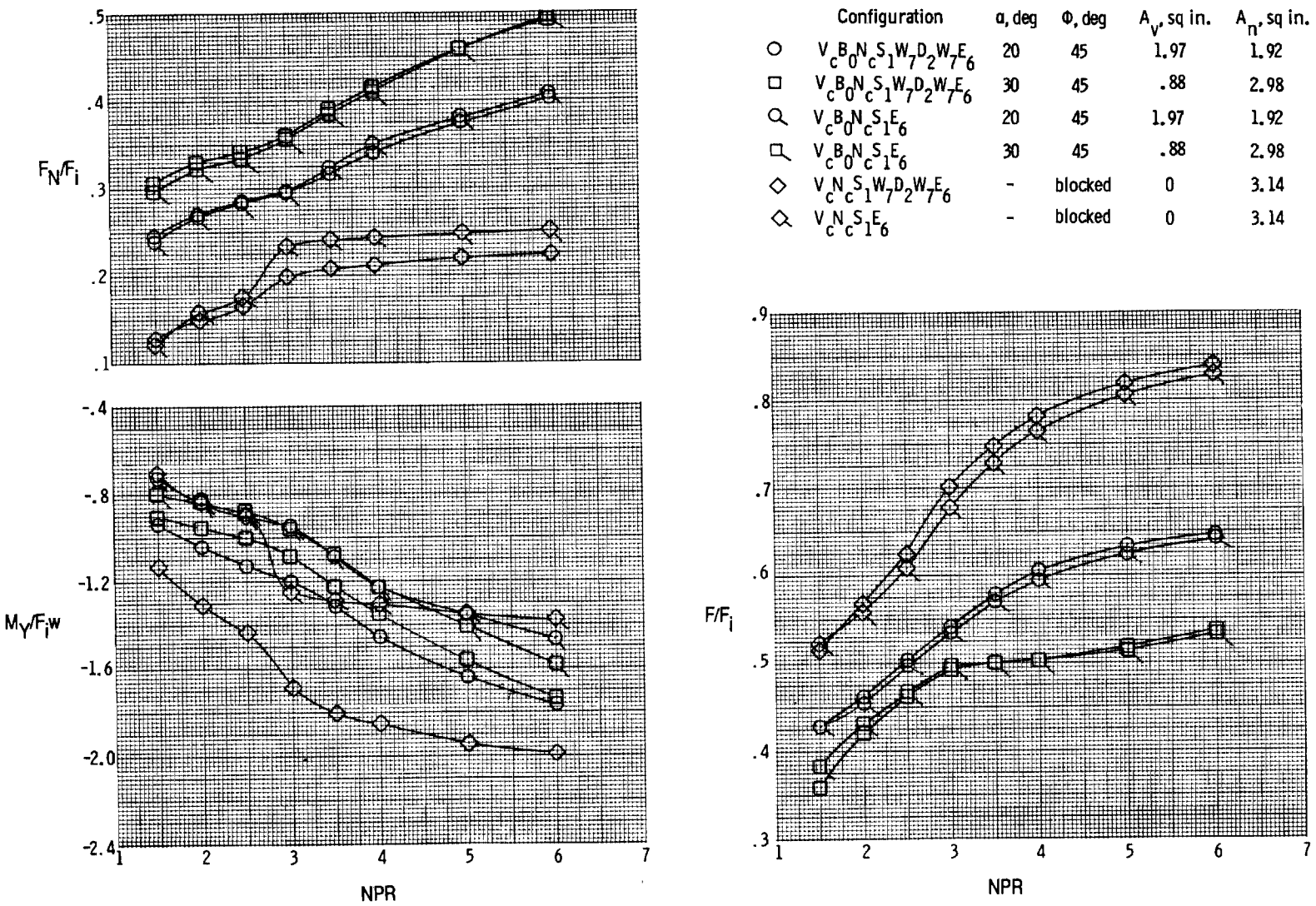

(b) Normal-force ratio, pitching-moment ratio, and thrust ratio.

Figure 33. Concluded.

	Configuration	δ_n, deg	ϕ, deg	A_n, sq in.	A_v, sq in.	α, deg	Flight regime
○	$V_{fc}N_bS_1W_7D_2W_7E_6$	15	–	4.00	–	–	Cruise
□	$V_cB_0N_cS_1W_7D_2W_7E_6$	15	45	1.92	1.97	20	Transition
◇	$V_cB_0N_cS_1W_7D_2W_7E_6$	15	45	2.98	.88	30	Transition
△	$V_cB_1N_cS_1E_9$	–	90	–	2.43	Closed	Vertical
◺	$V_cB_2N_cS_1E_9$	–	90	–	2.43	Closed	Vertical

	Configuration	δ_n, deg	ϕ, deg	A_n, sq in.	A_v, sq in.	β, deg	Flight regime
◺	$V_cB_0N_bS_1W_7D_2W_7E_7$	15	45	3.28	1.64	45	Transition
⌓	$V_cB_0N_bS_1W_7D_2W_7E_8$	15	45	1.71	2.64	65	Transition
◇	$V_cB_0N_bS_1W_7D_2W_7E_9$	–	45	–	2.64	90	Vertical
◇	$V_cB_1N_bS_1E_9$	–	90	–	2.43	90	Vertical

(Shaded symbols indicate geometric throat area (A_t) for each of the above configurations)

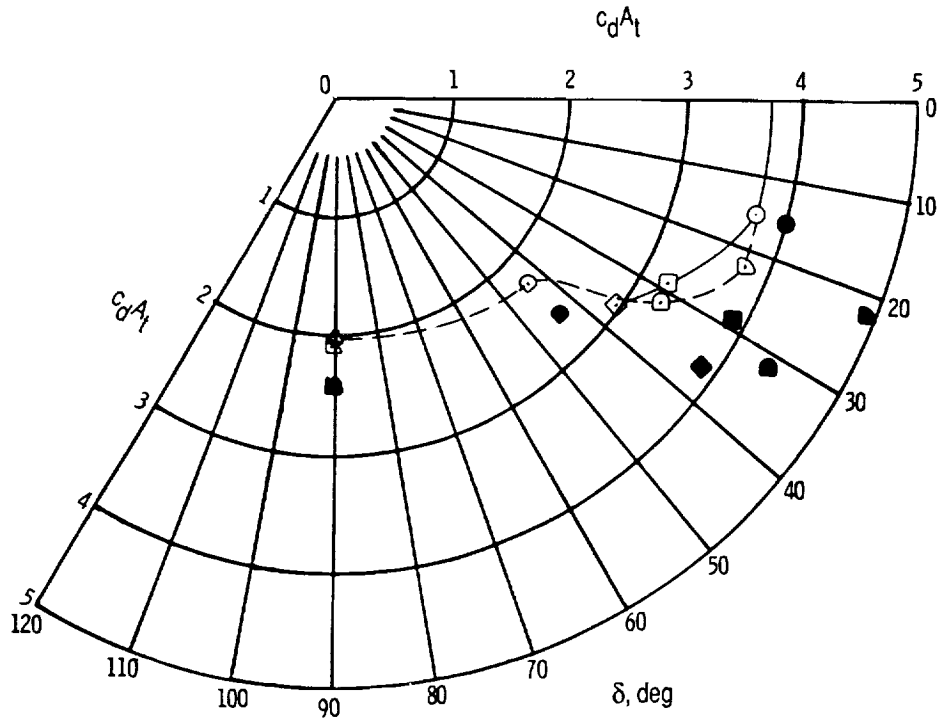

Figure 34. Variation of effective throat area c_dA_t with resultant-thrust-vector angle from cruise to vertical flight for axisymmetric rear nozzle configurations with clamshell diverter and butterfly door ventral nozzles at NPR = 3.0. Dashed line indicates fairing of configurations with butterfly door ventral nozzle.

	Configuration	δ_n, deg	ϕ, deg	A_n, sq in.	A_v, sq in.	α, deg	Flight regime
○	$V_{fc}N_bS_1W_7D_2W_7E_6$	15	-	4.00	-	-	Cruise
□	$V_cB_0N_cS_1W_7D_2W_7E_6$	15	45	1.92	1.97	20	Transition
◇	$V_cB_0N_cS_1W_7D_2W_7E_6$	15	45	2.98	.88	30	Transition
△	$V_cB_1N_cS_1E_9$	-	90	-	2.43	Closed	Vertical
▷	$V_cB_2N_cS_1E_9$	-	90	-	2.43	Closed	Vertical

	Configuration	δ_n, deg	ϕ, deg	A_n, sq in.	A_v, sq in.	β, deg	Flight regime
▷	$V_cB_0N_bS_1W_7D_2W_7E_7$	15	45	3.28	1.64	45	Transition
□	$V_cB_0N_bS_1W_7D_2W_7E_8$	15	45	1.71	2.64	65	Transition
○	$V_cB_0N_bS_1W_7D_2W_7E_9$	-	45	-	2.64	90	Vertical
◇	$V_cB_1N_bS_1E_9$	-	90	-	2.43	90	Vertical

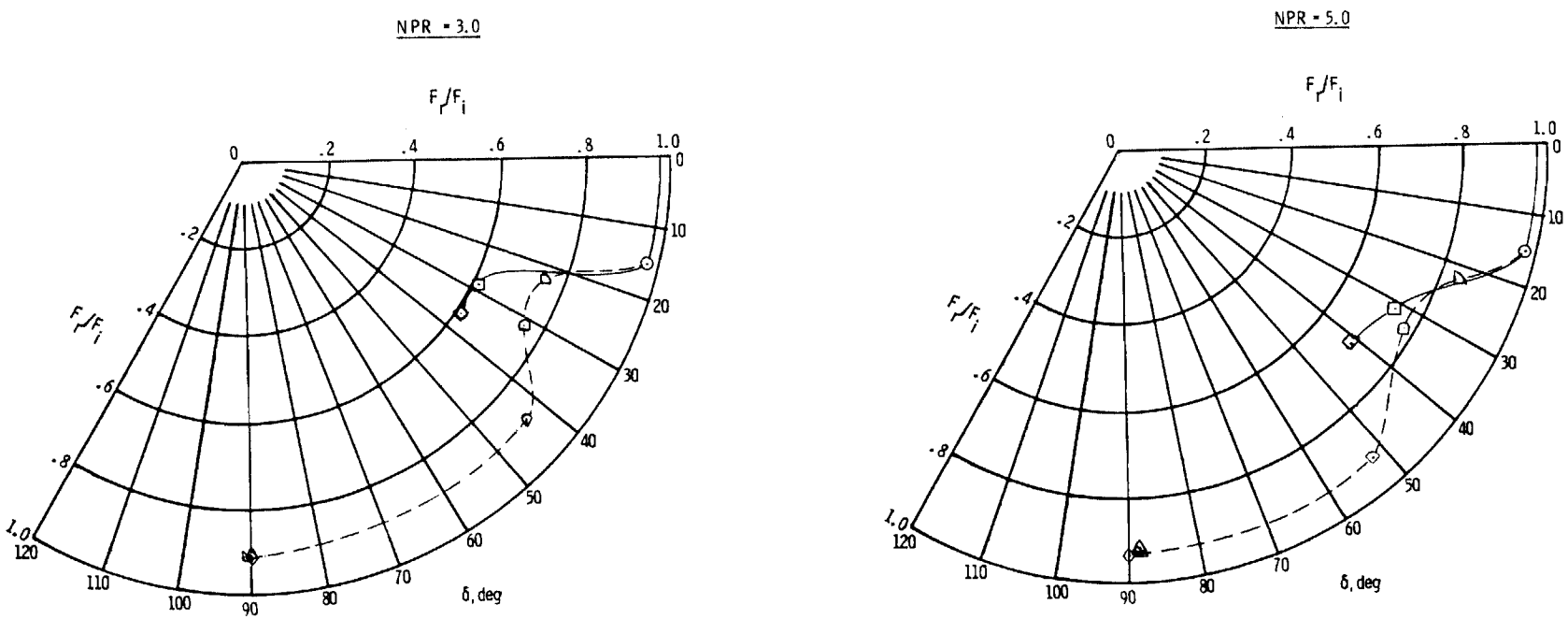

Figure 35. Variation of resultant-thrust ratio with resultant-thrust-vector angle from cruise to vertical flight for axisymmetric rear nozzle configurations with clamshell diverter and butterfly door ventral nozzles at two nozzle pressure ratios. Dashed lines indicate fairing of configurations with butterfly door ventral nozzle.

NASA
National Aeronautics and Space Administration

Report Documentation Page

1. Report No.	2. Government Accession No.	3. Recipient's Catalog No.
NASA TP-3103		

4. Title and Subtitle	5. Report Date
Static Internal Performance of Ventral and Rear Nozzle Concepts for Short-Takeoff and Vertical-Landing Aircraft	September 1991
	6. Performing Organization Code
7. Author(s)	8. Performing Organization Report No.
Richard J. Re and George T. Carson, Jr.	L-16902
	10. Work Unit No.
9. Performing Organization Name and Address	505-62-30-01
NASA Langley Research Center Hampton, VA 23665-5225	11. Contract or Grant No.
12. Sponsoring Agency Name and Address	13. Type of Report and Period Covered
National Aeronautics and Space Administration Washington, DC 20546-0001	Technical Paper
	14. Sponsoring Agency Code

15. Supplementary Notes

16. Abstract

An investigation has been conducted to determine the internal performance of two exhaust system concepts applicable to single-engine short-takeoff and vertical-landing tactical fighter configurations. These concepts involved blocking (or partially blocking) tail-pipe flow to the rear (cruise) nozzle and diverting it through an opening to a ventral nozzle for vertical thrust. A set of variable-angle vanes at the ventral nozzle exit was used to vary ventral nozzle thrust angle between 45° and 110° relative to the positive-axial-force direction. In the vertical flight mode the rear nozzle (or tail-pipe flow to it) was completely blocked. In the transition flight mode flow in the tail pipe was split between the rear and ventral nozzles, and the flow was vectored at both exits for aircraft control purposes throughout this flight regime. In the cruise flight mode the ventral nozzle was scaled and all flow exited through the rear nozzle.

17. Key Words (Suggested by Author(s))	18. Distribution Statement
STOVL Short takeoff Vertical landing Ventral nozzle	Unclassified— Unlimited Subject Category 02

19. Security Classif. (of this report)	20. Security Classif. (of this page)	21. No. of Pages	22. Price
Unclassified	Unclassified	69	A04

NASA FORM 1626 OCT 86

NASA-Langley, 1991

For sale by the National Technical Information Service, Springfield, Virginia 22161-2171